ANALYSIS AND MODELING OF INNOVATIVE HYBRID PLC-WIRELESS COOPERATIVE SYSTEM

A Dissertation

Presented to the Faculty of the Graduate School

of Cornell University

in Partial Fulfillment of the Requirements for the Degree of

Doctor of Philosophy

by

Tae Eung Sung

February 2010

ANALYSIS AND MODELING OF INNOVATIVE HYBRID PLC-WIRELESS COOPERATIVE SYSTEMS

Tae Eung Sung, Ph.D.

Cornell University 2010

Wireline and wireless communications have become indispensable part of our daily life. A variety of devices, such as cellular phones and wireless laptops, have changed the way people communicate and interact. The demand for broadband internet and ubiquitous connectivity such as 3G/4G cellular telephony and wireless LANs has been steadily growing.

However wireless devices are hampered by challenges such as fading, mobility, battery life, etc. Recently power line communication which exploits existing infrastructures has emerged as a medium that could overcome these challenges. The ultimate goal of such system is to support the required high data rates within limited resources. Hence, we propose to combine wireline and wireless technologies and investigate coding and modulation schemes that improve transmission date rates. This work consists of three major communication systems of wireline, wireless and hybrid scheme.

First, we deal with a discrete time-varying block model that captures cyclostationary nature of power line channel response. In fact, power line channel is time-varying since appliances connected to power lines often exhibit input impedance that is a function of instantaneous amplitude of the mains voltage. Our time-varying block transmission model is suitable to simulate more realistically the effect of the medium, but also facilitates the design of precoders and bit loading methods to better cope with the periodically time-varying channel distortion. This

analysis is essential for understanding how precoders deal with time variation of the channel.

Second, we investigate wireless cooperative communications with randomized space-time coding, exploiting the advantages of co-located antenna systems. Starting with decentralized randomization schemes and their attainable diversity in flat fading channels, we show these schemes are desirable in the presence of time dispersion due to asynchronism among nodes and frequency selectivity. We then study packet transmission policies in the cross-layer perspective, which is called *modified-linear-rule* (MLR), that minimize the average power consumed by transmitter under average delay constraints. We generalize the scheme of MLR scheduler to multiuser wireless fading environment and compare it with the performance of the optimal scheduler and the log-linear scheduler.

Third, we elaborate on a hybrid PLC/wireless link which is realizable in typical indoor communication networks. We derive analytic forms of single-user and multiuser MIMO channel capacities, and then evaluate relay channel capacities for two channel scenarios; one when channel is perfectly known to transmitter and the other when channel is unknown. We propose adaptive PLC-embedded relaying scheme which involves both decode-and-forward coding and OFDM modulation. We investigate the optimal allocation of transmit powers for the scheme at both source and relay nodes under total power constraints.

BIOGRAPHICAL SKETCH

Tae Eung Sung was born in 1976 in Busan, Republic of Korea. He received the B.S. degree with honors (*cum laude*) in Electrical Engineering from Seoul National University, Korea, in 2002, and the M.S. degree in Electrical and Computer Engineering from University of Texas at Austin, Austin, TX, in 2004. From 2004 to 2009, he worked towards his Ph.D. degree in the School of Electrical and Computer Engineering at Cornell University, Ithaca, NY, while having spent a valuable internship at Princeton Laboratory of Panasonic North America in 2008.

His research interests include the areas of communications theory and system design, power line communications (PLC), space-time coding (STC) and multiple input multiple output (MIMO) systems, cross-layer designs and optimal resource allocation, information theory, channel estimation and signal processing for communications. His recent work focuses on cooperative communications over cognitive radio networks, and convergence of advanced information-communications technology and smart power grid systems.

To my family.

ACKNOWLEDGEMENTS

My five years at Cornell have been an invaluable journey with a mixture of hardships and delights. The rewards in waiting to see the end of my doctoral studies are undoubtedly sweet.

This dissertation could not have been completed without the support of many faculty members, my colleagues, family, and friends. First and foremost, I would like to thank my advisor, Prof. Adam Bojanczyk, for his guidance and support during the preparation of this work. Since he joined my academic committee as the Chair, he has always been available for discussion and full of insightful suggestions. I would also like to thank him for generously respecting and listening to my opinions and wishes. I have no doubt that his influence in shaping me will be ever-lasting throughout my career.

Next, I would further like to thank Prof. Stephen Wicker and Prof. Tsuhan Chen for serving on my academic committee and providing many fruitful suggestions and comments. My special thanks go to my mentors, Stefano Galli and Dr. Anna Scaglione, for giving me the opportunity of an internship in Panasonic Laboratory. Without the research experience in system solution development in power line communications, probably, I would have never felt my Ph.D. is complete. I am also grateful to Prof. Edward J. Powers in the Electrical and Computer Engineering at University of Texas at Austin for having steadily encouraged my research and career, and Prof. Minkoo Han and Prof. Sung June Kim in Seoul National University for serving as advisors and supporters during my undergraduate days in Korea.

In addition, there are still many grateful mentors in Korea, Prof. Minho Kang, Prof. Seongjoon Baek, Prof. Joonhyuk Kang, Prof. Youngmin Jang, Prof. Kyungbin Song, Prof. Heung-Gyoon Ryu, Prof. Goo Yeon Lee, Prof. Yong Lee, and Dr.

Seongkyu Song, for helping me direct and shape on a right track towards my ultimate goal.

My appreciation extends to my close friends at Cornell, Daniel Seung Lee, Dr. Kyusoon Lee, Seung-Keun Yoon and Joshua Gabet, who would listen to all my research related and non-related questions and give me useful feedback, and of course, Prof. Youngchul Sung and Prof. Ki-Il Kim, with whom I had countless pleasant experiences and guidance. Last but not the least, I would like to thank my alumni and friends, Dr. Byungchul Jang, Dr. Larkhoon Leem, Changyoung Park, Kyuwoong Choi, Jinho Shin, Kyungchang Moon, Sangjoon Kim, Jaeil Kwon, Seongbong Seo, Jeonghyung Park, Taewoo Kim, and Junyoung Park, for their warm-hearted friendship and support on me, and I also owe a debt of gratitude to all my Korean ECE graduate students, Dr. Jeonghyun Hwang, Dr. Moon Kyung Kim, Sang Hyeon Lee, Ji Hyuk Park, Wooram Lee, Jaesung Lee, Eugene Hwang, Jin Sub Kim, and Daniel Juhyung Joe for sharing delightful moments together. They are hard-working, sincere people, and I wish the best in their career path from the bottom of my heart.

I am indebted to Il-Hwan Jeon, Dae-Jin Baik and Eunjoo Lee, for sharing almost everything in my lifetime, who are ones of the most pleasant and reliable persons on earth. I have been very fortunate to have amazingly delightful, supportive people as above.

Finally, my greatest thanks goes to my family for their dedicated love and encouragement: my parents, Mr. Sae-Yong Sung and Mrs. Yu-Song Lee, who I love and respect most in the world; my eldest brother, Tae-Gyu Sung, whose future will shine in full of prosperity; my old brother and favorite sister-in-law, Tae-Ho Sung and Hee-Jeong Kang, who have brought parents the best of happiness with lovely kids Won-Jae Sung and Min-Jae Sung. It has made me feel hard that I

has physically been so far away from them, but I hope that my success makes them proud. I wish all upcoming glorious, joyful moments to be shared with them together.

TABLE OF CONTENTS

LIST OF TABLES

LIST OF FIGURES

CHAPTER 1

INTRODUCTION

Wireline and wireless communications have become indispensable part of our daily life. Cellular phones and wireless laptops are devices that have changed the way people communicate and interact.

They have increased the demand for broadband internet and ubiquitous connectivity including 3G/4G cellular telephony and wireless LANs. However wireless devices are hampered by challenges like fading, mobility, battery life, etc. Recently power line communication which exploits existing infrastructures has emerged as a medium that could aid in overcoming those challenges. The ultimate goal of such system is to support the required high data rates within limited resources.

Hence, we propose to merge wireline and wireless technologies and investigate coding and modulation schemes that improve transmission data rates.

1.1 PLC-embedded Cooperative Systems

In radio propagation environments, there may be blind zones caused by surrounding buildings in the area covered by the transmitter. In such situations several terminals can serve as intermediate nodes which relay the signal to the receiver. Cooperative relaying is an effective communication technique that offers better quality of communication link and increased channel capacity, [1], [2]. Information-theoretically, channel capacity depends on the signal-to-noise (SNR) ratio of received signals. In practical systems, there exist resource constraints among those terminals involved in relaying, such as transmit power, encoding/decoding schemes,

etc. Therefore, finding the best transmit power allocation strategy between transmitter and relay which achieves maximum SNR at receiver and maximizes channel capacity is an important issue.

In this dissertation, we consider cooperative communication with single relay selection, [3]. In that scheme a relay selection mechanism is considered jointly with transmission power control. A set of potential relays determine their transmission power needed to participate in the cooperative communication. The relay which minimizes the overall power consumption is chosen. The relay selection is done in a distributed manner with minimum communication overhead. Due to spatial diversity multiple input multiple output (MIMO) techniques based on antenna arrays can dramatically reduce the required transmission power for certain throughput requirements. In cases when each node is limited to a single antenna, multiple nodes could collaborate to form a virtual antenna array to achieve spatial diversity, [4]. Compared with multinode cooperative communication schemes, single relay cooperation schemes need neither cooperative beamforming nor distributed space-time coding. Thus they incur less cooperation overhead and are much easier to implement. Besides, they can potentially achieve the same diversity multiplexing tradeoff as that of multinode cooperative schemes. Hence, single relay selection cooperative strategies are important considerations, [4]. Most of the work on selective cooperation schemes focus on the multiplexing-diversity tradeoff property, where a fixed power level is usually assumed at the source and relays. Power control issues are investigated in [5]- [8] from an information theoretic point of view based on the outage probability analysis.

It is well known that power line communication (PLC) offers a fully developed infrastructure of electrical power distribution grid for reliable data transmission.

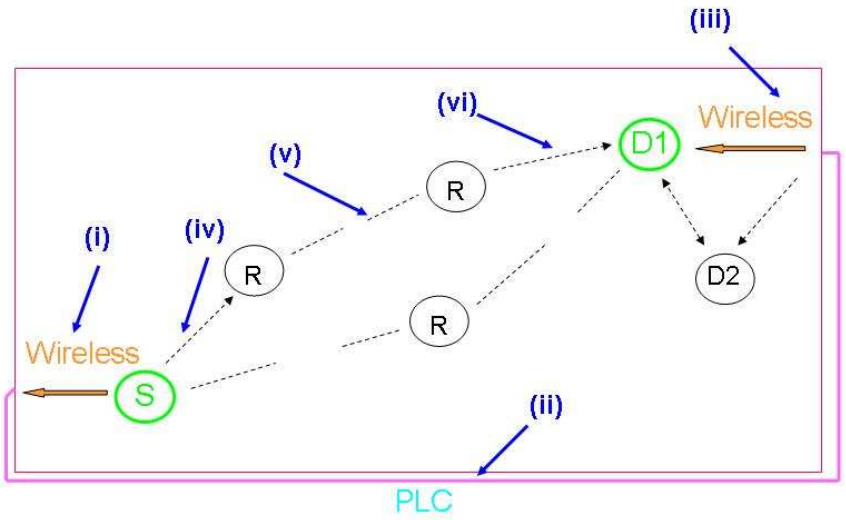

Figure 1.1: Convergence of PLC and wireless link

Thus we propose to replace a weak wireless link of (iv)-(v)-(vi) by a stable PLC link of (i)-(ii)-(iii) in Fig. 1.1. We show that such a hybrid scheme can improve overall communication quality. Based on single or two-hop relaying link which experiences Rayleigh fading, we propose an adaptive power allocation scheme under transmit power constraints which guarantees optimal system efficiency. Our scheme involves the decode-and-forward (DF) relaying and orthogonal frequency division multiplexing (OFDM). For a realistic relaying scenario in Fig. 1.1, numerical tests indicate that PLC/wireless link via (i)-(ii)-(iii) performs better than a typical wireless link via (iv)-(v)-(vi).

1.2 Outline of the Dissertation

This dissertation consists of three major communication systems of wireline (Chapter 2 and 3), wireless (Chapter 4 and 5) and hybrid scheme (Chapter 6).

In Chapter 2 we develop a discrete time-varying block channel model that captures the cyclostationary nature of the power line channel response. The power line channel is time-varying since appliances connected to power lines often exhibit input impedance that is a function of instantaneous amplitude of the mains voltage which, in turn, causes a periodically time-varying channel response. Our time-varying block transmission model allows us to simulate more realistically the effect of the medium, and also facilitates the design of precoders and bit loading methods which better cope with the periodically time-varying channel distortion. This analysis is essential for understanding how precoders deal with time variation of the channel.

In Chapter 3 addresses the problem of designing a simple, efficient power line network simulator which incorporates two types of multirate filter bank precoders, *weighted orthogonal frequency division multiplexing* (OFDM) and *wavelet-based maximally decimated filter bank* (MDFB). Using our simulator, we validate our time-varying block channel model on a real test channel taken from [10] and compare two precoder schemes in terms of error probability performance.

In Chapter 4, we investigate wireless cooperative communications with randomized space-time coding, exploiting the advantages of co-located antenna systems. The majority of current cooperative schemes require the knowledge of the number of cooperating nodes, and in many cases, specific knowledge of the encoding rule. Though the hardware resources may be distributed, the protocols employed

in these schemes are not. Starting with decentralized randomization schemes and their attainable diversity in flat fading channels, we show these schemes are desirable in the presence of time dispersion due to asynchronism among nodes and frequency selectivity, and they are easily adapted to block space-time precoding schemes which exploit both spatial and temporal diversity.

In Chapter 5, we investigate packet transmission policies in the cross-layer implementations that minimize the average power consumed by transmitter under average delay constraints. We present a simple packet scheduling policy which is influenced by both queue and channel states and which can be utilized to tradeoff queueing delay and transmission power allocation. Our scheduling policy uses a low-complexity *modified-linear-rule* (MLR) which causes the queue to evolve as a stable feed-back linear system. The MLR design parameter is chosen so as to reach the desired compromise between delay and power consumption. We generalize the scheme of the MLR scheduler to multiuser wireless fading environment and compare it with the performances of the optimal scheduler and the log-linear scheduler.

In Chapter 6, we exploit the results of wireline and wireless schemes obtained in earlier chapters, and design a hybrid PLC/wireless scheme which can be realized in typical indoor communication networks. We derive analytic forms of single-user and multiuser MIMO channel capacity, and then evaluate relay channel capacities for two channel scenarios; one when channel is perfectly known to transmitter and the other when channel is unknown. We propose adaptive PLC-embedded cooperative relaying scheme which involves both decode-and-forward (DF) coding and OFDM modulation. We investigate the optimal allocation of transmit powers for the scheme at both source and relay nodes under total power constraints. We

close the chapter with numerical results that justify validity of our analysis.

The last chapter summarize the main results of the dissertation and describes applications of the results to real world systems.

CHAPTER 2

NOVEL POWER LINE NETWORK DESIGN

2.1 Power Line Communications

Power Line Communication (PLC) utilizes existing power distribution cables to transmit data. Initially, the interest for PLCs was limited to "outdoor" applications, i.e. using the existing power line infrastructure for delivering broadband Internet access, [15], [26]. More recently, PLC is emerging as an excellent candidate for many other applications, e.g. for in-home, in-office and in-vehicle LANs, for "Smart Grids" applications, and in-building control and automation networks etc., [16], [19], [20].

Ethernet provides high speed networking, but requires dedicated category 5 cabling to be installed in the home. Although wireless devices based on 802.11 are now becoming more popular, their performance is limited by walls and other obstructions which drastically reduce their effective coverage; moreover, ensuring deterministic QoS in such networks is still problematic. On the other hand, PLCs are able to provide increased coverage at higher bit-rates when compared to wireless solutions, so that they well complement wireless LANs in the indoor environment.

PLC technology has the ability of communicating data or information signals via the electrical supply network (ESN), and therefore it can extend an existing local area network (LAN) or share an existing Internet connection through electric plugs with the installation of adapter units. The principle of PLC consists in superimposing a high-frequency (HF) signal (1.6 to 30 MHz) at low energy levels over the 50 Hz (Europe) or 60 Hz (USA) electrical signal. The combined signal is

transmitted via the power infrastructure, and decoded at remote locations.

2.1.1 Examples of Practical Applications

Electrical power is normally transmitted over high-voltage (HV) networks (110-380 kV) at a considerably long distance within a continent, distributed over medium-voltage (MV) (10-30 kV) networks at a size of large cities and big commercial vendors, and used at low-voltage (LV) (220 V in Europe, 110 V in USA) for the end user supply inside buildings or private homes. Most PLC technologies limit themselves to a set of wires such as premises wiring, but sometimes cross-leveled technology between the distribution network and premises wiring is also realizable.

From the viewpoint of customer side applications, PLC is becoming an alternative to existing wireless technology for a seamless in-home network environment where the wireless applications cannot supply consistently stable, high throughput service. As shown in Fig. 2.1. (a) and (b), every PC or peripheral devices are attached to PLC connecting outlets or adapters which behave as modems. Fig. 2.1. (c) illustrates an integrated powerline MAC/PHY transceiver which requires no new wiring to support transmission at speeds of up to 14 Mbps. It provides the ability to inter-connect multiple interfaces to the external MAC controller. Fig. 2.1. (d) shows a smart coffee maker which communicates via PLC when it is plugged to an AC outlet and communicates wirelessly via radio frequency (RF) when operated on batteries.

(a)

(b)

(c)

(d)

Figure 2.1: Various PLC products: (a) powerline PC networking connectors; (b) powerline network adapter; (c) integrated powerline MAC/PHY transceiver; and (d) HLT-smart coffeemaker

2.1.2 Characteristics of Power Line Channel and Noise

The challenge in developing PLC technology is that power cables were designed for the purpose of power distribution and not data communications. Power lines are a very hostile medium that offer many technical challenges to the design of high speed data communications devices [25]. Power line channel is a very harsh and noisy transmission medium that is very difficult to model; the power line channel is frequency-selective, time-varying, and is impaired by colored background noise and impulsive noise; many transformers along the power line are fed by a single

high voltage line, with the earth itself being used for the return electrical path (a very noisy configuration for telecommunications signals); the structure of the grid differs from country to country and also within a country (and the same applies for indoor wiring practices); power line cables are often unshielded, thus becoming both sources and targets of electromagnetic interference (EMI).

The response of the power line channel may vary abruptly when the topology changes, i.e. when devices are plugged in or out, and switched on or off. Interestingly, even if the topology of the network and the loads (appliances) attached to it do not undergo abrupt changes, the channel response is still time-varying.

In particular, the power line channel exhibits a short-term variation because the high-frequency parameters of electrical devices depend on the instantaneous amplitude of the AC mains voltage. Some initial work on the modeling of this unique aspect of the power line channel can be found in [21], [23], and [57], and references therein.

A fundamental property of the power line channel is that the time varying behavior mentioned above is periodic, where the period T_0 is typically half the AC mains period (50 or 60 Hz). Parallel to the channel input-output response behavior, are the noise statistics, that exhibit a cyclostationary component with the same period. An example of this behavior unique to the power line channel is shown in Fig. 2.2. In Fig. 2.2.(a), we observe time variation of an indoor power line channel transfer function along time axis (ms), whereas for fixed time scale ranging from 0 to 15 (ms) the magnitude gain has several deep fades over active power line region of 30 MHz. In Fig. 2.2.(b), the noise waveform generated by the dimmer of a halogen light shows the periodic cycle of 8.3 (ms), where it follows the shape of the measured AC envelope.

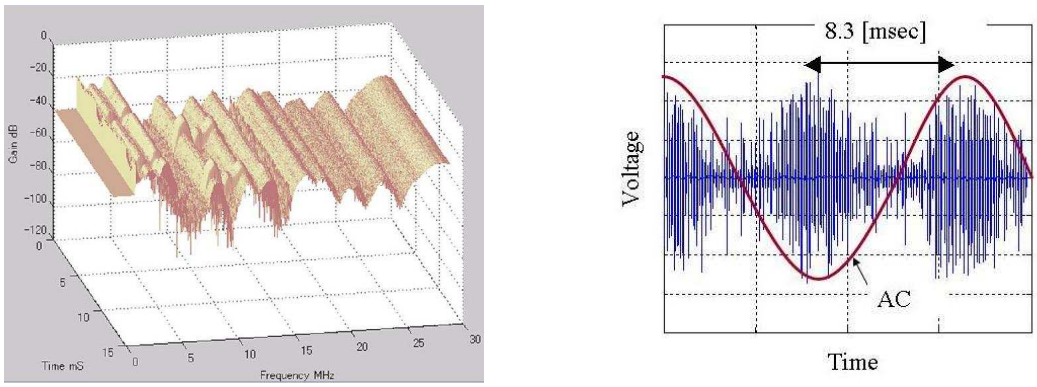

(a) (b)

Figure 2.2: (a) Measured time variation of indoor powerline channel; (b) the noise waveform generated by the dimmer of an halogen light

2.1.3 Motivation

Despite the importance and uniqueness of this behavior, to the best of the authors' knowledge there are no time-varying discrete time models for the channel response in the literature where the time variability of the channel is taken into consideration.

We here propose to model the input/output (I/O) relationship by what we refer to as a *lifting-trailing-zeros* (LTZ) technique, which provides a matrix vector form representation for the I/O relationship between the modulated symbols and the samples of the complex envelope of the output of the time-varying channel. The LTZ technique removes the inter-block interference (IBI) which occurs between adjacent transmission blocks of length P sufficiently large, by forcing the last L symbols to zeros, where L is equal to the duration of the channel impulse response in number of symbol periods; the *lifting* operation is what is commonly done when looking at filter bank processing of signals and in this context gives the advantage of providing a one-to-one mapping between the discrete time input and output data blocks of length P, [18]. We show how to derive the overall time-varying

channel response of multiple cascaded subsystems and indicate how this strategy can be used to design precoders that obtain the maximum (achievable) information rate in the specific configuration.

The main advantage of the proposed time-varying block channel model compared to that in [57] is that it captures the effect of non-stationary channel response, while operating directly on the symbols in discrete-time. Hence, with the time-varying block model we eliminate the need to convert the signals into wavelet coefficients. Not only my method is suitable to simulate more realistically the effect of the medium but also naturally leads to design precoders and bit loading methods that are tailored to better cope with the periodically time-varying channel distortion. This analysis is essential for understanding how different forms of precoding deal with time variation of the channel as well as for providing tools for improving over existing schemes.

In notational consistency, we denote vectors by boldfaced lower-case letters ($\mathbf{s}$, $\mathbf{x}$, $\mathbf{w}$, $\cdots$), matrices by bold-faced upper-case letters ($\mathbf{H}$, $\mathbf{R}_*$, $\cdots$), and scalars by lower-case roman letters (s, x, h, w, $\cdots$).

2.2 System Model

A time-varying linear channel can be represented by a linear operator $\mathcal{L}[\cdot]$. The impulse response for such a channel at time t depends on the time in which the impulse is applied at the input, say at time τ, hence $\mathcal{L}[\delta(t-\tau)] = g(t,\tau)$. Since any signal can be decomposed as follows:

$$x(t) = \int_{-\infty}^{\infty} x(\tau)\delta(t-\tau)d\tau.$$

By interchanging this integral with $\mathcal{L}[\cdot]$, the output can be written as

$$y(t) = \mathcal{L}[x(t)] = \int_{-\infty}^{\infty} x(\tau)\mathcal{L}[\delta(t-\tau)]d\tau = \int_{-\infty}^{\infty} x(\tau)g(t,\tau)d\tau, \tag{2.1}$$

where $g(t,\tau)$ is the classical input delay spread function defined in [29]. For channels that have limited memory, it is often more convenient to utilize the equivalent time-varying impulse response $h(t,t-\tau) = g(t,\tau)$. Since the second argument of $h(\cdot,\cdot)$ is the difference between time index of the output and time of the value that contributes to form that output, for channels with finite memory Δ we have $h(t,t-\tau) = 0$ for $|t-\tau| > \Delta$, which implies that support of the function $h(t,\xi)$ with respect to the second argument ξ is essentially the delay spread. Hence,

$$y(t) = \mathcal{L}[x(t)] = \int_{t-\Delta}^{t+\Delta} x(\tau)h(t,t-\tau)d\tau = \int_{-\Delta}^{\Delta} x(t-\xi)h(t,\xi)d\xi. \tag{2.2}$$

If the linear channel is also stationary, then $h(t,t-\tau) \triangleq \bar{h}(t-\tau)$, which represents the continuous-time impulse response at time t to an impulse at time $t-\tau$.

We note that for any ξ the impulse response $h(t,\xi)$ of the power line channel with period T_0 can be expanded into Fourier series, thus we have

$$h(t,\xi) = \sum_{m=-\infty}^{+\infty} h_m(\xi)e^{j\frac{2\pi m}{T_0}t}. \tag{2.3}$$

Hence the output can be represented as a sum of components $y_m(t) = h_m(t) * x(t)$

$$y(t) = \sum_{m=-\infty}^{+\infty} y_m(t)e^{j\frac{2\pi m}{T_0}t}, \tag{2.4}$$

where $'*'$ denotes convolution. The digitally modulated signal $x(t)$ can be represented as the base-band complex equivalent pulse amplitude modulation (PAM) waveforms

$$x(t) = \sum_{n=-\infty}^{\infty} x[n]p(t-nT_s), \tag{2.5}$$

where $p(t)$ is a pulse-shaping filter which is assumed to have a Nyquist characteristic and T_s is the symbol duration. In order to be able to assess the link performance

for a certain modulation and coding, we need to be able to describe the system directly in terms of the modulated symbols $x[n]$. In the following, we will express the samples of the output signal directly as a function of the channel response $h[k,n]$ and the input values $x[n]$.

Let us define $y[k] := y(kT)$ and assume that $x(t)$ can be expressed as in (2.5). Then, the output samples of a single input single output (SISO) time-varying system in (2.2) are

$$y[k] = \sum_{n=-\infty}^{\infty} x[n]h[k,k-n], \tag{2.6}$$

where

$$h[k,k-n] := \int_{-\infty}^{\infty} h(kT_s,\tau)p((k-n)T_s-\tau)d\tau. \tag{2.7}$$

Also, noting that for an LTI channel $h(t,\tau) = \mathcal{L}[\delta(t-\tau)]$ and letting $l \triangleq k-n$ we obtain

$$\bar{h}[l] = \int_{-\infty}^{\infty} \bar{h}(kT_s-\tau)p(\tau-nT_s)d\tau \tag{2.8}$$

$$= \int_{-\infty}^{\infty} p(lT_s-\tau')\bar{h}(\tau')d\tau'. \tag{2.9}$$

Substituting (2.7) in (2.6) we find the well-known fact that the system behaves as a discrete-time linear time-invariant (LTI) system with discrete-time impulse response $\bar{h}[l]$.

We note that for all τ the sampled channel response $h(kT_s, t-\tau)$ is the projection of $h(t,\tau)$ onto the space spanned by *sinc* functions $sinc(\pi t/T_s)$, and the discrete time-varying response $h[k,n]$ is the projection of the $h(kT_s,\tau)$ onto the space spanned by pulse functions $p(\tau-nT_s)$, which are orthogonal because they are Nyquist pulses. Since the digitally modulated signal $x(t)$ is directly generated using the basis $p(\tau-nT_s)$, the sample signal $\{x[n]\}$ is, in turn, a compact

representation for $x(t)$ as well. Considering (2.3) and (2.7), we have

$$h[k,k-n] = \sum_{m=-\infty}^{+\infty} e^{j\frac{2\pi T_s}{T_0}mk} \int_{-\infty}^{\infty} h_m(\tau)p((k-n)T_s-\tau)d\tau = \sum_{m=-\infty}^{+\infty} e^{j\frac{2\pi T_s}{T_0}mk} h_m(k-n). \tag{2.10}$$

This leads to writing the output as a sum of components

$$y[k] = \sum_{m=-\infty}^{+\infty} e^{j\frac{2\pi T_s}{T_0}mk} y_m[k], \tag{2.11}$$

where $y_m[k] = h_m[k] * x[k]$.

2.2.1 Lifting

The previous section shows that it is quite straightforward to obtain a discrete-time equivalent model where each sample is a function of infinite number of input symbols. However, since the system will generally have finite memory, only few symbols will actually contribute to each output sample. The technique we use next parses the data in blocks of size P larger than the maximum memory L of the discrete-time equivalent system. The objective is to account explicitly in notation for inter-block interference (IBI), while hiding the parameters that cause the inter-symbol interference (ISI) inside the mixing matrices that map input blocks into output blocks. If the blocks are large enough and the system is causal only the previous block will interfere with the current block, allowing us to describe the I/O relationship in a compact form.

For a length-P block, let us define the i-th block as follows:

$$\underline{\mathbf{x}}[i] = \begin{bmatrix} x[iP] \\ x[iP+1] \\ \vdots \\ x[iP+P-1] \end{bmatrix}, \qquad \underline{\mathbf{y}}[i] = \begin{bmatrix} y[iP] \\ y[iP+1] \\ \vdots \\ y[iP+P-1] \end{bmatrix}. \tag{2.12}$$

Then, (2.6) becomes

$$\underline{\mathbf{y}}[i] = \sum_{j=-\infty}^{\infty} \mathbf{H}_{i,i-j}\underline{\mathbf{x}}[j], \tag{2.13}$$

where $\mathbf{H}_{i,i-j}$ is P-by-P and its (k,n)-th element is defined as

$$\{\mathbf{H}_{i,i-j}\}_{k,n} = h[iP+k, (i-j)P+k-n], \quad (k,n = 0, \cdots, P-1). \tag{2.14}$$

For LTI system $\mathbf{H}_{i,i-j} = \mathbf{H}_{i-j}$ with the (k,n)-th element defined as in (2.14). Hence (2.13) becomes

$$\underline{\mathbf{y}}[i] = \sum_{j=-\infty}^{\infty} \mathbf{H}_{i-j}\underline{\mathbf{x}}[j]. \tag{2.15}$$

Lemma 1 *If the channel memory L (i.e. $L+1$ taps) is finite and $L < P$, then $\mathbf{H}_{i,i-j}$ is nonzero only for $i-j = 0$, 1, i.e.*

$$\mathbf{H}_{i,i-j} = \begin{cases} \mathbf{H}_{i,0}, & \textit{iff} \quad i = j \\ \mathbf{H}_{i,1}, & \textit{iff} \quad i = j+1 \\ \mathbf{0}, & \textit{otherwise} \end{cases} \tag{2.16}$$

and we can express (2.13) as follows:

$$\underline{\mathbf{y}}[i] = \mathbf{H}_{i,0}\underline{\mathbf{x}}[i] + \mathbf{H}_{i,1}\underline{\mathbf{x}}[i-1], \tag{2.17}$$

where $\mathbf{H}_{i,0} \triangleq \mathbf{H}_{i,0}^{(L)}$ and $\mathbf{H}_{i,1} \triangleq \mathbf{H}_{i,0}^{(L)}$ are lower-banded and upper-triangular with memory order L as in Fig. 2.3.

Proof: Refer to Appendix 2.A.

For LTI system (2.17) then becomes

$$\underline{\mathbf{y}}[i] = \underbrace{\mathbf{H}_0}_{Toeplitz}\ \underline{\mathbf{x}}[i] + \underbrace{\mathbf{H}_1}_{Toeplitz}\ \underline{\mathbf{x}}[i-1]. \tag{2.18}$$

We point out that products of $\mathbf{H}_{i,0}^{(L)}$ and $\mathbf{H}_{i,1}^{(L)}$ take special structures and we have

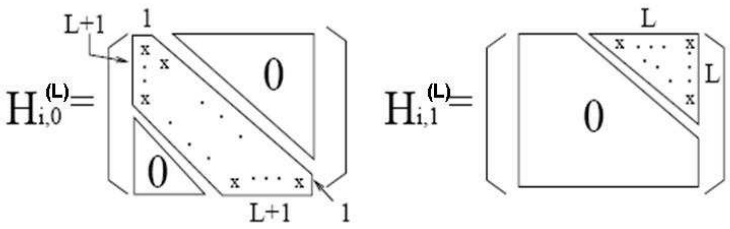

Figure 2.3: Special structures of time-varying block matrices with memory order L; $\mathbf{H}_{i,0}^{(L)}$ and $\mathbf{H}_{i,1}^{(L)}$ are lower-banded and an upper triangular, respectively.

the followings.

$$\mathbf{H}_{i,0}^{(L_1)} \cdot \mathbf{H}_{i,0}^{(L_2)} = \mathbf{H}_{i,0}^{(L_1+L_2)} \qquad \text{iff} \qquad L_1 + L_2 \leq P \tag{2.19}$$

$$\mathbf{H}_{i,1}^{(L_1)} \cdot \mathbf{H}_{i,1}^{(L_2)} = \mathbf{0} \qquad \text{iff} \qquad L_1 + L_2 \leq P \tag{2.20}$$

$$\mathbf{H}_{i,0}^{(L_1)} \cdot \mathbf{H}_{i,1}^{(L_2)} = \quad \text{V-trapezoidal matrix} \tag{2.21}$$

$$\mathbf{H}_{i,1}^{(L_1)} \cdot \mathbf{H}_{i,0}^{(L_2)} = \quad \text{H-trapezoidal matrix} \tag{2.22}$$

From (2.21) and (2.22) it follows that

$$\mathbf{H}_{i,0}^{(L_1)} \cdot \mathbf{H}_{i,1}^{(L_2)} + \mathbf{H}_{i,1}^{(L_1)} \cdot \mathbf{H}_{i,0}^{(L_2)} = \mathbf{H}_{i,0}^{(L_1+L_2)} \qquad \text{iff} \qquad L_1 + L_2 \leq P. \tag{2.23}$$

From the Lemma above, a useful corollary follows.

Corollary 1 *If* $\underline{\mathbf{x}}[i]$ *has* L *trailing zeros, where* L *is the channel memory, then for all* i

$$\mathbf{H}_{i,1}\underline{\mathbf{x}}[i-1] = 0 \tag{2.24}$$

and hence (2.17) becomes

$$\underline{\mathbf{y}}[i] = \mathbf{H}_{i,0}\underline{\mathbf{x}}[i]. \tag{2.25}$$

Proof: Note that $\mathbf{H}_{i,1}$ is an upper triangular matrix and $\underline{\mathbf{x}}[i-1]$ has trailing zeros. Therefore, since $\{\mathbf{H}_{i,1}\}_{k,n} = h[iP+k, P+k-n] \neq 0$ only for $P-L \leq n \leq P-1$ while $\{\underline{\mathbf{x}}[i-1]\}_n = 0$ for $P-L \leq n \leq P-1$.

We then have that for every i and every k

$$\sum_{n=0}^{P-1} \{\mathbf{H}_{i,1}\}_{k,n} \{\underline{\mathbf{x}}[i-1]\}_n = 0. \tag{Q.E.D}$$

For LTI system (2.25) then becomes

$$\underline{\mathbf{y}}[i] = \mathbf{H}_0\underline{\mathbf{x}}[i]. \tag{2.26}$$

2.2.2 Cascading Multiple Time-Varying Linear Systems

We now introduce a useful theorem that allows us to describe the cascade of N linear systems recursively.

Theorem 1 *If the memory of the i-th system is finite and equal to L_i, then the memory of the cascade of all N linear systems is equal to $L^{(1,\ldots,N)}=\sum_{j=1}^{N} L_j$. Now, choosing $P \geq L^{(1,\ldots,N)}$, we can apply Lemma 1 and obtain*

$$\mathbf{H}_{i,i-j}^{(1,\ldots,N)} = \begin{cases} \prod_{j=N}^{1} \mathbf{H}_{i,0}^{(j)} & \text{iff} \quad i = j \\ \mathbf{H}_{i,0}^{(N)} \mathbf{H}_{i,1}^{(1,\ldots,N-1)} + \mathbf{H}_{i,1}^{(N)} \mathbf{H}_{i-1,0}^{(1,\ldots,N-1)} & \text{iff} \quad i = j+1 \end{cases} \tag{2.27}$$

where $\mathbf{H}_{i,0}^{(1,\ldots,N)}$ is still a lower-banded matrix while $\mathbf{H}_{i,1}^{(1,\ldots,N)}$ is an upper-triangular matrix.

Proof: Refer to Appendix 2.B.

2.3 Transmission Lines as Two-Port Networks (2PNs)

The response of a transmission line to an input signal can be described through the telegraph-equations, [13], [17]. A general result of transmission line (TL) theory is that every uniform TL can be modeled as a Two-Port Network (2PN), thus allowing us to replace a distributed parameter circuit with a single lumped network. In the next two sub-sections, we will address separately the two cases of linear time-invariant (LTI) and linear time-varying (LTV) transmission line.

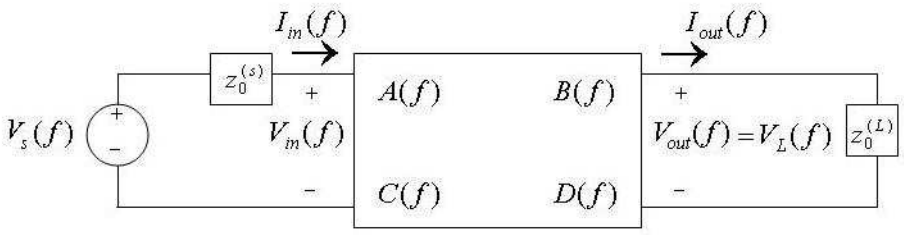

Figure 2.4: Schematic representation of a two-port network

2.3.1 Time-Invariant Transmission Lines

In TL theory, a common way to represent a 2PN is to use the transmission matrix, also known as the ABCD matrix (see [14], and references therein). The relationship between current and voltage (in the frequency domain) at the two ports of a 2PN

is given by the following expression, (cf. see Fig. 2.4).

$$\begin{bmatrix} V_{in}(f) \\ I_{in}(f) \end{bmatrix} = \underbrace{\begin{bmatrix} A(f) & B(f) \\ C(f) & D(f) \end{bmatrix}}_{\triangleq \Phi_{fw}} \begin{bmatrix} V_{out}(f) \\ I_{out}(f) \end{bmatrix} \tag{2.28}$$

where $\Phi_{fw} \triangleq [A(f)\ B(f);\ C(f)\ D(f)]$ is defined as forward transmission matrix, and the quantities above are all complex phasors. This description can be easily mapped into an overall system transfer function. Considering a load $z_0^{(L)}$ constant in time and frequency closing the output port and a generator transmitting a signal with Fourier transform $V_S(f)$ with in series an impedance $z_0^{(s)}$ constant in time and frequency, the overall transfer function of the two-port equivalent network is

$$H(f) = \frac{V_L(f)}{V_S(f)} \tag{2.29}$$

$$= \frac{z_0^{(L)}}{A(f)z_0^{(L)} + B(f) + C(f)z_0^{(L)}z_0^{(s)} + D(f)z_0^{(s)}}. \tag{2.30}$$

It is possible to express the I/O relationship of a 2PN using Fourier transforms

$$V_{out}(f) = \widetilde{A}(f)V_{in}(f) + \widetilde{B}(f)I_{in}(f) \tag{2.31}$$

$$I_{out}(f) = \widetilde{C}(f)V_{in}(f) + \widetilde{D}(f)I_{in}(f), \tag{2.32}$$

where $\Phi_{bw} \triangleq [\widetilde{A}(f)\ \widetilde{B}(f);\ \widetilde{C}(f)\ \widetilde{D}(f)]$ is defined as backward transmission matrix and the Fourier transforms above are well-defined in the LTI case. In fact, TL theory in [14] verifies $\Phi_{bw} = \Phi_{fw}^{-1} = \Phi_{fw}$ with $det(\Phi_{fw}) = 1$, where the signs of $B(f)$ and $C(f)$ do not have to be changed because the direction of the current flowing from the source to the load is regarded as positive.

From (2.31) and (2.32), we obtain two different representations of $V_{out}(f)$

$$V_{out}(f) = \frac{1}{A(f)}V_{in}(f) - \frac{B(f)}{A(f)}I_{out}(f) \tag{2.33}$$

$$V_{out}(f) = \frac{1}{C(f)}I_{in}(f) - \frac{D(f)}{C(f)}I_{out}(f). \tag{2.34}$$

(2.33) and (2.34) imply that the output voltage and current can be expressed as a filtered version of the input voltage and current.

In general, a power line point-to-point link consists of several sections of power cables including bridged taps. The end-to-end system can be decomposed in the cascade of several sub-systems (where a sub-system is a section of power cable), and each sub-system can be modeled with an appropriate 2PN. A convenient rule known as the "Chain Rule" allows us to obtain the overall transmission matrix by simply multiplying the transmission matrices of each subsystem, [13].

2.3.2 Time-Varying Transmission Lines

In the case of time-varying system, the expressions in (2.33) and (2.34) do not hold. Nevertheless, the relations between current and voltage remain linear and, as such, one can still express the dependency of the output voltage as functions of the input voltage, the input current and the output current via the following two distinct integral relationships

$$v_{out}(t) = \int_{-\infty}^{\infty} v_{in}(\tau)a(t,t-\tau)d\tau + \int_{-\infty}^{\infty} i_{out}(\tau)b(t,t-\tau)d\tau \qquad (2.35)$$

$$v_{out}(t) = \int_{-\infty}^{\infty} i_{in}(\tau)c(t,t-\tau)d\tau + \int_{-\infty}^{\infty} i_{out}(\tau)d(t,t-\tau)d\tau, \qquad (2.36)$$

where $a(t,t-\tau)$, $b(t,t-\tau)$, $c(t,t-\tau)$, $d(t,t-\tau)$ are defined as the time-varying kernels of frequency responses $\frac{1}{A(f)}$, $\frac{-B(f)}{A(f)}$, $\frac{1}{C(f)}$, $\frac{-D(f)}{C(f)}$, respectively. We express each of the continuous-time convolutions into their discrete-time equivalent as done in Section 2.2 and write the following discrete-time model, (cf. see (2.6))

$$v_{out}[k] = \sum_{n=-\infty}^{\infty} v_{in}[n]a[k,k-n] + \sum_{n=-\infty}^{\infty} i_{out}[n]b[k,k-n] \qquad (2.37)$$

$$v_{out}[k] = \sum_{n=-\infty}^{\infty} i_{in}[n]c[k,k-n] + \sum_{n=-\infty}^{\infty} i_{out}[n]d[k,k-n] \quad (2.38)$$

where $a[k,k-n]$, $b[k,k-n]$, $c[k,k-n]$, $d[k,k-n]$ are defined as in (2.7).

The relationship between source and load voltages and the output voltage and current can also be easily expressed in the discrete time

$$v_{in}[k] = v_s[k] - z_0^{(s)} i_{in}[k] \quad (2.39)$$

$$v_{out}[k] = z_0^{(L)} i_{out}[k]. \quad (2.40)$$

Similarly to (2.12), let us define $\{\underline{\mathbf{v}}_s[i]\}_k \triangleq v_s[iP+k]$, $\{\underline{\mathbf{v}}_{out}[i]\}_k \triangleq v_{out}[iP+k]$, $\{\underline{\mathbf{v}}_{in}[i]\}_k \triangleq v_{in}[iP+k]$, $\{\underline{\mathbf{i}}_{out}[i]\}_k \triangleq i_{out}[iP+k]$ and $\{\underline{\mathbf{i}}_{in}[i]\}_k \triangleq i_{in}[iP+k]$.

If the system memory is finite and $L < P$, (2.37)-(2.40) can be cast in their lifted form as follows:

$$\underline{\mathbf{v}}_{out}[i] = \mathbf{A}_{i,0}\underline{\mathbf{v}}_{in}[i] + \mathbf{A}_{i,1}\underline{\mathbf{v}}_{in}[i-1] + \mathbf{B}_{i,0}\underline{\mathbf{i}}_{out}[i] + \mathbf{B}_{i,1}\underline{\mathbf{i}}_{out}[i-1] \quad (2.41)$$

$$\underline{\mathbf{v}}_{out}[i] = \mathbf{C}_{i,0}\underline{\mathbf{i}}_{in}[i] + \mathbf{C}_{i,1}\underline{\mathbf{i}}_{in}[i-1] + \mathbf{D}_{i,0}\underline{\mathbf{i}}_{out}[i] + \mathbf{D}_{i,1}\underline{\mathbf{i}}_{out}[i-1] \quad (2.42)$$

$$\underline{\mathbf{v}}_{in}[i] = \underline{\mathbf{v}}_s[i] - z_0^{(s)}\underline{\mathbf{i}}_{in}[i] \quad (2.43)$$

$$\underline{\mathbf{v}}_{out}[i] = z_0^{(L)}\underline{\mathbf{i}}_{out}[i], \quad (2.44)$$

where we define $\mathbf{A}_{i,0}$, $\mathbf{B}_{i,0}$, $\mathbf{C}_{i,0}$ and $\mathbf{D}_{i,0}$ as in (2.14),

$$\{\mathbf{A}_{i,i-j}\}_{k,n} = a[iP+k,(i-j)P+k-n] \quad (k,n=0,\cdots,P-1) \quad (2.45)$$

$$\{\mathbf{B}_{i,i-j}\}_{k,n} = b[iP+k,(i-j)P+k-n] \quad (k,n=0,\cdots,P-1) \quad (2.46)$$

$$\{\mathbf{C}_{i,i-j}\}_{k,n} = c[iP+k,(i-j)P+k-n] \quad (k,n=0,\cdots,P-1) \quad (2.47)$$

$$\{\mathbf{D}_{i,i-j}\}_{k,n} = d[iP+k,(i-j)P+k-n] \quad (k,n=0,\cdots,P-1). \quad (2.48)$$

2.4 Discrete-Time I/O Relationship of Transmission Lines

For the overall channel impulse response $h^{(1,\cdots,N)}(t,\tau)$ in the time domain, we can write

$$v_{out}(t) = \int_{-\infty}^{\infty} v_s(\tau) h^{(1,\cdots,N)}(t,\tau) d\tau, \tag{2.49}$$

which maps to the discrete-time equivalent relationship

$$v_{out}[k] = \sum_{n=-\infty}^{\infty} v_s[n] h^{(1,\cdots,N)}[k, k-n]. \tag{2.50}$$

Our objective is to calculate

$$\underline{\mathbf{v}}_{out}[i] = \mathbf{H}_{i,0}^{(1,\cdots,N)} \underline{\mathbf{v}}_s[i] + \mathbf{H}_{i,1}^{(1,\cdots,N)} \underline{\mathbf{v}}_s[i-1]. \tag{2.51}$$

In order to do this, we first tackle the single system case and then extend our results to the cascade of multiple systems.

2.4.1 Single System

There are various ways to find the I/O relationship in the single system case. First, on the basis of Lemma 1, we can prove the following Theorem.

Lemma 2 *Given a system with finite memory $L < P$, the I/O relationship in terms of $\underline{\mathbf{v}}_{out}[i]$, $\underline{\mathbf{v}}_s[i]$ and $\underline{\mathbf{v}}_{in}[i]$ is given by the expression*

$$\mathbf{G}_{i,0} \cdot \underline{\mathbf{v}}_{out}[i] + \mathbf{G}_{i,1} \cdot \underline{\mathbf{v}}_{out}[i-1] = \underline{\mathbf{v}}_s[i] + \mathbf{J}_{i,1} \underline{\mathbf{v}}_s[i-1] + \mathbf{Q}_{i,1} \underline{\mathbf{v}}_{in}[i-1], \tag{2.52}$$

where $\mathbf{G}_{i,0}$, $\mathbf{G}_{i,1}$, $\mathbf{J}_{i,1}$ *and* $\mathbf{Q}_{i,1}$ *are defined as follows:*

$$\mathbf{G}_{i,0} = \mathbf{A}_{i,0}^{-1}(\mathbf{I} - 1/z_0^{(L)}\mathbf{B}_{i,0}) + z_0^{(s)}\mathbf{C}_{i,0}^{-1}(\mathbf{I} - 1/z_0^{(L)}\mathbf{D}_{i,0}) \quad (2.53)$$

$$\mathbf{G}_{i,1} = -1/z_0^{(L)}\mathbf{A}_{i,0}^{-1}\mathbf{B}_{i,1} - z_0^{(s)}/z_0^{(L)}\mathbf{C}_{i,0}^{-1}\mathbf{D}_{i,1} \quad (2.54)$$

$$\mathbf{J}_{i,1} = \mathbf{C}_{i,0}^{-1}\mathbf{C}_{i,1} \quad (2.55)$$

$$\mathbf{Q}_{i,1} = \mathbf{A}_{i,0}^{-1}\mathbf{A}_{i,1} - \mathbf{C}_{i,0}^{-1}\mathbf{C}_{i,1}. \quad (2.56)$$

Proof: Refer to Appendix 2.C.

Corollary 2 *Forcing the last L input symbols to be zeros, the I/O relationship between* $\underline{\mathbf{v}}_{out}[i]$ *and* $\underline{\mathbf{v}}_s[i]$ *is*

$$\underline{\mathbf{v}}_s[i] = \underbrace{\left(\mathbf{A}_{i,0}^{-1}(\mathbf{I} - 1/z_0^{(L)}\mathbf{B}_{i,0}) + z_0^{(s)}\mathbf{C}_{i,0}^{-1}(\mathbf{I} - 1/z_0^{(L)}\mathbf{D}_{i,0})\right)}_{\triangleq \mathbf{G}_{i,0}} \underline{\mathbf{v}}_{out}[i], \quad (2.57)$$

where the overall I/O transmission matrix is $\mathbf{H}_{i,0} \triangleq \mathbf{G}_{i,0}^{-1}$.

Proof: The thesis is readily obtained by forcing to zero the upper triangular matrices that account for IBI (cf. see lifted representation in Corollary 1). The proof in details is provided in Appendix 2.D. (Q.E.D)

Next, we propose a second way to represent the I/O relationship in the following theorem.

Theorem 2 *Given a system with finite memory* $L < P$*, the overall I/O relationship is expressed as*

$$\begin{bmatrix} \underline{\mathbf{v}}_{out}[i] \\ \underline{\mathbf{i}}_{out}[i] \end{bmatrix} = \underbrace{\begin{bmatrix} \Lambda_{i,0} & \mathbf{0} \\ \mathbf{0} & \Delta_{i,0} \end{bmatrix}}_{\triangleq \Sigma_{i,0}} \begin{bmatrix} \underline{\mathbf{v}}_{in}[i] \\ \underline{\mathbf{i}}_{in}[i] \end{bmatrix} + \underbrace{\begin{bmatrix} \Lambda_{i,1} & \mathbf{0}_{P\times 2P} \\ \mathbf{0}_{P\times 2P} & \Delta_{i,1} \end{bmatrix}}_{\triangleq \Sigma_{i,1}} \begin{bmatrix} \overline{\mathbf{v}}_{IBI}[i-1] \\ \overline{\mathbf{i}}_{IBI}[i-1] \end{bmatrix}, \quad (2.58)$$

where $\mathbf{0}_{P\times 2P}$ *is* $P\times 2P$ *zero matrix,* $\overline{\mathbf{v}}_{IBI}[i-1]=[\underline{\mathbf{v}}_{in}[i-1]\ \underline{\mathbf{v}}_{out}[i-1]]^T$, $\overline{\mathbf{i}}_{IBI}[i-1]$ $=[\underline{\mathbf{i}}_{in}[i-1]\ \underline{\mathbf{i}}_{out}[i-1]]^T$ *and we have*

$$\Lambda_{i,0} = (\mathbf{I}-1/z_0^{(L)}\mathbf{B}_{i,0})^{-1}\mathbf{A}_{i,0} \tag{2.59}$$

$$\Delta_{i,0} = (z_0^{(L)}\mathbf{I}-\mathbf{D}_{i,0})^{-1}\mathbf{C}_{i,0} \tag{2.60}$$

$$\Lambda_{i,1} = [(\mathbf{I}-1/z_0^{(L)}\mathbf{B}_{i,0})^{-1}\mathbf{A}_{i,1}\ \ 1/z_0^{(L)}(\mathbf{I}-1/z_0^{(L)}\mathbf{B}_{i,0})^{-1}\mathbf{B}_{i,1}] \tag{2.61}$$

$$\Delta_{i,1} = [(z_0^{(L)}\mathbf{I}-\mathbf{D}_{i,0})^{-1}\mathbf{C}_{i,1}\ \ (z_0^{(L)}\mathbf{I}-\mathbf{D}_{i,0})^{-1}\mathbf{D}_{i,1}], \tag{2.62}$$

where $\mathbf{I}$ *is the* $P\times P$ *identity matrix.*

Proof: Refer to Appendix 2.E.

Corollary 3 *Under the assumption of input blocks with the last* L *trailing zeros, the I/O relationship between* $\underline{\mathbf{v}}_{out}[i]$ *and* $\underline{\mathbf{v}}_s[i]$ *becomes (cf. see (2.58).)*

$$\begin{bmatrix}\underline{\mathbf{v}}_{out}[i]\\ \underline{\mathbf{i}}_{out}[i]\end{bmatrix} = \underbrace{\begin{bmatrix}\Lambda_{i,0} & \mathbf{0}\\ \mathbf{0} & \Delta_{i,0}\end{bmatrix}}_{\triangleq\Sigma_{i,0}}\begin{bmatrix}\underline{\mathbf{v}}_{in}[i]\\ \underline{\mathbf{i}}_{in}[i]\end{bmatrix} \tag{2.63}$$

$$= \begin{bmatrix}(\mathbf{I}-1/z_0^{(L)}\mathbf{B}_{i,0})^{-1}\mathbf{A}_{i,0} & -z_0^{(s)}(\mathbf{I}-1/z_0^{(L)}\mathbf{B}_{i,0})^{-1}\mathbf{A}_{i,0}\\ \mathbf{0} & (z_0^{(L)}\mathbf{I}-\mathbf{D}_{i,0})^{-1}\mathbf{C}_{i,0}\end{bmatrix}\begin{bmatrix}\underline{\mathbf{v}}_s[i]\\ \underline{\mathbf{i}}_{in}[i]\end{bmatrix}, \tag{2.64}$$

where we can easily relate $\underline{\mathbf{v}}_{in}[i]$ *to* $\underline{\mathbf{v}}_s[i]$ *using*

$$\begin{bmatrix}\underline{\mathbf{v}}_{in}[i]\\ \underline{\mathbf{i}}_{in}[i]\end{bmatrix} = \begin{bmatrix}\mathbf{I} & -z_0^{(s)}\mathbf{I}\\ \mathbf{0} & \mathbf{I}\end{bmatrix}\begin{bmatrix}\underline{\mathbf{v}}_s[i]\\ \underline{\mathbf{i}}_{in}[i]\end{bmatrix}. \tag{2.65}$$

Proof: Forcing the last L symbols in input blocks to zero makes the IBI term disappear and then (2.58) reduces to (2.63). In addition, plugging (2.65) into (2.63) leads to (2.64). (Q.E.D)

By including all parameters in (2.45)-(2.48), we can arrive at a third way to find the I/O relationship in the following corollary.

Corollary 4 *Assume that the system memory is finite with $L < P$, then we can construct the overall I/O relationship as follows:*

$$\underbrace{\begin{bmatrix} \mathbf{A}_{i,0} & \mathbf{0} & \mathbf{B}_{i,0} & -\mathbf{I} \\ \mathbf{0} & \mathbf{C}_{i,0} & \mathbf{D}_{i,0} & -\mathbf{I} \\ \mathbf{I} & z_0^{(s)}\mathbf{I} & \mathbf{0} & \mathbf{0} \\ \mathbf{0} & \mathbf{0} & -z_0^{(L)}\mathbf{I} & \mathbf{I} \end{bmatrix}}_{\triangleq\overline{\Psi}_{i,0}} \underbrace{\begin{bmatrix} \underline{\mathbf{v}}_{in}[i] \\ \underline{\mathbf{i}}_{in}[i] \\ \underline{\mathbf{i}}_{out}[i] \\ \underline{\mathbf{v}}_{out}[i] \end{bmatrix}}_{\triangleq\overline{\mathbf{Y}}[i]}$$

$$= \underbrace{\begin{bmatrix} \mathbf{0} \\ \mathbf{0} \\ \underline{\mathbf{v}}_s[i] \\ \mathbf{0} \end{bmatrix}}_{\triangleq\overline{\mathbf{X}}[i]} + \underbrace{\begin{bmatrix} -\mathbf{A}_{i,1} & \mathbf{0} & -\mathbf{B}_{i,1} & \mathbf{0} \\ \mathbf{0} & -\mathbf{C}_{i,1} & -\mathbf{D}_{i,1} & \mathbf{0} \\ \mathbf{0} & \mathbf{0} & \mathbf{0} & \mathbf{0} \\ \mathbf{0} & \mathbf{0} & \mathbf{0} & \mathbf{0} \end{bmatrix} \begin{bmatrix} \underline{\mathbf{v}}_{in}[i-1] \\ \underline{\mathbf{i}}_{in}[i-1] \\ \underline{\mathbf{i}}_{out}[i-1] \\ \underline{\mathbf{v}}_{out}[i-1] \end{bmatrix}}_{\triangleq\overline{\mathbf{Y}}[i-1](i.e.IBI)} \tag{2.66}$$

where $\Psi_{i,0}$ is non-singular.

Proof: Using (2.45) through (2.48), we can build $\overline{\Psi}_{i,0}$ explicitly. (Q.E.D)

2.4.2 Cascaded System

Let us consider (2.58) in the presence of IBI. In that case the chain rule, which is valid in the phasor domain, does not hold true any longer. However by forcing the last L input symbols to be zeros, the cumulative response of the cascade of multiple systems can be obtained recursively, exploiting the following theorem.

Theorem 3 *Under the input block assumption with the last L trailing zeros, we express the I/O relationship of the cascade of 2PN systems using the lifted form as follows:*

$$\begin{bmatrix} \underline{\mathbf{v}}_{out}[i] \\ \underline{\mathbf{i}}_{out}[i] \end{bmatrix} = \begin{bmatrix} \Lambda_{i,0}^{(1,\cdots,N)} & \mathbf{0} \\ \mathbf{0} & \Delta_{i,0}^{(1,\cdots,N)} \end{bmatrix} \begin{bmatrix} \underline{\mathbf{v}}_{in}[i] \\ \underline{\mathbf{i}}_{in}[i] \end{bmatrix} \tag{2.67}$$

$$= \begin{bmatrix} \Lambda_{i,0}^{(1,\cdots,N)} & -z_0^{(s)}\Lambda_{i,0}^{(1,\cdots,N)} \\ \mathbf{0} & \Delta_{i,0}^{(1,\cdots,N)} \end{bmatrix} \begin{bmatrix} \underline{\mathbf{v}}_{s}[i] \\ \underline{\mathbf{i}}_{in}[i] \end{bmatrix}, \tag{2.68}$$

where

$$\Lambda_{i,0}^{(1,\cdots,N)} = \prod_{p=N}^{1} \Lambda_{i,0}^{(p)} = \prod_{p=N}^{1} (\mathbf{I} - 1/z_0^{(L)}\mathbf{B}_{i,0}^{(p)})^{-1}\mathbf{A}_{i,0}^{(p)} \tag{2.69}$$

$$\Delta_{i,0}^{(1,\cdots,N)} = \prod_{p=N}^{1} \Delta_{i,0}^{(p)} = \prod_{p=N}^{1} (z_0^{(L)}\mathbf{I} - \mathbf{D}_{i,0}^{(p)})^{-1}\mathbf{C}_{i,0}^{(p)} \tag{2.70}$$

and $\Lambda_{i,0}^{(p)}$ *and* $\Delta_{i,0}^{(p)}$ *represent the p-th subsystem.*

Proof: For simplicity, consider the cascade of two subsystems. Then, the multiplication of those block matrices (keeping the order) is quite straight-forward and the proof is completed recursively. (Q.E.D)

When no IBI is present, the discrete-time case admits the chain rule analogue of the phasor domain and the I/O relationship in (2.67) is a practical and efficient representation of cascaded system.

2.5 Discrete-Time Representation of the Classical ABCD Parameters

Certain appliances exhibit an input impedance that varies smoothly with the amplitude of the AC mains voltage(e.g. coffee maker), while other appliances have a bistatic behavior, i.e. their impedance switches between two values (e.g. TVs, refrigerator, etc.). These appliances essentially alternate between two discrete states, and these changes occur with a period that is generally equal to half or to one quarter of the reciprocal of the AC mains frequency, i.e. $T_{AC} = 1/60(s)$. Depending on the appliances plugged into the network, the channel transfer function may vary continuously with time, or switch between two responses that remain static for a portion of the AC cycle period. Note that all appliances in the network switch synchronously with the mains (indeed, phase shifts).

Let us now consider the case of switched impedances. We can approximate the transition between the two responses as instantaneous and decompose the time-varying load impedance $Z(t, f)$ into the sum of two alternating contributions characterized by the locally time invariant base-band equivalent impedances $Z_1(f)$, $Z_2(f)$ as follows:

$$Z(t, f) \simeq \mathbf{S}_A(t)Z_1(f) + (1 - \mathbf{S}_A(t))Z_2(f), \tag{2.71}$$

where $\mathbf{S}_A(t)$ is indicator function for set $\mathbf{S}$,

$$\mathbf{S}_A(t) = \begin{cases} 1 & \text{if} \quad t \in A \\ 0 & \text{elsewhere} \end{cases} \tag{2.72}$$

where $A \triangleq \{t | t \in [2nT_s, (2n+1)T_s]\}$ and $T_s = KT_{AC}$ with $K = \frac{1}{2}$ or $\frac{1}{4}$ is a symbol duration transmitted.

Time-domain version of classical ABCD parameters are generalized as $a(t,\tau)$, $b(t,\tau)$, $c(t,\tau)$ and $d(t,\tau)$ in (2.35) and (2.36), which are the quantities evaluated by the inverse Fourier transform as follows:

$$a(t,\tau) = \mathcal{F}^{-1}\{A(t,f)\}, \tag{2.73}$$

where $A(t,f)$ is approximated as bistatic impedances in (2.71); similarly, we can find $b(t,\tau)$, $c(t,\tau)$ and $d(t,\tau)$. In Fig. 2.5, all these parameters are found from signal theory in a two-port network, see [28].

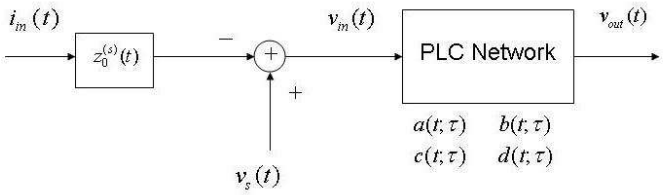

Figure 2.5: Time-domain equivalent representation of classical ABCD parameters in Fig. 2.4

Firstly, when a load is placed as a shunt impedance across hot-and-return and exhibits a linear time-invariant (LTI) impedance $Z(f)$, we consider a continuous time-domain impedance matrix which corresponds to the ABCD parameters in a function of frequency,

$$\Phi(f) = \begin{bmatrix} 1 & 0 \\ \frac{1}{Z(f)} & 1 \end{bmatrix} \leftrightarrow \begin{bmatrix} a_0(t) & b_0(t) \\ c_0(t) & d_0(t) \end{bmatrix} = \begin{bmatrix} \delta(t) & 0 \\ g_0(t) & \delta(t) \end{bmatrix} \tag{2.74}$$

where $g_0(t) = \mathcal{F}^{-1}\{Z^{-1}(f)\}$.

As in (2.74) above, we can find the discrete-time model parameters for linear time-invariant (LTI) lines, which generally interconnect time-varying loads,

$$c[k, k-n] \equiv c_0[k-n] = \int_{-\infty}^{+\infty} P(f)C(f)e^{j2\pi f(k-n)T}df$$

$$\mathbf{C}_{i,0} \equiv \mathbf{C}_0 \tag{2.75}$$

where $\{\mathbf{C}_0\}_{k,n} = c_0[k-n]$ and $\mathbf{C}_0$ does not depend on i.

Here we provide a simple network example to compare the response through lifted block model with that obtained by taking the inverse Fourier transform of the overall frequency domain response. The ABCD matrix for transmission line with the bridge tap length l_{br} is well known to be

$$\begin{bmatrix} A(f) & B(f) \\ C(f) & D(f) \end{bmatrix} = \begin{bmatrix} \cosh(\gamma_c l_{br}) & Z_c \sinh(\gamma_c l_{br}) \\ \frac{1}{Z_c}\sinh(\gamma_c l_{br}) & \cosh(\gamma_c l_{br}) \end{bmatrix}, \tag{2.76}$$

where Z_c and γ_c are the characteristic impedance and the propagation constant, respectively. With per-unit-length resistance(R), inductance(L), conductance(G) and capacitance(C), Z_c and γ_c can be expressed as

$$Z_c = \sqrt{\frac{R + j2\pi fL}{G + j2\pi fC}}, \qquad \gamma_c = \sqrt{(R + j2\pi fL)(G + j2\pi fC)}. \tag{2.77}$$

In fact, since the general ABCD parameters cannot be formed explicitly in terms of inverted time-domain responses, to check whether our model leads to the same response with classical Fourier transform we will consider a particular case of shunt impedance in Fig. 2.6 (a) with l_{br} sufficiently large such that $l_{br} \to \infty$ (which implies $\tanh(l_{br}) \approx 1$). Then we have $Z(f) = Z_c \frac{Z_{br} + Z_c \tanh(\gamma_c l_{br})}{Z_c + Z_{br} \tanh(\gamma_c l_{br})}$ which approaches Z_c.

Without loss of generality, assume that for any real numbers K_1 and K_1, characteristic impedance Z_c of an LTI shunt case in Fig. 2.6(a) can be expressed as

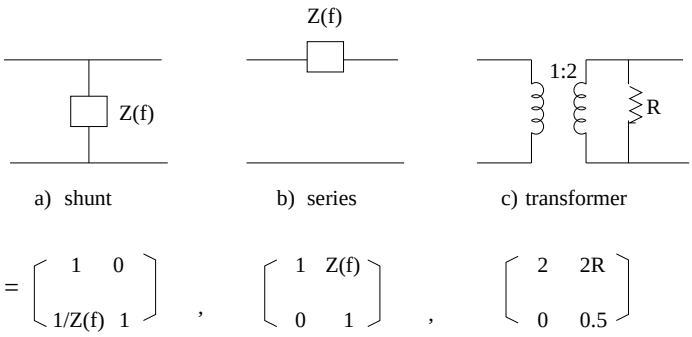

Figure 2.6: Various types of impedance configuration: (a) shunt, (b) series and (c) transformer

$Z_c = K_1 + j2\pi f K_2$. Then we have

$$\frac{1}{Z(f)} \approx \frac{1}{Z_c} = \frac{1}{K_1 + j2\pi f K_2}, \tag{2.78}$$

where K_1 and K_2 satisfy

$$K_1 + j2\pi f K_2 = \sqrt{\frac{R + j2\pi f L}{G + j2\pi f C}}, \tag{2.79}$$

or equivalently,

$$K_1^2 - (j2\pi f)^2 K_2^2 = \frac{RG + (j2\pi f)^2 LC}{G^2 + (j2\pi f)^2 C^2} \quad \text{and} \quad 2K_1 K_2 = \frac{GL - RC}{G^2 + (j2\pi f)^2 C^2}$$

then by (2.74) and (2.75) we obtain the discrete-time equivalent responses as follows:

$$\begin{bmatrix} a_0[k-n] & b_0[k-n] \\ c_0[k-n] & d_0[k-n] \end{bmatrix} = \begin{bmatrix} \delta[k-n] & 0 \\ \frac{1}{K_2} e^{-\frac{K_1}{K_2}(k-n)} U[k-n] & \delta[k-n] \end{bmatrix}, \tag{2.80}$$

where $U[k-n]$ is the discrete version of unit step function which takes value 1 for $k \geq n$ and 0 elsewhere.

In (2.80), $\frac{1}{K_1 + j2\pi f K_2}$ has a Fourier transform pair of $1/K_2 e^{-K_1/K_2 t} u(t)$ where $u(t)$ is a unit-step response. Now, we are able to construct the block matrices for $\mathbf{A}_0$, $\mathbf{B}_0$, $\mathbf{C}_0$ and $\mathbf{D}_0$ and find the output sequence $\underline{\mathbf{v}}_{out}[i]$ in terms of the input block

$\underline{\mathbf{v}}_{in}[i]$, see (2.13) or (2.17). Hence, we can compare it with the response which is obtained by taking convolutions in a symbol-by-symbol manner using (2.80).

Secondly, for linear time-varying (LTV) load impedances, the continuous-time model parameters are found according to various specific configurations as follows, see Fig. 2.6,

(a) Shunt:

$$a(t,\tau) = d(t,\tau) = \delta(t-\tau), \quad b(t,\tau) = 0 \tag{2.81}$$

$$c(t,\tau) = \mathbf{S}_A(kT)\mathcal{F}^{-1}\{Z_1^{-1}(f)\} + (1-\mathbf{S}_A(kT))\mathcal{F}^{-1}\{Z_2^{-1}(f)\} \tag{2.82}$$

(b) Series:

$$a(t,\tau) = d(t,\tau) = \delta(t-\tau), \quad c(t,\tau) = 0 \tag{2.83}$$

$$b(t,\tau) = \mathbf{S}_A(kT)\mathcal{F}^{-1}\{Z_1(f)\} + (1-\mathbf{S}_A(kT))\mathcal{F}^{-1}\{Z_2(f)\} \tag{2.84}$$

(c) Transformer:

$$\frac{a(t,\tau)}{2} = \frac{b(t,\tau)}{2R} = \frac{d(t,\tau)}{0.5} = \delta(t-\tau), \quad c(t,\tau) = 0. \tag{2.85}$$

Now, we investigate the discrete-time model parameters corresponding to $a(t,\tau)$, $b(t,\tau)$, $c(t,\tau)$, and $d(t,\tau)$ in three cases above. For a specific time-varying impulse response $a(t,\tau)$, we can define a time-varying frequency response which consists of bistatic impedances, denoted as $A_1(f)$ and $A_2(f)$, as in (2.71),

$$A(t,f) = \int_{-\infty}^{\infty} a(t,\tau)e^{-j2\pi f\tau}d\tau \tag{2.86}$$

$$\simeq \mathbf{S}_A(t)A_1(f) + (1-\mathbf{S}_A(t))A_2(f). \tag{2.87}$$

Then, we have

$$a(t,\tau) = \mathbf{S}_A(t)\mathcal{F}^{-1}[A_1(f)] + (1-\mathbf{S}_A(t))\mathcal{F}^{-1}[A_2(f)] \tag{2.88}$$

$$\simeq \mathbf{S}_A(t)\underbrace{\int_{-\infty}^{\infty} A_1(f)e^{j2\pi f\tau}df}_{\triangleq a_1(\tau)} + (1-\mathbf{S}_A(t))\underbrace{\int_{-\infty}^{\infty} A_2(f)e^{j2\pi f\tau}df}_{\triangleq a_2(\tau)} \tag{2.89}$$

For simplicity, we look into the time instance kT_s for $A_1(f)$ or $a_1(\tau)$, i.e., for $\mathbf{S}_A(kT_s) = 1$ such that we can regard it as the linear time-invariant model. In a similar way, we find $b(t,\tau)$, $c(t,\tau)$ and $d(t,\tau)$.

In particular, using a pulse shape filter $p(t)$ for the discrete-time sampling, we get the following lemma.

Lemma 3 *For a time-varying shunt load with the impedance $Z(t,f)$ in (2.71), we have*

$$a[k,k-n] = d[k,k-n] = \delta[k-n], \quad b[k,k-n] = 0 \tag{2.90}$$

$$c[k,k-n] \simeq \mathbf{S}_A(kT_s)\cdot\int_{-\infty}^{+\infty}\frac{P(f)}{Z_1(f)}e^{j2\pi f(k-n)T}df+(1-\mathbf{S}_A(kT_s))\cdot\int_{-\infty}^{+\infty}\frac{P(f)}{Z_2(f)}e^{j2\pi f(k-n)T}df$$
$$+(1-\mathbf{S}_A(kT_s))\cdot\int_{-\infty}^{+\infty}\frac{P(f)}{Z_2(f)}e^{j2\pi f(k-n)T}df \tag{2.91}$$

where $P(f) = \int_{-\infty}^{+\infty} p(t)e^{-j2\pi ft}df$ is the Fourier transform of a pulse shaping filter $p(t)$ in (2.5).

Proof: Refer to Appendix 2.F.

2.6 Average Channel Capacity over Power Lines

In typical transmission lines, since the channel variations are very regular and could be potentially predicted, it is reasonable to evaluate the capacity bound that corresponds to full channel knowledge at the transmitter side. The FCC imposes a constraint on the power spectrum. For k-th block transmission, let $\mathbf{R}_{\underline{\mathbf{v}}_s}[k]$ and $\mathbf{R}_{\underline{\mathbf{n}}}[k]$ be the input symbol covariance matrix and the noise covariance matrix, respectively. Also let $\mathbf{R}_{\underline{\mathbf{v}}_s}[k] = U[k]\Phi[k]U^H[k]$ be the eigenvalue decomposition,

where $\{U[k]\}_{i,l} = \delta[i-l]u_{ii}(k)$. Then, the maximum information rate for the k-th block is

$$I(\underline{\mathbf{v}}_{out}[k]; \underline{\mathbf{v}}_s[k]) = \frac{1}{P}\sum_{i=1}^{\overline{P}} \log(1 + \lambda_{ii}(k)\phi_{ii}(k)), \tag{2.92}$$

where $\overline{P} : 1 \leq \overline{P} \leq P$ is the number of non-zero eigenvalues of $\mathbf{R}_{\underline{\mathbf{v}}_s}[k]$, $\{\Phi[k]\}_{i,l} = \delta[i-l]\phi_{ii}(k)$ and for the overall I/O transmission matrix $\mathbf{H}_{k,0}$ defined in Corollary 2, $\lambda_{ii}(k)$s are eigenvalues of $\mathbf{H}_{k,0}^H \mathbf{R}_{\underline{\mathbf{n}}}^{-1}[k]\mathbf{H}_{k,0}$. For i-th symbol of k-th block the eigenvalues $\phi_{ii}(k)$ meet the FCC constraints.

In general, the m-th Fourier basis vector e_m ($m = 1, \cdots, P$) can be defined as e_m=[1 $e^{-j2\pi\frac{m-1}{P}}$ $\cdots$ $e^{-j2\pi\frac{(P-1)(m-1)}{P}}$ $]^T$. Then, the energy of the signal over a certain frequency can be evaluated by the following quadratic form:

$$e_m^H \mathbf{R}_{\underline{\mathbf{v}}_s}[k] e_m \leq FCC_m, \tag{2.93}$$

where FCC_m is a power constraint for m-th symbol. From the eigenvalue decomposition of $\mathbf{R}_{\underline{\mathbf{v}}_s}[k]$, for k-th transmission block (2.93) implies that

$$\sum_{i=1}^{P} \phi_{ii}(k) \left(\underbrace{e_m^H u_{ii}(k) u_{ii}^H(k) e_m}_{\triangleq v_{i,m}[k]} \right) \leq FCC_m, \tag{2.94}$$

where for fixed k the magnitude of $v_{i,m}[k]$ is bounded by unity. This system of inequalities has all nonnegative coefficients and $FCC_m \geq 0$. Hence, a nonnegative solution of the system with equality exists and it provides the optimum power.

Let us assume that the noise is stationary and white, so that $\mathbf{R}_{\underline{\mathbf{n}}}[k] = N_0\mathbf{I}$. Since the channel switches at every half cycle of the 60Hz, we set the block duration to be equal to half a cycle, i.e. $PT_s = 1/120sec$. In the large part of each block duration, the channel is stationary and therefore we can obtain the power line channel capacity by averaging maximum information rates in each of the two states. For a linear time invariant channel channel, if the number of orthogonal dimensions

available is high, i.e., if

$$P \approx (f_{\max} - f_{\min})/120 \gg 1,$$

thanks to Szego's theorem [27] it is well known that one can approximate the eigenfunctions of the channel as complex exponentials $exp(j2\pi f_i t)$, where $f_{i+1} - f_i = (PT_s)^{-1}$, $f_1 = f_{\min}$ and $f_P = f_{\min} + \frac{P-1}{PT_s}$. If we define $H^{(j)}(f_i)$ as an extensive form of $H(f)$ in (2.29) where $i = 1, \cdots, P$ and $j = 1, 2$ are symbol and bistate index, respectively, then the k-th eigenvalue $\lambda_{ii}(k)$ is determined by one of two values $\frac{|H^{(j)}(f_i)|^2}{No}$ for $j = 1, 2$.

In addition, when the FCC constraints become directly the tight constraints on $\phi_{ii}(k) \leq FCC_i$, by averaging the bistatic channels we obtain the average capacity C_{PLC} of power lines as follows,

$$C_{PLC} = \frac{0.5}{PT_s} \sum_{j=1}^{2} \sum_{i=1}^{P} \log \left(1 + \frac{|H^{(j)}(f_i)|^2}{No} FCC_i \right). \tag{2.95}$$

One can compute C_{PLC} for two schemes; one is the bistatic capacity with water-filling power-loading [11] and the other is that with uniform power bit-loading (as commercial modems do now).

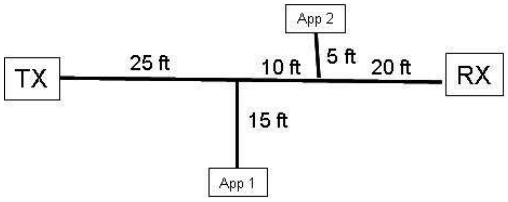

(a)

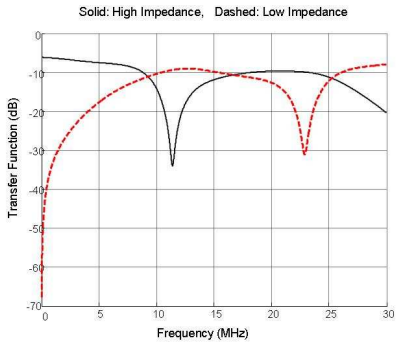

(b)

Figure 2.7: (a) Schematic diagram of a simple model; and (b) its corresponding transfer functions

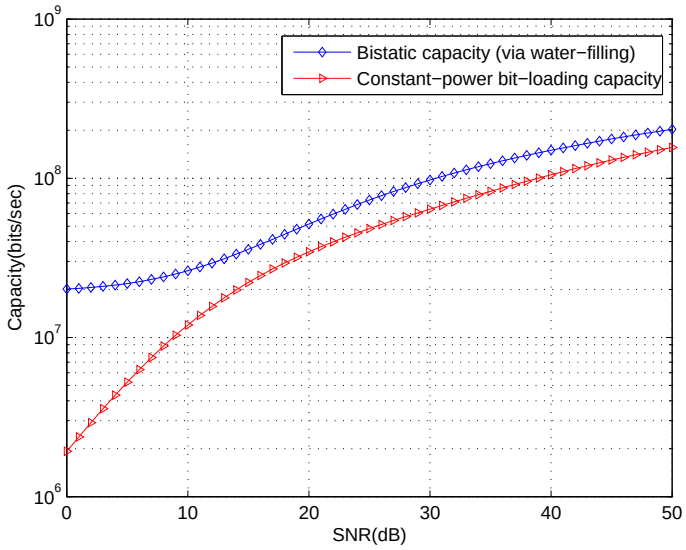

Figure 2.8: Bistatic channel capacity and uniform power-loading capacity over various SNRs (dB)

2.7 Numerical Results

Fig. 2.7 illustrates a simple model with two appliances, where each of them has time-varying characteristic of either high impedance for half AC cycle and low impedance for the other half. High impedance corresponds to a scenario in which both appliances switch on, and low impedance corresponds to that in which both switch off. In Fig. 2.7 we observe two deep fades around 11.5 MHz and 23 MHz, which explain the scenario when both appliances are in destructive impedance matching in phases. The actual values of the transfer functions are calculated using the PLC model given in [13]. We have found the achievable capacity in the band 2-30 MHz for bistatic channels in (2.95), and the bistatic waterfilling capacity is compared with uniform power bit-loading capacity as seen in Fig. 2.8. As shown in the figure, the capacity of adaptive power-loading scheme we propose is larger than that of uniform power bit-loading scheme for all SNR values.

2.8 Summary

In this chapter, we have proposed a discrete-time equivalent model for the time-varying response of the power line channel. The time-varying block transmission model provides a practical simulation and analysis tool for realistic PLCs since it takes into account the time-varying characteristics of the channel. Moreover, the proposed model can also be applied to DC PLC networks, i.e. to the case of in-vehicle PLCs. In this case, load variations are not periodic and may be more complex than bistatic. Nevertheless, the I/O relationship we have found for AC networks still holds.

APPENDIX 2.A

PROOF OF LEMMA 1

Matrix $\mathbf{H}_{i,i-1}$ will have non zero elements if and only if we have $0 \leq (i-j)P + k - n \leq L$. Let us look at three notable cases.

(a) $i - j = 0$: $\mathbf{H}_{i,0}$ will have non zero elements iff $0 \leq k - n \leq L$. Since $0 \leq k, n \leq P-1$, we have that $-(P-1) \leq k - n \leq P-1$. Therefore, there are always k, n values for which $0 \leq k - n \leq L \leq P-1$ and we conclude that $\mathbf{H}_{i,0}$ is always a non-zero matrix.

(b) $i - j = 1$: $\mathbf{H}_{i,1}$ will have non zero elements iff $0 \leq P + k - n \leq L$. Since we have that $1 \leq P + k - n \leq 2P - 1$, there are always k, n values that satisfy the non-zero condition for $\mathbf{H}_{i,1}$.

(c) $|i - j| > 1$: In this case, $\mathbf{H}_{i,i-j}$ will have non zero elements iff $0 \leq (i - j)P + k - n \leq L$. It is easy to verify that there are no k, n values that satisfy $0 \leq (i-j)P+k-n \leq L$ and also the constraint $(i-j-1)P+1 \leq (i-j)P+k-n \leq (i-j+1)P-1$ so that $\mathbf{H}_{i,i-j}$ is always zero for every $|i-j| \geq 2$. (Q.E.D)

APPENDIX 2.B

PROOF OF THEOREM 1

Let us consider the cascade of N systems as in Fig. 2.9.

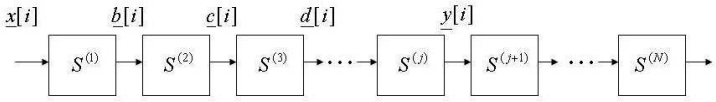

Figure 2.9: Block diagram for the cascade of N systems

If the memory of system $S^{(1)}$ is finite and equal to $L_1 < P$, we can express $\underline{\mathbf{b}}[i]$ exploiting *Lemma 1*

$$\underline{\mathbf{b}}[i] = \mathbf{H}_{i,0}^{(1)}\underline{\mathbf{x}}[i] + \mathbf{H}_{i,1}^{(1)}\underline{\mathbf{x}}[i-1]. \tag{2.96}$$

Similarly if the memory of $S^{(2)}$ is finite and equal to $L_2 < P$, we can also write

$$\underline{\mathbf{c}}[i] = \mathbf{H}_{i,0}^{(2)}\underline{\mathbf{b}}[i] + \mathbf{H}_{i,1}^{(2)}\underline{\mathbf{b}}[i-1]. \tag{2.97}$$

Substituting (2.97) in (2.96) we then obtain

$$\underline{\mathbf{c}}[i] = \mathbf{H}_{i,0}^{(2)}\mathbf{H}_{i,0}^{(1)}\underline{\mathbf{x}}[i] + \left(\mathbf{H}_{i,0}^{(2)}\mathbf{H}_{i,1}^{(1)} + \mathbf{H}_{i,1}^{(2)}\mathbf{H}_{i-1,0}^{(1)}\right)\underline{\mathbf{x}}[i-1] + \mathbf{H}_{i,1}^{(2)}\mathbf{H}_{i-1,1}^{(1)}\underline{\mathbf{x}}[i-2]. \tag{2.98}$$

The last term in (2.98) is the product of two upper triangular matrices of the kind shown in Fig. 2.3. It is easy to recognize that, if $L_1 + L_2 \leq P$, the product of two upper triangular matrices is always zero. We can then rewrite (2.98) as

$$\underline{\mathbf{c}}[i] = \underbrace{\mathbf{H}_{i,0}^{(2)}\mathbf{H}_{i,0}^{(1)}}_{\triangleq \mathbf{H}_{i,0}^{(1,2)}}\underline{\mathbf{x}}[i] + \underbrace{\left(\mathbf{H}_{i,0}^{(2)}\mathbf{H}_{i,1}^{(1)} + \mathbf{H}_{i,1}^{(2)}\mathbf{H}_{i-1,0}^{(1)}\right)}_{\triangleq \mathbf{H}_{i,1}^{(1,2)}}\underline{\mathbf{x}}[i-1]. \tag{2.99}$$

Now, exploiting the properties of the mixed products of the lower-banded and upper-triangular matrices reported in (2.19)-(2.22), we can state that

$$\mathbf{H}_{i,0}^{(1,2)} \Rightarrow \text{Banded matrix of order } L_1 + L_2 \leq P \tag{2.100}$$

$$\mathbf{H}_{i,0}^{(2)}\mathbf{H}_{i,1}^{(1)} \Rightarrow \text{V-trapezoidal matrix } (L_2 + L_1, L_1, L_2 + 1) \tag{2.101}$$

$$\mathbf{H}_{i,0}^{(2)}\mathbf{H}_{i-1,0}^{(1)} \Rightarrow \text{H-trapezoidal matrix } (L_1 + L_2, L_2, L_1 + 1) \tag{2.102}$$

$$\mathbf{H}_{i,1}^{(1,2)} \Rightarrow \text{Upper triangular matrix of order } L_1 + L_2 \leq P. \tag{2.103}$$

If we add a third system $S^{(3)}$ in cascade to system $S^{(2)}$, it is straightforward to obtain

$$\underline{\mathbf{d}}[i] = \mathbf{H}_{i,0}^{(3)}\mathbf{H}_{i,0}^{(1,2)}\underline{\mathbf{x}}[i] + \left(\mathbf{H}_{i,0}^{(3)}\mathbf{H}_{i,1}^{(1,2)} + \mathbf{H}_{i,1}^{(3)}\mathbf{H}_{i-1,0}^{(1,2)}\right)\underline{\mathbf{x}}[i-1] + \mathbf{H}_{i,1}^{(3)}\mathbf{H}_{i-1,1}^{(1,2)}\underline{\mathbf{x}}[i-2]. \tag{2.104}$$

Again, exploiting the properties listed in (2.19)-(2.22), we have

$$\mathbf{H}_{i,0}^{(1,2,3)} = \mathbf{H}_{i,0}^{(3)}\mathbf{H}_{i,0}^{(1,2)} \Rightarrow \text{Banded matrix of order } L_1 + L_2 + L_3 \leq P$$

$$\mathbf{H}_{i,1}^{(1,2,3)} = \mathbf{H}_{i,0}^{(3)}\mathbf{H}_{i,1}^{(1,2)} + \mathbf{H}_{i,1}^{(3)}\mathbf{H}_{i-1,0}^{(1,2)} \Rightarrow \text{Upper triangular of order } L_1 + L_2 + L_3 \leq P$$

$$\mathbf{H}_{i,1}^{(3)}\mathbf{H}_{i-1,1}^{(1,2)} = 0 \quad \text{iff } L_3 + L_{1,2} = L_1 + L_2 + L_3 \leq P.$$

It is easy to verify that at every level of recursion, we obtain that the output of the cascade $\underline{\mathbf{y}}[i]$ can be always expressed as a function of the last 3 input vectors $\underline{\mathbf{x}}[i]$, $\underline{\mathbf{x}}[i-1]$, $\underline{\mathbf{x}}[i-2]$ which are multiplied by $\mathbf{H}_{i,0}^{(1,\cdots,j)}$ (lower banded matrix of order $\sum_{k=1}^{j} L_k \leq P$), matrix $\mathbf{H}_{i,1}^{(1,\cdots,j)}$ (upper triangular matrix of order $\sum_{k=1}^{j} L_k \leq P$), and matrix $\mathbf{H}_{i,1}^{(j)}\mathbf{H}_{i-1,1}^{(1,\cdots,j-1)}$ (identically zero for any i, j, L_i), respectively. (Q.E.D)

APPENDIX 2.C

PROOF OF LEMMA 2

If the overall system be finite memory $L < P$, by rewriting (2.43) and (2.44) with respect to $\underline{\mathbf{i}}_{in}[i]$ and $\underline{\mathbf{i}}_{out}[i]$ and plugging into (2.41) and (2.42), we obtain as follows:

$$(\mathbf{I} - 1/z_0^{(L)}\mathbf{B}_{i,0})\underline{\mathbf{v}}_{out}[i] = \mathbf{A}_{i,0}\underline{\mathbf{v}}_{in}[i] + \mathbf{A}_{i,1}\underline{\mathbf{v}}_{in}[i-1] + 1/z_0^{(L)}\mathbf{B}_{i,1}\underline{\mathbf{v}}_{out}[i-1] \quad (2.105)$$

$$\begin{aligned}(\mathbf{I} - 1/z_0^{(L)}\mathbf{D}_{i,0})\underline{\mathbf{v}}_{out}[i] &= 1/z_0^{(s)}\mathbf{C}_{i,0}(\underline{\mathbf{v}}_s[i] - \underline{\mathbf{v}}_{in}[i]) \quad (2.106)\\ &\quad +1/z_0^{(s)}\mathbf{C}_{i,1}(\underline{\mathbf{v}}_s[i-1] - \underline{\mathbf{v}}_{in}[i-1]) + 1/z_0^{(L)}\mathbf{D}_{i,1}\underline{\mathbf{v}}_{out}[i-1],\end{aligned}$$

where since $\mathbf{B}_{i,0}$ and $\mathbf{D}_{i,0}$ are lower-banded Toeplitz matrices, both $\mathbf{I} - 1/z_0^{(L)}\mathbf{B}_{i,0}$ and $\mathbf{I} - 1/z_0^{(L)}\mathbf{D}_{i,0}$ are invertible, which can be verified numerically.

Since $\mathbf{A}_{i,0}$ and $\mathbf{C}_{i,0}$ are also lower-banded Toeplitz matrices, then both are invertible. Multiplying $\mathbf{A}_{i,0}^{-1}$ and $z_0^{(s)}\mathbf{C}_{i,0}^{-1}$ on both sides of (2.105) and (2.106), respectively, and rearranging them in terms of $\underline{\mathbf{v}}_{in}[i]$, we obtain as follows:

$$\underline{\mathbf{v}}_{in}[i] = \mathbf{A}_{i,0}^{-1}\left[(\mathbf{I} - 1/z_0^{(L)}\mathbf{B}_{i,0})\underline{\mathbf{v}}_{out}[i] - 1/z_0^{(L)}\mathbf{B}_{i,1}\underline{\mathbf{v}}_{out}[i-1] - \mathbf{A}_{i,1}\underline{\mathbf{v}}_{in}[i-1]\right] \quad (2.107)$$

$$\begin{aligned}\underline{\mathbf{v}}_{in}[i] &= z_0^{(s)}\mathbf{C}_{i,0}^{-1}\left[(1/z_0^{(L)}\mathbf{D}_{i,0} - \mathbf{I})\underline{\mathbf{v}}_{out}[i] + 1/z_0^{(L)}\mathbf{D}_{i,1}\underline{\mathbf{v}}_{out}[i-1]\right. \quad (2.108)\\ &\quad \left. +1/z_0^{(s)}\mathbf{C}_{i,0}\underline{\mathbf{v}}_s[i] + 1/z_0^{(s)}\mathbf{C}_{i,1}(\underline{\mathbf{v}}_s[i-1] - \underline{\mathbf{v}}_{in}[i-1])\right].\end{aligned}$$

Equating (2.107) to (2.108) and expressing in terms of $\underline{\mathbf{v}}_{out}[i]$, $\underline{\mathbf{v}}_{out}[i-1]$, $\underline{\mathbf{v}}_s[i]$, $\underline{\mathbf{v}}_s[i-1]$ and $\underline{\mathbf{v}}_{in}[i-1]$, we finally obtain the thesis. (Q.E.D)

APPENDIX 2.D

PROOF OF COROLLARY 2

The input blocks with trailing zeros have the ability of forcing to zero the IBI terms with upper triangular matrices. Therefore, in (2.41) and (2.42) are simply reduced as follows:

$$\underline{\mathbf{v}}_{out}[i] = \mathbf{A}_{i,0}\underline{\mathbf{v}}_{in}[i] + \mathbf{B}_{i,0}\underline{\mathbf{i}}_{out}[i] \tag{2.109}$$

$$\underline{\mathbf{v}}_{out}[i] = \mathbf{C}_{i,0}\underline{\mathbf{i}}_{in}[i] + \mathbf{D}_{i,0}\underline{\mathbf{i}}_{out}[i]. \tag{2.110}$$

By substituting $\underline{\mathbf{i}}_{out}[i] = 1/z_0^{(L)}\underline{\mathbf{v}}_{out}[i]$ into both (2.109) and (2.110) and plugging $\underline{\mathbf{i}}_{in}[i] = 1/z_0^{(s)}(\underline{\mathbf{v}}_s[i] - \underline{\mathbf{v}}_{in}[i])$ into (2.110), we have two intermediate representations.

$$\underline{\mathbf{v}}_{out}[i] = \mathbf{A}_{i,0}\underline{\mathbf{v}}_{in}[i] + 1/z_0^{(L)}\mathbf{B}_{i,0}\underline{\mathbf{v}}_{out}[i] \tag{2.111}$$

$$\underline{\mathbf{v}}_{out}[i] = 1/z_0^{(s)}\mathbf{C}_{i,0}(\underline{\mathbf{v}}_s[i] - \underline{\mathbf{v}}_{in}[i]) + 1/z_0^{(L)}\mathbf{D}_{i,0}\underline{\mathbf{v}}_{out}[i]. \tag{2.112}$$

Then, by rearranging (2.111) and (2.112) with respect to $\underline{\mathbf{v}}_{in}[i]$ and forcing both to be equal, we reach the final relationship given. (Q.E.D)

APPENDIX 2.E

PROOF OF THEOREM 2

Using (2.44), we can modify (2.41) and (2.42) as follows:

$$\underline{\mathbf{v}}_{out}[i] = \mathbf{A}_{i,0}\underline{\mathbf{v}}_{in}[i] + \mathbf{A}_{i,1}\underline{\mathbf{v}}_{in}[i-1] + \mathbf{B}_{i,0}1/z_0^{(L)}\underline{\mathbf{v}}_{out}[i] + \mathbf{B}_{i,1}1/z_0^{(L)}\underline{\mathbf{v}}_{out}[i-1] \tag{2.113}$$

$$z_0^{(L)}\underline{\mathbf{i}}_{out}[i] = \mathbf{C}_{i,0}\underline{\mathbf{i}}_{in}[i] + \mathbf{C}_{i,1}\underline{\mathbf{i}}_{in}[i-1] + \mathbf{D}_{i,0}\underline{\mathbf{i}}_{out}[i] + \mathbf{D}_{i,1}\underline{\mathbf{i}}_{out}[i-1]. \tag{2.114}$$

Grouping both equations with respect to the present voltage and current blocks as well as the previous voltage and current blocks, we can get to the relationship given. (Q.E.D)

APPENDIX 2.F

PROOF OF LEMMA 3

From (2.71), we reach as follows:

$$\frac{1}{Z(t,f)} \simeq \mathbf{S}_A(t)\frac{1}{Z_1(f)} + (1-\mathbf{S}_A(t))\frac{1}{Z_2(f)} \tag{2.115}$$

$$\Rightarrow g(t,\tau) = \mathbf{S}_A(t)g_1(\tau) + (1-\mathbf{S}_A(t))g_2(\tau). \tag{2.116}$$

As a counterpart of (2.74), we have a time-varying ABCD parameters as follows:

$$\begin{bmatrix} a(t,\tau) & b(t,\tau) \\ c(t,\tau) & d(t,\tau) \end{bmatrix} = \begin{bmatrix} \delta(t-\tau) & 0 \\ g(t,\tau) & \delta(t-\tau) \end{bmatrix}. \tag{2.117}$$

It is easy to verify for $a[k,k-n]$, $b[k,k-n]$ and $d[k,k-n]$. As for $c[k,k-n]$, we use (2.7):

$$\begin{aligned} c[k,k-n] &= \int_{-\infty}^{+\infty} p(\tau - nT_s)g(kT_s,\tau)d\tau \\ &= \mathbf{S}_A(kT_s)\int_{-\infty}^{+\infty} p(\tau-nT_s)g_1(kT_s-\tau)d\tau + (1-\mathbf{S}_A(kT_s))\int_{-\infty}^{+\infty} p(\tau-nT_s)g_2(kT_s-\tau)d\tau \\ &= \mathbf{S}_A(kT_s)\int_{-\infty}^{+\infty} \frac{P(f)}{Z_1(f)}e^{j2\pi f(k-n)T_s}df + (1-\mathbf{S}_A(kT_s))\int_{-\infty}^{+\infty}\frac{P(f)}{Z_2(f)}e^{j2\pi f(k-n)T_s}df. \end{aligned} \tag{2.118}$$

(Q.E.D)

CHAPTER 3

WAVELET-BASED MDFB AND WEIGHTED OFDM OVER POWER LINES

3.1 Multirate Signal Processing for High-speed PLC

Broadband power line modems are based on conventional OFDM modulation, which has the ability to cope with severe inter-symbol interference (ISI) channels. Despite the simplicity and popularity of the standard OFDM technology, there are several disadvantages in the context of PLC-enhanced applications such as high degree of spectral leakage, necessity of adequate guard interval and poor resiliency to impulsive noise. Hence, as alternative multi-carrier modulations (MCM), the error performance of *Weighted OFDM* and/or *Wavelet-based Maximally Decimated Filter Bank* (MDFB) will be investigated in this chapter. In addition, we develop an innovative PLC network simulator which can model cascaded time-varying I/O systems as a single I/O system.

3.1.1 Motivation

The main advantage of the time-varying block channel model proposed in chapter 2, when compared to that in [57], is that it captures the effect of non-stationary channel response, while operating directly on the symbols in discrete-time. The time-varying block channel model makes block transmission very efficient to combat with inter-symbol interference (ISI) caused by frequency selective, dispersive channels. However, we also need to consider the inter-block interference (IBI) occurring during block transmission. Let P be the precoder block size. In this chap-

ter we address the problem of finding the maximum input block M so that IBI is avoided and the redundancy measured by $\frac{P-M}{P}$ is minimized. In numerous designs for block transmission based on precoding and equalization, zero paddings (Z/P) or cyclic prefix (C/P) are used to mitigate IBI, which involves certain amount of redundancy in the FIR filter bank.

Typically, conventional OFDM utilizing C/P has recently received widespread attention for wireline or wireless communication by virtue of its excellent properties in frequency selective fading channels. Also, in order to mitigate the inter-carrier interference occurring between the adjacent carrier waveforms, we study here *weighted OFDM* with weighting factors for each subcarrier. To demonstrate the effectiveness of weighted OFDM (non-maximally decimated), we introduce wavelet-based MDFB (maximally decimated) with minimum redundancy, in particular we investigate a wavelet-modulated technique with cosine-modulated band-pass pulse filters.

3.2 System Model

3.2.1 General Transmultiplexer Structure

We consider a time-varying block transmission model based on the multirate precoding and decoding shown in Fig. 3.1, (cf. see also [18]). The noise-free I/O relationship in such a time-varying channel was formulated in (2.6) as

$$r[n] = \sum_{l=-\infty}^{\infty} h[n,l]x[n-l] + w[n], \tag{3.1}$$

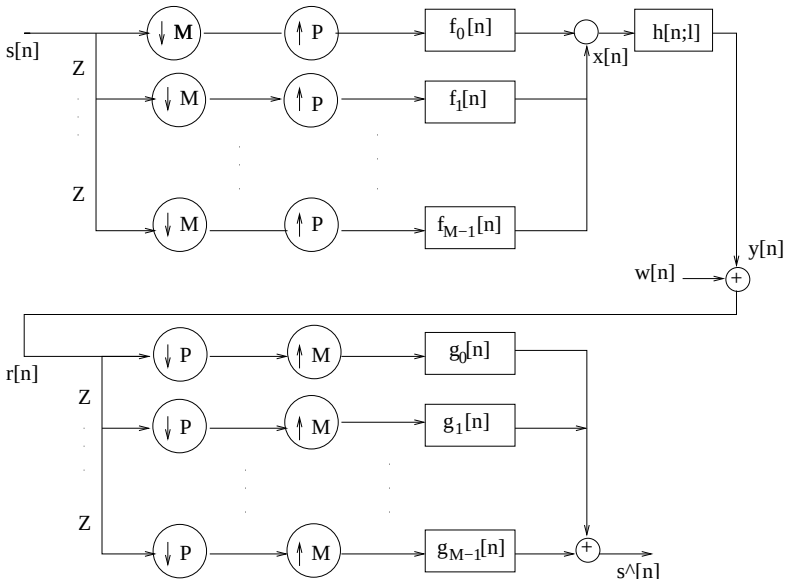

Figure 3.1: Transmultiplexer structure before post-detection

where $h[n,l]$ is a time-varying impulse response of the l-th tap at time n and $w[n]$ is assumed to be additive Gaussian noise. Suppose the multirate filterbank precoder shown in the upper part of Fig. 3.1 is used in the transmitter of our block transmission model. Such an precoder separates $s[n]$ into the M polyphase components, followed by upsampling by P and then passing through the filters with impulse response $f_m[n]$ of order L_f. Leaving $M>P$ (oversampled) for an unlikely useful case, we focus the case on $M\leq P$. A system with $M=P$ is referred to as *maximally decimated* and that with $M<P$ *non-maximally decimated*. From the precoder/decoder structures we see that the channel input $x[n]$ and the decoded output $\hat{s}[n]$ can be represented as

$$x[n] = \sum_{m=0}^{M-1} \sum_{i=-\infty}^{\infty} s[iM+m] f_m[n-iP] \tag{3.2}$$

$$\hat{s}[n] = \sum_{p=0}^{P-1} \sum_{j=-\infty}^{\infty} r[jP+p] g_p[n-jM], \tag{3.3}$$

where $f_m[n]$ and $g_p[n]$ are the impulse responses of transmit and receiver filters, respectively. Let us define the following vectors and matrices

$$\{\underline{\mathbf{s}}[i]\}_m = s[iM+m],\ \{\underline{\hat{\mathbf{s}}}[i]\}_m = \hat{s}[iM+m]$$

$$\{\underline{\mathbf{x}}[i]\}_k = x[iP+k],\ \{\underline{\mathbf{y}}[i]\}_k = y[iP+k]$$

$$\{\underline{\mathbf{r}}[i]\}_k = r[iP+k],\ \{\underline{\mathbf{w}}[i]\}_k = w[iP+k]$$

$$\{\mathbf{H}_{i,i-j}\}_{k,n} = h[iP+k,(i-j)P+k-n]$$

$$(m = 0,\cdots,M-1 \text{ and } n,k = 0,\cdots,P-1).$$

The k-th output of the i-th block, $y[iP+k]$, is expressed by

$$y[iP+k] = \sum_{j=-\infty}^{\infty}\sum_{n=0}^{P-1} h[iP+k,(i-j)P+k-n]x[jP+n]. \tag{3.4}$$

Thus a lifted form is (cf. see [58] and Chapter 2)

$$\underline{\mathbf{y}}[i] = \sum_{j=-\infty}^{\infty} \mathbf{H}_{i,i-j}\underline{\mathbf{x}}[j]. \tag{3.5}$$

Also, by Theorem 2.1 in Chapter 2, if the block size P is larger than the maximum memory L of the discrete-time equivalent system, then

$$\mathbf{H}_{i,i-j} \triangleq \mathbf{H}_{i,0}\delta[i-j] + \mathbf{H}_{i,1}\delta[i-j-1], \tag{3.6}$$

where $\mathbf{H}_{i,0}$, $\mathbf{H}_{i,1}$ were defined in (2.17) and Fig. 2.3.

3.3 Wavelet-based MDFB and Weighted OFDM

3.3.1 Wavelet-based MDFB

As a good candidate of the transmit filters, we introduce discrete wavelet multitone scheme (DWMT, [59]), which is known to be robust to noise impairments and receiver structure limitations.

Bandpass pulses used in DWMT are cosine-modulated wavelets with filter banks (M=P),

$$f_m[n] = 2p[n]\cos(\omega_l n + \phi_l) \tag{3.7}$$

$$g_p[n] = 2p[n]\cos(\omega_l n - \phi_l), \tag{3.8}$$

where the pulses $p[n]$ behaves like a low-pass prototype filter and the filter length is L_f=QM where Q is the overlap factor, [56]. For example, the DWMT scheme with Q=4 has a precoder that last for duration of four blocks, ω_l=$(l-\frac{1}{2})\frac{\pi}{M}$ and the phase ϕ_l=$(-1)^m\frac{\pi}{4}$, [55].

Requirement of such a system that there is no ISI within symbol stream is known as the *orthogonality condition* in [55]. In particular, if $f_m[n]$ is such that

$$\sum_{n=0}^{M-1} f_{m_1}[n]f^*_{m_2}[n-iM] = \gamma\delta[i]\delta[m_1-m_2], \tag{3.9}$$

where $\delta[k]$ is a Kronecker delta and $p[n]$ is a rectangular window for $0{\leq}n{\leq}M{-}1$, then the filters of impulse response $f_m[n]$ of order L_f construct a complete orthonormal set, scaled by γ. This type of cosine-modulated wavelet filter banks are designed to minimize stopband energy and optimize subchannel spectral components. The constraint required is that the set of $f_m[n]$ and their time shifts by integer multiples of M renders a set of orthonormal waveforms.

In fact, as a hybrid scheme from wavelet-based MDFB and weighted OFDM, *wavelet-OFDM* is known as a high frequency efficient data transmission technology, where each subcarrier centered around $\frac{m}{M}$ is orthogonalized by wavelet transform, allowing the smallest side lobes, [60].

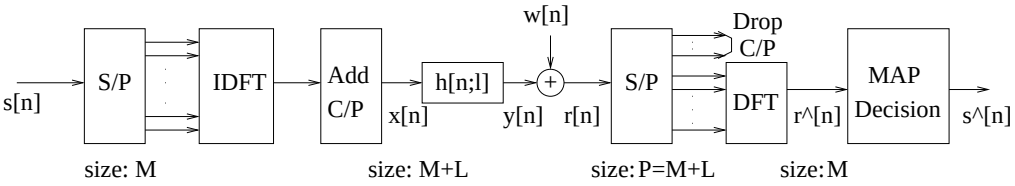

Figure 3.2: Multirate OFDM encoder and decoder equivalent to Fig. 3.1

3.3.2 Weighted OFDM

When $M < P$, the OFDM system with cyclic prefix (C/P) shown in Fig. 3.2 is an example of non-maximally decimated filter banks. The C/P operation takes the last L (the order of channel memory) elements of each block and appends them to the beginning of the i-th transmitted block. By inserting the redundant C/P into the precoder, we obtain the OFDM input vector $\underline{\mathbf{x}}_{OFDM} \triangleq [x[iM+M-L],\cdots,x[iM+M-1],x[iM],\cdots,x[iM+M-1]]$ of length $P{=}M{+}L$. For MDFB system we use

$$f_m[n] = \begin{cases} e^{j\frac{2\pi}{M}m(n-L)}, & n \in [0, \mathrm{M+L-1}] \\ 0 & \text{otherwise} \end{cases} \tag{3.10}$$

From typical OFDM system with N-point IFFT operations, we propose a weighted OFDM whereby

$$x[n] = \frac{1}{N}\sum_{m=0}^{N-1} s[m]\alpha_m e^{j\frac{2\pi}{N}mn}, \quad (n = 0,\cdots,N+L-1 \text{ and } N = M) \tag{3.11}$$

where α_m is chosen as either raised cosine (RC) or Gaussian weighting functions [54],

$$\text{Raised cosine} : \alpha_m = \begin{cases} Asin^2(\pi\frac{m}{N}), & 0 \le m \le N-1 \\ 0 & \text{otherwise} \end{cases} \tag{3.12}$$

$$\text{Gaussian} : \quad \alpha_m = \begin{cases} Ae^{-\frac{(m-N/2)^2}{2\sigma^2}}, & 0 \le m \le N-1 \\ 0 & \text{otherwise} \end{cases} \tag{3.13}$$

Table 3.1: Basic PHY parameters of Weighted OFDM and Wavelet-OFDM.

Communication method	Weighted OFDM	Wavelet OFDM
FFT/DWT points	3072, 6144	512, 1024
Sampling frequency (MHz)	75, 150	62.5, 125
Symbol length (μ s)	40.96	8.192
Guard interval (μ s)	5.56, 7.56, 47.12	Not necessary
Primary modulation (per subcarrier)	BPSK, QPSK, M-QAM	BPSK, M-PAM
Frequency band (MHz)	2-30	2-28
Error correction	Turbo convolutional coding	RS, RS-CC; LDPC (optional)
Maximum transmission speed (Mb/s)	548 (CTC)	544 (239/255 RS)
Diversity modes	Normal ROBO	MAC header, payload

where A is determined by the normalization constraint such that $\sum_{m=0}^{N-1} \alpha_m^2 = 1$. It turns out that such defined weighted OFDM reduces inter-carrier interference.

In the physical layer (PHY) perspective, basic parameters of Weighted OFDM and Wavelet-OFDM are shown in Table 3.1, and optimal values and schemes are chosen depending on the computational complexity and desired performance level.

3.3.3 Cyclostationary Noise

The test channel described in Section 2.7 incorporates cyclostationary noise with period of 60Hz [58], we analyze the characteristics of this cyclostationarity.

Suppose $s[n]$ is a zero-mean white stationary process. Then, we are interested in characterizing the noise-free output $y[n]$ (and its noisy output $r[n]$). Defining $R_{yy}(n;\tau) := E[y^*[n+\tau]y[n]]$, the time-varying correlation of $r[n]$ is found from (3.1)

$$R_{rr}(n;\tau) = \bar{E}_s \sum_{l_1=-\infty}^{\infty} \sum_{l_2=-\infty}^{\infty} h^*[n+\tau, n+\tau-l_1]h[n, n-l_2]$$

$$\cdot \sum_{m=0}^{M-1} \sum_{i=-\infty}^{\infty} f_m^*[l_1 - iP] f_m[l_2 - iP] + R_{ww}(n;\tau), \tag{3.14}$$

where $\bar{E}_s$:=$E[s^*[iM+m]s[iM+m]]$ (m=$0,\cdots,M-1$) and we reduce summations over m_1, m_2, i_1, i_2 to summations over m, i because of the orthogonality condition in (3.9). Setting $l = l_2$ and $\rho = l_1 - l_2$, and recalling the fact that $f_m[n]$ is of the finite order L_f, we can rewrite (3.14) as

$$R_{rr}(n;\tau) = \bar{E}_s \sum_{l=-\infty}^{\infty} \sum_{\rho=-L_f}^{L_f} h^*[n+\tau, n+\tau-\rho-l]h[n, n-l]$$

$$\cdot R_{ff}(l;\rho) + R_{ww}(n;\tau), \tag{3.15}$$

where we have defined

$$R_{ff}(l;\rho) := \sum_{m=0}^{M-1} \sum_{i=-\infty}^{\infty} f_m^*[l+\rho-iP]f_m[l-iP].$$

Because $R_{ff}(l;\rho)$ is generally P-periodic in l and we assumed that the noise has the cyclostationarity with period equal to 60 Hz, then we can say the same about $R_{rr}(n;\tau)$.

In case of MDFB (M=P), we intend to eliminate the insertion of redundancy, so under the condition (3.9) $R_{ff}(l;\rho)$ (and also $R_{rr}(n;\tau)$) is periodic.

In case of weighted OFDM (P=$M+L$), OFDM symbols without C/P lose the cyclostationarity by (3.9)

$$R_{ff}(l;\rho) = \sum_{m=0}^{M-1} \sum_{i=-\infty}^{\infty} e^{-j\frac{2\pi}{M}m(l+\rho-iP)} e^{j\frac{2\pi}{M}m(l-iP)} = M\delta(\rho), \tag{3.16}$$

and hence is not periodic. On the other hand, OFDM with C/P for $\rho$$\in$$[-M-L,M+L]$ has the correlation depending on l,

$$R_{ff}(l;\rho) = \sum_{m=0}^{M-1} \sum_{k_1=-\infty}^{\infty} \sum_{k_2=-\infty}^{\infty} e^{-j\frac{2\pi}{M}mk_2} e^{j\frac{2\pi}{M}mk_1} \cdot \delta(l-k_1)\delta(l+\rho-k_2). \tag{3.17}$$

In order to preserve the cyclostationarity for complete orthonormal sets in (3.17), we consider non-maximally decimated OFDM with M<P and filters of impulse

response $f_m[n]$ of order $L{=}P{-}M$, where L corresponds to the number of zero-padding (Z/P) superimposed on the input symbols of length M. Then, we have $R_{ff}(l;\rho) = \sum_{m=0}^{M-1} e^{-j\frac{2\pi}{P}\rho m}$, which implies the cyclostationarity of $r[n]$.

3.4 Time-Varying Power Line Channel

Considering the discrete-time I/O block model equivalent to the frequency domain two-port network in Fig. 2.4, similarly as in Section 3.2.1 we define $\{\underline{\mathbf{v}}_s[i]\}_k \triangleq v_s[iP{+}k]$, $\{\underline{\mathbf{v}}_{out}[i]\}_k \triangleq v_{out}[iP{+}k]$ and $\{\underline{\mathbf{i}}_{in}[i]\}_k \triangleq i_{in}[iP{+}k]$.

3.4.1 Power Line Network Simulator

In this section, we design a generalized network simulator, which has the ability of describing the unknown parameters in terms of the past and present values, which does not use the LTZ technique from chapter 2. If we denote a blocked version of $s[n]$ as $\underline{\mathbf{s}}[i]{=}\,[s[iM]\cdots s[iM{+}M{-}1]]^T$ and $\underline{\mathbf{v}}_s[i]{=}\,[v_s[iP]\cdots v_s[iP{+}P{-}1]]^T$, we find the relationship between the source voltage $\underline{\mathbf{v}}_s[i]$ and the input symbol vector $\underline{\mathbf{s}}[i]$ as follows:

$$\underline{\mathbf{v}}_s[i] = \sum_{l=-\infty}^{\infty} \mathbf{F}_l \underline{\mathbf{s}}[i-l], \tag{3.18}$$

where $\mathbf{F}_l$ is a precoder filter of order L_f such that $\{\mathbf{F}_l\}_{p,m}{=}f_m[lP{+}p]$ for $p{=}0,\cdots,P{-}1$ and $m{=}0,\cdots,M{-}1$.

Let the time-varying block matrices $\mathbf{A}_{i,i-j}$,$\mathbf{B}_{i,i-j}$,$\mathbf{C}_{i,i-j}$,$\mathbf{D}_{i,i-j}$ defined in (2.45)-(2.48) be of finite orders, respectively, N_A, N_B, N_C and N_D, and suppose that all these values are greater than 1. Source impedance $z_0^{(s)}$ and load impedance $z_0^{(L)}$ in Section 2.3.1 are time-invariant, and without loss of generality we can interchange

the second index $i-j$ of channel matrix with the index j of input vector in (3.5). When precoding from (3.18) is superimposed on the original source voltage vector $\underline{\mathbf{v}}_s[i]$, we can reformulate (2.41)-(2.44) in lifted block forms as follows:

$$\underline{\mathbf{v}}_{out}[i] = \sum_{j=0}^{N_A} \mathbf{A}_{i,j}\underline{\mathbf{v}}_{in}[i-j] + \sum_{j=0}^{N_B} \mathbf{B}_{i,j}\underline{\mathbf{i}}_{in}[i-j] \tag{3.19}$$

$$\underline{\mathbf{i}}_{out}[i] = \sum_{j=0}^{N_C} \mathbf{C}_{i,j}\underline{\mathbf{v}}_{in}[i-j] + \sum_{j=0}^{N_D} \mathbf{D}_{i,j}\underline{\mathbf{i}}_{in}[i-j] \tag{3.20}$$

$$\underline{\mathbf{v}}_{in}[i] = \sum_{l=0}^{L_f} \mathbf{F}_l\underline{\mathbf{s}}[i-l] - z_0^{(s)}\underline{\mathbf{i}}_{in}[i-l] \tag{3.21}$$

$$\underline{\mathbf{v}}_{out}[i] = z_0^{(L)}\underline{\mathbf{i}}_{out}[i-l]. \tag{3.22}$$

If we choose a block size P sufficiently large such that $P>>\max(N_A, N_B, N_C, N_D, L_f)$, we can apply the results from (3.6) and (3.18) can be subdivided into two terms

$$\underline{\mathbf{v}}_s[i] = \mathbf{F}_0\underline{\mathbf{s}}[i] + \mathbf{F}_1\underline{\mathbf{s}}[i-1], \tag{3.23}$$

where $\mathbf{F}_0$ is a lower-banded matrix which is multiplied by the current input $\underline{\mathbf{s}}[i]$ of interest and $\mathbf{F}_1$ is an upper-triangular matrix which is multiplied by the past input $\underline{\mathbf{s}}[i]$ (IBI term).

Under the assumption of $P>>\max(N_A, N_B, N_C, N_D, L_f)$, (3.19)-(3.22) can be represented as

$$\underline{\mathbf{v}}_{out}[i] = \mathbf{A}_{i,0}\underline{\mathbf{v}}_{in}[i] + \mathbf{B}_{i,0}\underline{\mathbf{i}}_{in}[i] + \underbrace{\mathbf{A}_{i,1}\underline{\mathbf{v}}_{in}[i-1] + \mathbf{B}_{i,1}\underline{\mathbf{i}}_{in}[i-1]}_{\triangleq \mathrm{IBI}_{\underline{\mathbf{v}}_{out}}[i-1]} \tag{3.24}$$

$$\underline{\mathbf{i}}_{out}[i] = \mathbf{C}_{i,0}\underline{\mathbf{v}}_{in}[i] + \mathbf{D}_{i,0}\underline{\mathbf{i}}_{in}[i] + \underbrace{\mathbf{C}_{i,1}\underline{\mathbf{v}}_{in}[i-1] + \mathbf{D}_{i,1}\underline{\mathbf{i}}_{in}[i-1]}_{\triangleq \mathrm{IBI}_{\underline{\mathbf{i}}_{out}}[i-1]} \tag{3.25}$$

$$\underline{\mathbf{v}}_{in}[i] = \mathbf{F}_0\underline{\mathbf{s}}[i] - z_0^{(s)}\underline{\mathbf{i}}_{in}[i] + \underbrace{\mathbf{F}_1\underline{\mathbf{s}}[i-1] - z_0^{(s)}\underline{\mathbf{i}}_{in}[i-1]}_{\triangleq \mathrm{IBI}_{\underline{\mathbf{v}}_{in}}[i-1]} \tag{3.26}$$

$$\underline{\mathbf{v}}_{out}[i] = z_0^{(L)}\underline{\mathbf{i}}_{out}[i] + \underbrace{z_0^{(L)}\underline{\mathbf{i}}_{out}[i-1]}_{\triangleq \mathrm{IBI}'_{\underline{\mathbf{v}}_{out}}[i-1]}, \tag{3.27}$$

where as seen from (3.24)-(3.27), $\mathrm{IBI}_{\underline{\mathbf{v}}_{out}}[i-1]$, $\mathrm{IBI}_{\underline{\mathbf{i}}_{out}}[i-1]$, $\mathrm{IBI}_{\underline{\mathbf{v}}_{in}}[i-1]$, and $\mathrm{IBI}'_{\underline{\mathbf{v}}_{out}}[i-1]$ are determined by the past values of $\underline{\mathbf{v}}_{in}[i-1]$, $\underline{\mathbf{i}}_{in}[i-1]$, and $\underline{\mathbf{i}}_{out}[i-1]$. If the two-port network is activated at rest, we can rearrange (3.24)-(3.27) to the following system equation.

$$\underbrace{\begin{bmatrix} \mathrm{IBI}_{\underline{\mathbf{v}}_{out}}[i-1] \\ \mathrm{IBI}_{\underline{\mathbf{i}}_{out}}[i-1] \\ \mathrm{IBI}_{\underline{\mathbf{v}}_{in}}[i-1] \\ \mathrm{IBI}'_{\underline{\mathbf{v}}_{out}}[i-1] \end{bmatrix}}_{\triangleq \overline{\mathbf{Y}}_{i-1}} + \underbrace{\begin{bmatrix} \mathbf{0} \\ \mathbf{0} \\ \mathbf{F}_0 \underline{\mathbf{S}}_i \\ \mathbf{0} \end{bmatrix}}_{\triangleq \overline{\mathbf{S}}_i}$$

$$= \underbrace{\begin{bmatrix} -\mathbf{A}_{i,0} & -\mathbf{B}_{i,0} & \mathbf{0} & \mathbf{I} \\ -\mathbf{C}_{i,0} & -\mathbf{D}_{i,0} & \mathbf{I} & \mathbf{0} \\ \mathbf{I} & -z_0^{(s)}\mathbf{I} & \mathbf{0} & \mathbf{0} \\ \mathbf{0} & \mathbf{0} & -z_0^{(L)}\mathbf{I} & \mathbf{I} \end{bmatrix}}_{\triangleq \overline{\Psi}_i} \underbrace{\begin{bmatrix} \underline{\mathbf{v}}_{in}[i] \\ \underline{\mathbf{i}}_{in}[i] \\ \underline{\mathbf{i}}_{out}[i] \\ \underline{\mathbf{v}}_{out}[i] \end{bmatrix}}_{\triangleq \overline{\mathbf{Y}}_i} \tag{3.28}$$

In fact, for the real test channel in Section 2.7 the coefficients of these filter matrices can be found from the relationship between the characteristic impedance and the propagation constant, see (2.77) and [17]. Since the structure of $\overline{\Psi}_i$ is itself invertible and $\overline{\mathbf{Y}}_{i-1}$ is IBI-term which is removable, we can find $\overline{\mathbf{Y}}_i$ in terms of $\overline{\mathbf{S}}_i$ and $\overline{\Psi}_i$. Thus (3.28) forms a basis for the design of our multistage network simulator, which includes the precoding stage of (3.18) in addition to precoding-free network simulator in (2.66).

3.4.2 Cascading Time-Varying Transmission Lines

The cumulative response of multistage system can be obtained recursively, just as in the case of a single input-output time-varying system. Considering that $\underline{\mathbf{v}}_{in}^{(1)}[j]$,

$\underline{\mathbf{i}}_{in}^{(1)}[j]$ (j=1,$\cdots$,i−1) in (3.28) are connected to the source and $\underline{\mathbf{v}}_{out}^{(n)}[i]$, $\underline{\mathbf{i}}_{out}^{(n)}[i]$ to the load, we can represent the n-cascaded power line network by replacing $\mathbf{A}_{i,0}$ by $\mathbf{A}_{i,0}^{(n,\cdots,1)}$ (similarly with $\mathbf{B}_{i,0}$,$\mathbf{C}_{i,0}$,$\mathbf{D}_{i,0}$), also $\underline{\mathbf{W}}_{i-1}$ by $\overline{\mathbf{Y}}_{i-1}^{(n,\cdots,1)}$, where $\overline{\mathbf{Y}}_{in}^{(1)}[i]$, $\underline{\mathbf{i}}_{in}^{(1)}[i]$ are substituted for $\underline{\mathbf{v}}_{in}[i]$, $\underline{\mathbf{i}}_{in}[i]$, and $\underline{\mathbf{v}}_{out}^{(n)}[i]$, $\underline{\mathbf{i}}_{out}^{(n)}[i]$ for $\underline{\mathbf{v}}_{out}[i]$, $\underline{\mathbf{i}}_{out}[i]$ (cf. (3.28)).

Hence, with the knowledge of the time-varying block channel model and the input current and voltage of the previous block at the first stage, we are capable of estimating the output current and voltage at the last stage. Or equivalently, if we find the inverse of $\overline{\Psi}_i^{(n,\cdots,1)}$, then $\overline{\mathbf{v}}_{out}^{(n)}[i]$ and $\overline{\mathbf{i}}_{out}^{(n)}[i]$ can be found from

$$\overline{\mathbf{Y}}_i = \overline{\Psi}_i^{(n,\cdots,1)^{-1}}[\overline{\mathbf{S}}_i + \overline{\mathbf{Y}}_{i-1}^{(n,\cdots,1)}], \tag{3.29}$$

where $\overline{\mathbf{Y}}_{i-1}^{(n,\cdots,1)}$ are determined from the input current and voltage in the previous block at the first stage and the current in the previous block at the last stage.

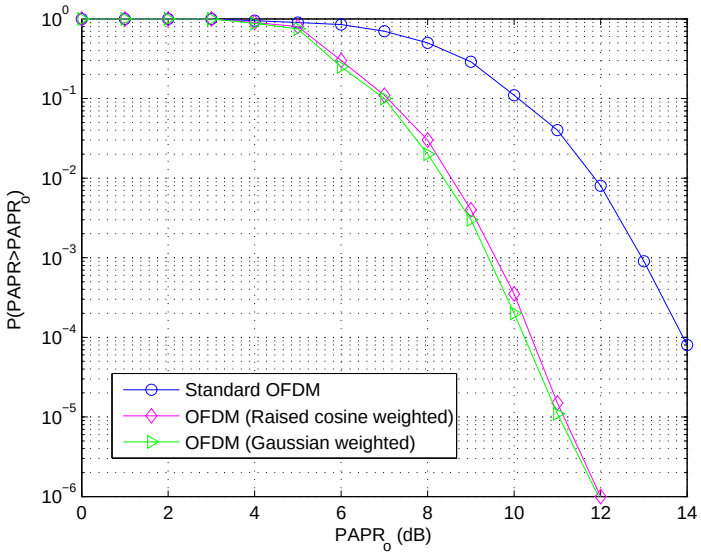

Figure 3.3: PAPR performance of Standard OFDM and Weighted OFDM for 80 subcarriers

3.5 Numerical Results

To validate the relationship in (3.29) works or not, we performed 1000 Monte Carlo simulations for the test channel used in [58] and Chapter 2.

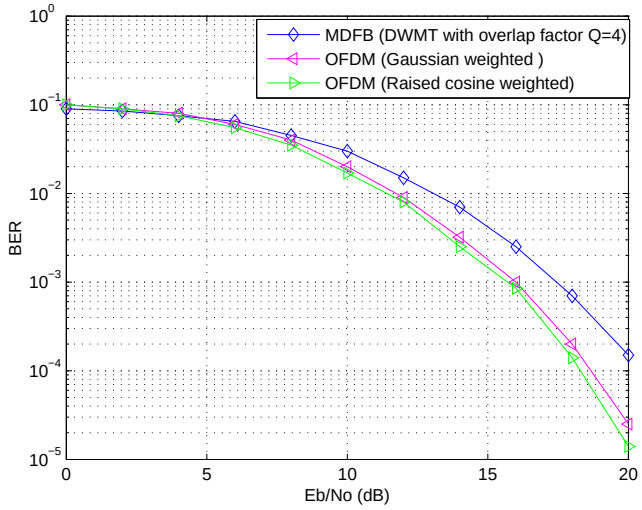

Figure 3.4: Bit error rate (BER) versus signal-to-noise (SNR) ratio via Monte Carlo simulations

In Fig. 3.3, peak-to-average power ratio (PAPR) performance of two weighted OFDMs are compared with that of standard OFDM, where 10 percent of weighted OFDM symbols has a PAPR of approximately 7 dB, and the standard OFDM has a PAPR of 9.6 dB. For Gaussian weighting function, we used $\sigma=\frac{N}{8}$. All the ABCD parameters are found in [17], and we set $Z_{L,0}=Z_{s,0}=100$ [ohms]. 128 QPSK symbols were modulated by this system architecture. Two weighted OFDM simulations (Gaussian/Raised cosine) have the parameter triplets of $(P,M,L)=(80,72,8)$, and discrete wavelet-based MDFBs have $P=M=72$ with no redundancy, where 3.63-30 MHz is the band of operation.

Combining the OFDM receiver output with the post-detection equalization and symbol-by-symbol MAP detection, the results in Fig. 3.4 shows that the

probability of error of weighted OFDM outperforms that of MDFB at high SNR.

3.6 Summary

In this chapter, we proposed a discrete-time equivalent model for the time-varying response of the power line channel and the corresponding (cascade) I/O relationship for power line network simulator. We run practical simulations over our real PLC model combined with two multirate precoders (weighted OFDM and wavelet-based MDFB) over the time-varying channels. With the cyclostationary noise with period of 60 Hz, the weighted OFDM system outperforms the wavelet-based MDFB system in having lower BER at the cost of redundancy (C/P) at high SNR.

CHAPTER 4

RANDOMIZED MULTI-ANTENNA SYSTEMS IN MULTI-PATH CHANNELS

4.1 Cooperative Communications

The advantages of multiple input multiple output (MIMO) systems are well documented. These systems combat the effects of fading with spatial diversity. In the setting of ad-hoc wireless networks or distributed large scale wireless networks, the users are typically limited in size or hardware resources to a single antenna. Cooperative communications were proposed to exploit the advantages of MIMO systems to single antenna users in multi-user environment. In cooperative communications the nodes collaborate to increase their performance, creating a virtual MIMO system.

There are many cooperative transmission schemes, including the amplify-and-forward (AF) and decode-and-forward (DF) scheme. In systems such as ad-hoc networks and sensor networks, there is typically no centralized control. Therefore, distributed forms of cooperation are used, where users independently decide when to cooperate. If transmitting users do not have access to the channel state information and the receivers are not cooperating, distributed forms of space-time coding designed for multiple input single output (MISO) systems are desirable, [44], [51], [52]. Interestingly, schemes such as [43], require only the knowledge of the number of cooperating nodes but not the code assignment. With the exception of several papers, [38], [39], [45], the majority of the other schemes considered in literature assume the nodes either know the code assignment or the number of cooperating nodes. The tight management of relay activities adds to the over-

head, limiting scalability to larger networks, and therefore, does not fit well within ad-hoc networking.

4.1.1 Motivation

Suppose that a node transmits a message $\mathbf{s}$ and has an unknown number of nodes in its vicinity which are qualified to decode and forward the message. Qualified nodes satisfy some performance criterion (e.g, they are not in outage capacity, or the SNR is above a certain threshold). We assume a set of these cooperating nodes, denoted by $\mathcal{S}$, can synchronize to the source message using a preamble sequence, and will retransmit in unison in the following time slot. Assuming these nodes correctly decode the message, and considering the decode-and-forward strategy, we want to investigate what decoding strategy is.

In [41], we showed how fully decentralized protocols could be designed in general, and analyzed the diversity that could be achievable over flat-fading channels. These architectures include [38], [39], [45] as special cases. In our model all users agree on a common coding scheme. Specifically, each node is unaware of the effective code being employed by the other nodes, as well as the number of cooperating nodes. A local independent random assignment of the code is performed at each node. The randomized coding rule targets a fixed order of diversity L, which is independent of the number of actual cooperating nodes.

Our contribution is to extend the applicability of the randomized model presented in [41] to that of non-ideal channel conditions such as the frequency selective model, capturing the effects of time-delays amongst the cooperating nodes as well as the inherent selectivity of the broadband links. A thorough analysis of its per-

formance is presented using different options for the utilized code. This is an important generalization, since in practice it is difficult to obtain perfect symbol synchronization among the cooperating nodes. We develop a randomized strategy that generalizes strategies presented in [41], as well as previously proposed schemes which use cooperative multi-path to generate diversity, such as in [15], [38], [39] and [45].

4.2 System Model

We consider a cooperative network with T cooperating radios. The jth radio has a baseband equivalent, discrete-time transmit signal $X_j[k]$ with an average power constraint $\sum_{k=0}^{K-1} |X_j[k]|^2 \leq KP_j$ where K is the duration of the signal. Let $W_i[k]$ be a sequence of mutually independent, circularly-symmetric, complex Gaussian random variables with common variance N_0 modeling thermal noise and other interference at the ith radio. Also denote the complex, baseband equivalent, continuous, time-varying channel impulse response by $h_{ij}(t, \tau)$, and its corresponding discrete-time channel between the i-th and j-th radios by $H_{ij}[k, l]$. Then $h_{ij}(t, \tau)$ captures the combined effects of a frequency selective time-varying multi-path fading environment, as well as shadowing and path-loss between radios i and j, and last but not least, symbol and carrier asynchronism among the cooperative nodes. Assuming that the physical channel has a given channel response, $c_{ij}(t, \tau)$, possibly time-varying itself, a time-delay τ_{ij} and carrier offset ν_{ij} of user j relative to the time and carrier synchronism estimated at node i, can be captured by considering the channel as having the equivalent response

$$h_{ij}(t, \tau) = c_{ij}(t - \tau_{ij}, \tau - \tau_{ij}) e^{j2\pi\nu_{ij}t}.$$

We will assume, for the purpose of our diversity analysis, that the discrete-time channel impulse response $H_{ij}[k,l]$ follows a *block-fading model*, that is, it remains constant over the duration of one transmission block and is perfectly estimated at the ith receiver. If the channel bandwidth of $h_{ij}(t,\tau)$ is denoted by B, then the discrete time channel $H_{ij}[k,l]$ can be found by

$$H_{ij}[k,k-l] = \int_{-\infty}^{\infty}\int_{-\infty}^{\infty} h_{ij}(k/B - v, \tau)p((k-l)/B - v - \tau)p(-v)d\tau dv,$$

where $p(t)$ is the pulse-shaping filter at the transmitter.

Then, assuming a 'half-duplex' constraint, that is, a transmitting user cannot simultaneously receive and vice versa, the discrete-time received signal $Y_j[k]$ at the ith user at time sample k is

$$Y_i[k] = \begin{cases} \sum_{j\in\mathcal{S}, j\neq i}^{T} \sum_{l=-\infty}^{+\infty} H_{ij}[k,k-l]\cdot X_j[l] + W_i[k] & \text{if radio } i \text{ receives} \\ 0, & \text{if radio } i \text{ transmits} \end{cases} \tag{4.1}$$

where $\mathcal{S}$ is the set of users transmitting cooperatively. We use this system model for diversity analysis in cooperative space-time coding in the next.

4.2.1 Cooperative Space-Time Coding

As stated previously, when the transmitting nodes do not have channel state information and the receivers do not cooperate, appropriate encoding schemes are those of distributed space-time coding [44]. Cooperating nodes share a common message, previously transmitted by one or more nodes and received by the group of cooperating nodes. We can represent the common message to transmit as a vector of length M denoted by $\mathbf{s} = (S[0], \ldots, S[M-1])^T$. Each of the T cooperating relay nodes transmits a specific column $\mathbf{x}_t = (X_t[0], ...X_t[K-1])^T$ of a $K \times T$

matrix code $\mathbf{X} = \mathbf{G}_{K\times T}(\mathbf{s})$. The rate of the code is therefore M/K. The number of columns of $\mathbf{G}(\mathbf{s})$ corresponds to the number of cooperating nodes. Cooperative schemes including the early examples in [40] and [34], as well as simple amplify and forward or decode and forward strategies can all be cast into the mapping $\mathbf{s} \rightarrow \mathbf{G}(\mathbf{s})$. These schemes all provide diversity, because the effect of the linear channel can be cast into a vector of receiver observations as:

$$\mathbf{y} = \mathbf{G}(\mathbf{s})\mathbf{R}\mathbf{h} + \mathbf{w} \tag{4.2}$$

As eloquently stated in [48], all forms of channel diversity can be mapped into (4.2). Therefore, the definition of coding gain in [44] and the considerations as to what codes can or cannot provide diversity, have a much more general impact than indicated.

4.3 Randomized Cooperative Coding in Flat Fading

4.3.1 Deep Fade Event Probability

In [41] the cooperating nodes generate their codes by forming a predetermined matrix code $\mathbf{X} = \mathbf{G}_{K\times L}(\mathbf{s})$. Instead of transmitting a pre-assigned column of the matrix code, each of the T cooperating nodes projects the rows of the matrix over a random, independently generated, $L \times 1$ vector $\mathbf{r}_t$, $t = 1, \ldots, T$. In flat-fading, the discrete-time channel $H_{ij}[k, l] \equiv H_{ij}\delta[l]$ and thus, the data at the i-th receiver is (4.1):

$$\mathbf{y}_i = \sum_{t=1}^{T} H_{it}\mathbf{G}(\mathbf{s})\mathbf{r}_t + \mathbf{w}_i \tag{4.3}$$

$$= \mathbf{G}(\mathbf{s})\mathbf{R}\mathbf{h}_i + \mathbf{w} = \mathbf{G}(\mathbf{s})\tilde{\mathbf{h}}_i + \mathbf{w}_i. \tag{4.4}$$

This randomized coding rule targets a fixed order of diversity L, which is strictly independent of the actual number of cooperating nodes as can be seen in the previous equation. It can be observed from the last equation that the system behaves as an equivalent set of L co-located transmit antennas with fading coefficients, relative to the ith receiver, composing the entries of the vector $\tilde{\mathbf{h}}_i$. Therefore, in order to decode at the receiver, knowledge of the number of cooperating nodes as well as the randomization matrix $\mathbf{R}$ are required. The receiver can simply estimate $\tilde{\mathbf{h}}_i$ directly leading to a great simplification of the decoding process. We will omit the receiver index i for simplicity.

The diversity in terms of the probability of error is defined as, [41], [42],

$$d^{(Pe)} \triangleq \lim_{SNR\to\infty} -\frac{\ln(Pe(SNR))}{\ln(SNR)}. \tag{4.5}$$

Assume that the codes satisfy the following *rank criterion* for flat-fading channels:

C1) *The Rank Criterion for* $\mathbf{G}$ *- (Flat Fading)*: For all $k \neq i$, the matrix $(\mathbf{G}(\mathbf{s}_k) - \mathbf{G}(\mathbf{s}_i))$ has full rank L.

Lemma 1 in [41] states that the probability of error $P_e(SNR)$ of a maximum likelihood (ML) detector has the following bounds:

$$P_e(SNR) \geq \frac{1}{M} Q\left(\sqrt{\lambda_{\max}/2}\right) \Pr(||\mathbf{Rh}||^2 \leq SNR^{-1}), \tag{4.6}$$

$$P_e(SNR) \leq \Pr(||\mathbf{Rh}||^2 \leq SNR^{-\alpha}) + E_{\mathbf{R}}\left\{e^{-\lambda_{\min} SNR||\mathbf{Rh}||^2} \;\middle|\; ||\mathbf{Rh}||^2 \leq SNR^{-\alpha}\right\}, \quad \forall \alpha \in (0,1) \tag{4.7}$$

where $Q(x) = \frac{1}{\sqrt{2\pi}} \int_x^\infty exp(-\frac{u^2}{2})du$, and $E_{\mathbf{R}}(\cdot)$ and M are expectation over all realizations of $\mathbf{R}$ and the cardinality of the code book $\mathbf{s}_k$, respectively. $\lambda_{\max}$ and $\lambda_{\min}$ are the maximum and minimum eigenvalues, respectively, of $\mathbf{A}_{ik} \triangleq (\mathbf{G}(\mathbf{s}_i) -$

$\mathbf{G}(\mathbf{s}_k))^H(\mathbf{G}(\mathbf{s}_i) - \mathbf{G}(\mathbf{s}_k))$. For $i \neq k$, and assuming *C1* is satisfied, all eigenvalues will be strictly positive.

In lieu of the diversity in terms of probability of error $d^{(Pe)}$, the *deep fade* event diversity $d^{(deep-fade)}$ can be analyzed. The deep fade event diversity is defined as:

$$d^{(deep-fade)} \triangleq \lim_{SNR\to\infty} -\frac{\ln(\Pr(||\mathbf{Rh}||^2 \leq SNR^{-1}))}{\ln(SNR)} \tag{4.8}$$

and is independent of the code.

As *Lemma 1* in [41] argues, as $SNR \to \infty$ and $\alpha \to 1$, both the upper and lower bounds in (4.6) and (4.7) will be normalized by $ln(SNR)$ in log-scale, and converge to the following deep fade event diversity in (4.8). We restate these results in the following lemma.

Lemma 4 *If the rank condition C1 is satisfied,* $d^{(deep-fade)} \equiv d^{(Pe)}$. *(cf. See Lemma 1 in [41])*

In [41], the deep fade event diversity was examined under arbitrary random matrix distributions for Rayleigh fading $\mathbf{h}_i \sim \mathcal{CN}(\mathbf{0}, \mathbf{\Phi_h})$. We briefly review this analysis. Let $\eta = \min(L, T)$, where T is the number of cooperating nodes and L is the targeted diversity. Further let λ_{min} denote the eigenvalues of $\mathbf{R}\mathbf{\Phi}_h^{1/2}$ where $\mathbf{\Phi}_h^{1/2}$ is $T \times T$ and generally of full rank. Clearly, $\text{rank}(\mathbf{\Phi}_h^{1/2}) \leq \eta$. Then, by *Theorem 1* and the deep fade event exponents of the singular values $\alpha_i \in [0, 1]$ in [41] we reach the following deep fade event diversity

$$d^{(deep-fade)} = \inf_{(\alpha_1,\ldots,\alpha_\eta)} \left(\sum_{i=1}^{\eta} (1 - \alpha_i) + \Gamma(\alpha_1, \ldots, \alpha_\eta) \right), \tag{4.9}$$

where

$$\Gamma(\alpha_1, \ldots, \alpha_\eta) = Pr\left(\bigcap_{i=1}^{\eta} (\lambda_i < SNR^{-\alpha_i}) \right). \tag{4.10}$$

Using sufficient conditions on the distribution of $\mathbf{R}$, shown in [41], there are several options for the randomization matrix $\mathbf{R}$ which enable the full diversity L of the code $\mathbf{G}(\mathbf{s})$ to be achieved, provided that the number of cooperating nodes T exceeds the number of virtual antenna L by at least one node. For the case where $T \leq L$, the same random selection rules provide a diversity $O(T)$. Under a wide variety of continuum distributions of $\mathbf{R}$ it was shown in [42]

$$d = \begin{cases} T & \text{if} \quad L \geq T+1 \\ L & \text{if} \quad L \leq T-1. \end{cases} \tag{4.11}$$

Since this is a fully decentralized design, obviously, the cooperating nodes independently generate columns of the randomization matrix $\mathbf{R}$. For example, these columns could be independent and identically distributed (i.i.d) complex Gaussian random variables, complex exponential random variables with uniformly distributed random phase, or the column could be a random vector uniformly distributed on an L-dimensional hypersphere. In numerical simulations it has been observed that the uniform spherical random vectors provide the best performance. The attainable diversity in (4.11) is significant as the diversity of randomized cooperation can be made as large as the minimum of the code order L or the number of cooperating users.

We note that there are tradeoffs in targeting large and small degrees L of diversity. Large degrees L allow the greatest gain in diversity if the number of nodes $T > L$, but add increased complexity and increases in either bandwidth or code length. This is a strong deterrent if the number of cooperating nodes is frequently less than L. Conversely, with small degrees of L, when the number of nodes is much larger than L, we are not taking full advantage of the potential diversity which could be obtained with a larger L.

4.3.2 Diversity Analysis over Randomization

We now extend the analysis in [41] of the deep-fade event probability. Again we assume T cooperative relays with a flat fading circularly symmetric complex Gaussian channel denoted by $\mathbf{h} \sim \mathcal{CN}(\mathbf{0}, \mathbf{\Phi}_h)$. We examine the obtainable diversity for a given $\mathbf{R}$ and note that $d^{(deep-fade)}(\mathbf{R}) = d^{(Pe)}(\mathbf{R})$ as long as the rank condition $C1$ is satisfied. The probability of the deep-fade event conditioned on the knowledge of $\mathbf{R}$ is:

$$\begin{aligned} \Pr(||\mathbf{Rh}||^2 \leq SNR^{-1}|\mathbf{R}) &= \Pr\left(\sum_{k=1}^{\eta} \lambda_k |\chi_k|^2 \leq SNR^{-1} \,|\mathbf{R}\right) \quad (4.12) \\ &= \sum_{k=1}^{\eta} \left(\prod_{m \neq k} \frac{\lambda_k}{\lambda_k - \lambda_m}\right) \left(1 - e^{-\frac{1}{SNR\lambda_k}}\right), \quad (4.13) \end{aligned}$$

where we used the eigenvalue decomposition $\mathbf{\Phi}_h^{H/2}\mathbf{R}^H\mathbf{R}\mathbf{\Phi}_h^{1/2} = \mathbf{U}\mathbf{\Lambda}\mathbf{U}^H$ and made the assumption that the nonzero eigenvalues are distinct. The random variable χ_k is an i.i.d. zero mean, unit norm complex Gaussian entry of the $T \times 1$ vector $\boldsymbol{\chi} = \mathbf{U}^H\mathbf{\Phi}^{-1/2}\mathbf{h} \Rightarrow \boldsymbol{\chi} \sim \mathcal{CN}(\mathbf{0}, \mathbf{I})$. We note that the sum in (4.12) is performed over the η greatest eigenvalues when eigenvalues of $\mathbf{\Phi}_h^{H/2}\mathbf{R}^H\mathbf{R}\mathbf{\Phi}_h^{1/2}$ are arranged in the decreasing order, and the corresponding entries of $\boldsymbol{\chi}$. The assumption that the non-zero eigenvalues are distinct is fairly reasonable for continuum distributions of $\mathbf{R}$. In order to derive (4.13), we note the density of the random variable $\lambda_k|\chi_k|^2$ is $f(y) = \frac{1}{\lambda_k} e^{-\frac{y}{\lambda_k}}$.

Another approach to calculate the obtainable diversity is based on the Laplace-Stieltjes transform of the random variable $SNR||\mathbf{Rh}||^2$. The following lemma expresses the obtainable diversity for a given $\mathbf{R}$.

Lemma 5 *The diversity of the randomized cooperative coding scheme for a given*

$\mathbf{R}$ *is*

$$d^{(deep-fade)}(\mathbf{R}) = \eta - \beta, \tag{4.14}$$

where $\beta = \sum_{k=1}^{\eta} \mathbf{1}\{\lambda_k = 0\}$*, i.e.* β *is the number of zero-eigenvalues in* $\mathbf{\Lambda}$*.*

Proof: Proof of the lemma is shown in Appendix 4.A.

The following corollary provides the necessary and sufficient condition to achieve full diversity given $\mathbf{R}$.

Corollary 5 *In order to achieve the full diversity* $d^{(deep-fade)}(\mathbf{R}) = \eta$ *for a given* $\mathbf{R}$*, the necessary and sufficient condition*[1] *is* $|\mathbf{\Phi}_h^{H/2}\mathbf{R}^H\mathbf{R}\mathbf{\Phi}_h^{1/2}| \neq 0$*. If* $\mathbf{\Phi}_h$ *is full rank, in order to achieve full diversity the corresponding necessary and sufficient condition is* $|\mathbf{R}^H\mathbf{R}| \neq 0$*.*

This corollary implies that the η largest eigenvalues of $|\mathbf{\Phi}_h^{H/2}\mathbf{R}^H\mathbf{R}\mathbf{\Phi}_h^{1/2}|$ must be non-zero in order to achieve the full diversity. The decrease in diversity β is a function of both $\mathbf{\Phi}_h$ and $\mathbf{R}$. We further extend these results to the case of the average diversity, providing an alternative characterization of the diversity compared to [41]. We assume that randomization matrix $\mathbf{R}$ changes several times during the transmission of a packet. Therefore, the probability of the deep fade event is given as

$$\Pr(||\mathbf{Rh}||^2 \leq SNR^{-1}) = E_{\mathbf{R}}\{\Pr(||\mathbf{Rh}||^2 \leq SNR^{-1}|\mathbf{R})\}. \tag{4.15}$$

The average obtainable diversity and the sufficient and necessary condition to obtain the full diversity $d^{(deep-fade)} = \eta$ are given in the following lemma and its corresponding corollary.

[1]If $\mathbf{A}$ is an $L \times T$ matrix, when $L \leq T$ the notation $|\mathbf{A}^H\mathbf{A}| = \det(\mathbf{A}\mathbf{A}^H)$; when $L > T$, $|\mathbf{A}^H\mathbf{A}| = \det(\mathbf{A}^H\mathbf{A})$. Hence, this notation is used to define the product of the η largest eigenvalues of $\mathbf{A}^H\mathbf{A}$.

Lemma 6 *The average diversity of the randomized cooperative coding scheme is*

$$d^{(deep-fade)} = \eta - \lim_{SNR\to\infty} \frac{\ln E_{\mathbf{R}}\{((\eta-\beta)!)^{-1} SNR^{\beta} \prod_{k=1}^{\eta-\beta} \lambda_k\}}{\ln SNR}. \tag{4.16}$$

Corollary 6 *The average diversity $d^{(deep-fade)} = \eta$ if the following necessary and sufficient condition is satisfied*

$$E_{\mathbf{R}}\{|\mathbf{\Phi}_h^{H/2}\mathbf{R}^H\mathbf{R}\mathbf{\Phi}_h^{1/2}|^{-1}\} < \infty. \tag{4.17}$$

If $\mathbf{\Phi}_h$ is full rank, the necessary and sufficient condition reduces to

$$E_{\mathbf{R}}\{|\mathbf{R}^H\mathbf{R}|^{-1}\} < \infty. \tag{4.18}$$

If we assume that the entries of the matrix $\mathbf{R}$ are i.i.d. zero mean with variance $1/L$, using asymptotic random matrix theory (i.e. $T, L \to \infty$) with a constant ratio $c = T/L$, we have the following corollary.

Corollary 7 *If $\mathbf{\Phi}_h$ is full rank and the entries of the matrix $\mathbf{R}$ are i.i.d. zero mean with variance $1/L$ and $T \neq L$, as $T, L \to \infty, T/L \to c$, the average diversity $d^{(deep-fade)} = \eta$.*

Proof: Proof of this corollary is shown in Appendix 4.B.

In the asymptotic case, the empirical distribution of the η largest eigenvalues of $\mathbf{R}^H\mathbf{R}$ converges to a non-random density function. If the above conditions are met $|\mathbf{R}^H\mathbf{R}|$ is finite with probability 1.

4.3.3 Cooperative Multi-Path

Cooperative multi-path [38], [39] and [45] can also be cast in this randomized coding framework. It is easier to understand its operation by isolating the effect of

actual multi-path from induced multi-path created by intentionally staggering the cooperative transmissions to induce fading. To isolate the latter effect and draw conclusions from [41] that cover this case, it is easier to consider the case of flat fading channel.

In cooperative multi-path, the mapping $\mathbf{G}(\mathbf{s})$ has a Toeplitz structure, since the codes designed for each transmit antenna are simply staggered versions of the transmit sequence, i.e. $\{\mathbf{G}(\mathbf{s})\}_{i,j} = S[i-j]$. If the delays for each transmit antenna are chosen at random, the vector $\mathbf{r}_i$ at the ith node is simply a randomly chosen canonical vector. In a centralized scheme, the nodes must choose non-overlapping delays in order to achieve a diversity gain proportional to the number of users.

Instead of forming $\mathbf{G}(\mathbf{s})$ directly, it may be beneficial to construct it from precoded data. This method can be combined with spread spectrum techniques or with Orthogonal Frequency Division Multiplexing (OFDM). Combining OFDM with error correction coding, diversity can be achieved in a spectrally efficient manner compared to that of spread spectrum techniques. The code matrix for these two techniques can be constructed in the two following fashions:

- Spread spectrum techniques: $\mathbf{u}$=$\mathbf{c}$S[i], $\mathbf{c}$: spreading code
- Multi-carrier modulations: $\mathbf{u}$=$\mathbf{F}\mathbf{s}$, $\mathbf{F}$: IFFT matrix+prefix

In spread spectrum techniques, the coded vector $\mathbf{u}$ is obtained by multiplying each symbol of length $M = 1$ by spreading code $\mathbf{c}$, whereas in multi-carrier modulations multiple symbols are multiplexed into the same block, where the inverse Fourier transform is applied and the prefix is appended. In both cases, the relationship between the message vector $\mathbf{s}$ and the coded vector $\mathbf{u}$ provides a Toeplitz convolution matrix, denoted by $\mathcal{T}(\mathbf{u})$, which is taken as the mapping matrix $\mathbf{G}(\mathbf{s})$ such

that we have $\mathbf{G}(\mathbf{s}) = \mathcal{T}(\mathbf{u})$. For OFDM, in order to obtain a diversity L, the equivalent channel must have length L, and therefore, there will be a bandwidth expansion due to the use of a cyclic prefix or a zero padding sequence, of length $N > L - 1$. Space-time coding can be included either within the OFDM block, or across blocks.

Some redundancy is required in order to guarantee that the rank condition *C1* is satisfied. A simple approach to satisfy the rank condition is to assume that the number of appended zeros is equal to the number of delays used, which is equal to L. Therefore, to guarantee the rank condition, the size of $\mathcal{T}(\mathbf{u})$ is $(M+L)\times L$ with first column equal to $[\mathbf{u}^T, 0, ..., 0]^T$ and first row equal to $(u[0], 0, ..., 0)$ where $u[0]$ is the first element of $\mathbf{u}$. On the other hand, OFDM adds an equivalent amount of redundancy, but if not appropriately coded, does not guarantee the rank condition, and will lose diversity.

Cooperative multi-path has several advantages compared to that of space-time coding, which are seldom acknowledged. First, it enables reduced complexity receiver architectures, which are fairly standard and provide simple options for multiplexing multiple sources either using different spreading codes or sub-carriers. Second, cooperative multi-path in combination with with OFDM precoding, can provide diversity gains on the order of the equivalent channel memory D, while maintaining spectral efficiency. In fact, for large coherence time in the channel, a large number of sub-carriers can be used, reducing the inefficiency due to the addition of the cyclic prefix (or zero padding). This simple strategy leads to spectrally-efficient large dimension space-time codes.

The unintentional effects of time-asynchronism and carrier frequency offset (CFO) can be incorporated in the model by appropriately defining the code ma-

trix and randomization vector. The time-asynchronism can be captured in the channel response $h_{ij}(t,\tau)$ by including the time and frequency offset. The CFO induces variations in the equivalent channels $\tilde{\mathbf{H}}_{il}, l = 1,\ldots,L$ effectively increasing the Doppler spread. Therefore, dealing with a cooperative channel is equivalent to dealing with a multi-antenna transmission over time-varying, time-dispersive channels. This is still challenging, but within reach. Further, since randomized cooperative multi-path in [38]- [39] and [45] is constructed using randomized selection, an analog randomization would have greater performance, [41].

When the channels experienced by the nodes are affected by inter-symbol interference (ISI), time-reversal techniques may be appropriate, [50]. These techniques can be used to limit the increase in the duration of the channel impulse response used to harvest additional delay diversity through the addition of cooperative users. The multi-antenna and multi-path can be simultaneously leveraged in a more efficient fashion. In the following section we demonstrate how randomized cooperation can be used to solve the code assignment problem within this context. We analyze the diversity and provide conditions on the code assignment to provide this diversity.

4.4 Randomized Cooperative Coding in Frequency Selective Fading

In the previous section, each user experienced a flat fading channel. In this section we assume each user utilizes a randomized space-time code and its transmission is received through an inherently asynchronous and selective channel.

4.4.1 Asynchronous Dispersive Links

We extend the results in [41] to the frequency selective case as follows. The block discrete time model will now have each input vector mapped to an output vector through the following linear transformation:

$$\{\mathbf{H}_{ij}\}_{k,l} = H_{ij}[k, k-l]. \tag{4.19}$$

We assume that the channel has a finite memory D and therefore the transmission can be structured in blocks which are interleaved with guard interval sufficiently long to eliminate inter-block interference (IBI) for weighted OFDM modulation, but guard interval is not necessary for wavelet MDFB case. For simplicity, we assume the guard periods are created with at least D zeros, although the use of a cyclic prefix is also possible. A block of size $K > 2D$ is mapped into a vector of size $K + D$ (i.e. $\mathbf{H}_{ij}$ in (4.19) is a tall $(K + D) \times K$ matrix):

$$\begin{aligned} \mathbf{y}_i &= \sum_{j=1}^{T} \mathbf{H}_{ij} \underbrace{\mathbf{G}(\mathbf{s})}_{\mathbf{x}_{K\times L}} \mathbf{r}_j + \mathbf{w}_i \\ &= \sum_{l=1}^{L} \left(\sum_{j=1}^{T} \mathbf{H}_{ij} r_{jl} \right) \mathbf{x}_l + \mathbf{w}_i = \sum_{l=1}^{L} \tilde{\mathbf{H}}_{i,l} \mathbf{x}_l + \mathbf{w}_i. \end{aligned} \tag{4.20}$$

The diversity that can be obtained through this scheme depends on the statistics of the equivalent channels $\tilde{\mathbf{H}}_{il}, l = 1, \ldots, L$ and randomization matrix $\mathbf{R}$, as well as the particular code selection $\mathbf{G}(\mathbf{s})$. Clearly, the receiver i needs no knowledge of the randomization matrix $\mathbf{R}$, but needs only to acquire the parameters of the equivalent L frequency selective channels.

To assess the potential performance gains that can be obtained by randomized cooperation in multi-path channels with asynchronous cooperative nodes, we extend the diversity analysis in [41] to a stationary channel. We rewrite the model in such a way that it can be mapped one to one in a special instance of (4.3).

Assuming the presence of zero guard intervals between blocks of data, and a linear time-invariant channel, the product $\tilde{\mathbf{H}}_{il}\mathbf{x}_l = \mathcal{T}(\mathbf{x}_l)\tilde{\mathbf{h}}_{il}$, where $\mathcal{T}(\mathbf{x}_l)$ has the Toeplitz structure but the size now depends on the equivalent channel order D and not solely on the design parameter L. Hence, if we denote $\otimes$ as Kronecker product, we can express (4.20) as follows:

$$\begin{aligned} \mathbf{y}_i &= \sum_{l=1}^{L} \mathcal{T}(\mathbf{x}_l)\tilde{\mathbf{h}}_{il} + \mathbf{w}_i = \boldsymbol{\mathcal{X}}\tilde{\mathbf{h}}_i + \mathbf{w}_i \qquad (4.21) \\ &= \boldsymbol{\mathcal{X}}(\mathbf{R} \otimes \mathbf{I}_{D\times D})\mathbf{h}_i + \mathbf{w}_i, \qquad (4.22) \end{aligned}$$

where $\boldsymbol{\mathcal{X}} \triangleq (T(\mathbf{x}_1), \ldots, T(\mathbf{x}_L))$; $\tilde{\mathbf{h}}_i \triangleq (\tilde{\mathbf{h}}_{i1}^T, \ldots, \tilde{\mathbf{h}}_{iL}^T)^T$; and $\mathbf{h}_i \triangleq (\mathbf{h}_{i1}^T, \ldots, \mathbf{h}_{iT}^T)^T$. This is now in a form similar to (4.3), except for the structure of the equivalent code matrix and the random mapping.

4.4.2 Diversity Analysis over Randomization and Multipath

There are two questions to address in the analysis of the diversity. First, is it possible for the equivalent code matrix $\boldsymbol{\mathcal{X}}$ to meet the rank condition, and second, what sort of diversity can we anticipate with the structure of the randomized mapping $(\mathbf{R}\otimes\mathbf{I}_{D\times D})$? Given the structure of the code matrix $\boldsymbol{\mathcal{X}}$, the corresponding rank criterion is as follows:

C2) *Rank criterion for $\boldsymbol{\mathcal{X}}$ - (Inter-symbol interference channels)*: For all $k \neq i$, the matrix $(\boldsymbol{\mathcal{X}}_k - \boldsymbol{\mathcal{X}}_i)$ has full rank LD. The matrix $\boldsymbol{\mathcal{X}}_i$ is the Toeplitz matrix formed from the code matrix $\mathbf{G}(\mathbf{s}_i)$.

The following lemma gives conditions on the matrix $\boldsymbol{\mathcal{X}}$ such that it will satisfy the rank condition.

Lemma 7 *Cooperative space time coding in multi-path channels of length* $\leq D$ *will satisfy the rank condition C2 if and only if*

C3) *The code sequence* $\mathbf{x}_l$ *has length* K *such that* $K + D - 1 \geq LD$

C4) *For any two distinct sequences* $\mathbf{s}_k$ *and* $\mathbf{s}_i$ *the polynomials formed by taking the Z-transforms of the columns of the matrix:*

$$\mathbf{A}_{ki} = \boldsymbol{\mathcal{X}}_k - \boldsymbol{\mathcal{X}}_i = (\mathbf{a}_{ki}^{(1)}, \ldots, \mathbf{a}_{ki}^{(L)})$$

are co-prime so that $\mathbf{A}_{ki}$ *is of full rank.*

Proof: The first condition simply states that the matrix $\mathbf{A}_{ki}$ must be tall or at least square in order to have full column rank LD. For the second condition the Z-transforms of the columns of $\mathbf{A}_{ki}$ are:

$$A_{ki}^{(l)}(z) \triangleq \sum_{k=0}^{K-1} a_{ki}^{(l)}[k] z^{-k} = X_{kl}(z) - X_{il}(z). \tag{4.23}$$

If the $A_{ki}^{(l)}(z)$ are not co-prime for $l = 1, ..., L$, then it is possible to find a $G(z) \neq 0$ such that $\sum_{l=1}^{L} A_{ki}^{(l)}(z) G(z) = 0$, implying the null-space of the matrix is nonempty, and the columns are linearly dependent. This condition is equivalent to conditions invoked in several second-order blind channel identification methods [35]. (Q.E.D.)

Lemma 7 provides conditions on the codes $\mathbf{G}(\mathbf{s})$ such that they will satisfy the rank criterion C2 for frequency selective channels of order D. The question of the spectral efficiency one can obtain while satisfying the rank criterion is beyond the scope of this paper. Without focusing on the spectral efficiency, nothing appears to prevent the existence of such designs, and we proceed to analyze the diversity they can provide.

Assuming the Rayleigh fading model, which is conventional in the study of diversity, some additional assumptions are still needed for the multi-path scenario.

In the flat-fading case, it would be sensible to assume that the channel vector covariance $\mathbf{\Phi}_h$ is diagonal, since the different users links are likely to be uncorrelated. Further, for relays situated in a similar position relative to the destination, it is reasonable to use an i.i.d model. However, in the case of a frequency selective medium, the equivalent channel vector $\mathbf{h}_i$ at the i-th destination, consists of the discrete-time channel impulse responses of all the users' links stacked one on top of another. We assume all users have the same equivalent channel order D, which is an upper-bound on the channel length plus the symbol asynchronism of the users. Certain delays will be more likely than others, the power delay profile of the channel is likely to be non-uniform, and the paths are, in general, going to be correlated due to transmit and receive filters. This suggests the i.i.d. channel model will not be realistic.

However we assume that the covariance of the channel impulse response, has the same structure up to a certain scale, for all cooperating nodes. This scale can capture the presence of different large scale fading attenuations among cooperating nodes. An appropriate model for the combined channel vector is then $\mathbf{h}_i \sim \mathcal{CN}(\mathbf{0}, (\mathbf{\Phi}_h \otimes \mathbf{\Delta}_h))$, where $\mathbf{\Delta}_h$ is a scaled $D \times D$ multi-path covariance matrix and $\mathbf{\Phi}_h$ captures the effects of large-scale fading and average received power. If we satisfy the rank criterion C2, Lemma 1 in [41] is still valid, and allows us to calculate the probability of deep fade event in a similar fashion as that done for the flat fading case. First, let us use the following eigenvalue decompositions:

$$\mathbf{\Phi}_h^{H/2}\mathbf{R}^H\mathbf{R}\mathbf{\Phi}_h^{1/2} = \mathbf{U}\mathbf{\Lambda}\mathbf{U}^H \tag{4.24}$$

$$\mathbf{\Delta}_h = \mathbf{V}\mathbf{\Gamma}\mathbf{V}^H, \tag{4.25}$$

where $\mathbf{U}$ and $\mathbf{V}$ are Hermitian matrices, $\mathbf{\Lambda} = \mathrm{diag}(\lambda_1, \cdots, \lambda_\eta)$ are the η largest ordered eigenvalues of $\mathbf{\Phi}_h^{H/2}\mathbf{R}^H\mathbf{R}\mathbf{\Phi}_h^{1/2}$, and $\mathbf{\Gamma} = \mathrm{diag}(\gamma_1, \cdots, \gamma_{\eta_D})$ are the ordered

eigenvalues of $\mathbf{\Delta}_h$. In the following we define $\eta = \min\{L, T\}$ and $\eta_D = \text{rank}(\mathbf{\Delta}_h)$

The following theorem provides the exact diversity order of randomized codes in a multi-path fading environment in terms of the distribution of the eigenvalues λ_k in (4.24). We use the notation 0^- to denote a negative real number that is close to zero and let $\Gamma(\alpha_1, \cdots, \alpha_\eta)$ represent the following function:

$$\Gamma(\alpha_1, \ldots, \alpha_\eta) = \lim_{SNR \to \infty} \frac{-\log \Pr(\lambda_1 \leq SNR^{-\alpha_1}, \cdots, \lambda_\eta \leq SNR^{-\alpha_\eta})}{\log SNR} \tag{4.26}$$

where the parameters $\alpha_1, \cdots, \alpha_\eta$ were defined as *deep fade exponents of the eigenvalues* in (4.9). We now present the following theorem.

Theorem 4 *If the conditions C3 and C4 in Lemma 7 are satisfied, then the diversity order of the randomized space-time code with ISI is*

$$d^{(deep-fade)} = \inf_{(\alpha_1, \cdots, \alpha_\eta)} \left(\Gamma(\alpha_1, \ldots, \alpha_\eta) + \eta_D \sum_{i=1}^{\eta} (1 - \alpha_i) \right), \tag{4.27}$$

where the infimum is over $\alpha_i \in [0^-, 1],\ i = 1, \cdots, \eta$.

Proof: Using (4.26), the proof is a straight forward generalization of the proof of *Theorem 1* in [42]. We note that (4.27) simplifies to the formula obtained under flat fading [42] when $\eta_D = 1$. (Q.E.D.)

Using a similar analysis as that in Lemma 5, we have the following lemma specifying the obtainable diversity for a given $\mathbf{R}$ in a multi-path fading environment:

Lemma 8 *The diversity given* $\mathbf{R}$ *of the randomized scheme over frequency selective channels is*

$$d^{(deep-fade)}(\mathbf{R}) = (\eta - \beta)\eta_D, \tag{4.28}$$

where $\beta = \sum_{k=1}^{\eta} \mathbf{1}\{\lambda_k = 0\}$ *and* $\eta_D = rank(\mathbf{\Delta}_h)$.

Proof: Proof of the lemma is given in Appendix 4.C.

The following corollary gives the necessary and sufficient condition to obtain the full diversity.

Corollary 8 *In order to achieve the full diversity* $d^{(deep-fade)}(\mathbf{R}) = \eta\ \eta_D$*, the necessary and sufficient condition is*

$$|\mathbf{\Phi}_h^{H/2}\mathbf{R}^H\mathbf{R}\mathbf{\Phi}_h^{1/2}|^{-\eta_D} < \infty. \tag{4.29}$$

Proof: Proof of the corollary is given in Appendix 4.D.

Here we see the obtainable diversity in a multi-path fading environment can be increased by a factor η_D over the flat fading case in Corollary 6. We consider the average obtainable diversity, again noting the relationship (4.15). This leads to the following lemma stating the obtainable average diversity.

Lemma 9 *The average diversity of the randomized scheme over frequency selective channels is:*

$$d^{(deep-fade)} = \eta\eta_D - \lim_{SNR\to\infty} \frac{\ln\left(E_{\mathbf{R}}\{SNR^{\beta\eta_D}[(\eta-\beta)\eta_D]!\prod_{k=1}^{\eta-\beta}\lambda_k^{-\eta_D}\prod_{p=1}^{\eta_D}\gamma_p^{\beta}\}\right)}{\ln(SNR)} \tag{4.30}$$

where $\beta = \sum_{k=1}^{\eta}\mathbf{1}\{\lambda_k = 0\}$ *and* $\eta_D = rank(\mathbf{\Delta}_h)$.

Corollary 9 *The sufficient and necessary condition to achieve full average diversity* $\eta\eta_D$ *is*

$$E_{\mathbf{R}}\{|\mathbf{\Phi}_h^{H/2}\mathbf{R}^H\mathbf{R}\mathbf{\Phi}_h^{1/2}|^{-\eta_D}\} < \infty. \tag{4.31}$$

Therefore in order to achieve the full diversity, all of the η eigenvalues λ_ks must be non-zero. We see that the decrease in diversity β is still a function of $\mathbf{\Phi}_h$ and $\mathbf{R}$.

In general, any random matrix $\mathbf{R}$ with independent columns drawn from a continuous distribution is full rank with probability 1. We continue searching for the best distribution of $\mathbf{R}$ among continuous distributions. In the following we provide sufficient conditions such that the above sufficient condition is satisfied and, hence, $d^{(deep-fade)} = \eta\ \eta_D$. Let $P_t < \infty$ be the total relay power available to the network such that

$$Tr(\mathbf{R}\mathbf{R}^H) \leq P_t \ \text{ with probability 1.} \tag{4.32}$$

Theorem 5 *Let* $\mathbf{R}$ *be an* $L \times T$ complex *random matrix and denote* $p(\mathbf{R})$ *its probability density function. Assume that the function* $p(\mathbf{R})$ *is bounded and it satisfies the total power constraint (4.32). If* $|L - T| > \eta_D$ *and C3, C4 in Lemma 7 are satisfied, then* $E\{|\mathbf{R}\mathbf{R}^H|^{-\eta_D}\} < \infty$. *Therefore, the diversity order of the randomized space-time code is given by*

$$d^* = \begin{cases} T \cdot \eta_D & \text{if} \quad T \leq L - \eta_D \\ L \cdot \eta_D & \text{if} \quad T \geq L + \eta_D. \end{cases} \tag{4.33}$$

Proof: Proof of the theorem is given in Appendix 4.E.

In the following, we present different randomized space-time codes and Table 4.1 summarizes the diversity order of the proposed schemes when the multi-path order $\eta_D = 2$. Furthermore, in Section 4.7, the average error probabilities of these designs are obtained via Monte-Carlo simulations. In the following, we assume that $\mathbf{h} \sim \mathcal{N}(0, \mathbf{I})$.

Proposed Schemes:

- *Complex/Real Gaussian distribution*: The $L \times T$ dimensional randomization matrix $\mathbf{R}$ are zero-mean independent and complex/real Gaussian.

Table 4.1: Diversity order of various RSTCs under multi-path order $\eta_D = 2$.

Distribution of $\mathbf{R}$	Condition	Diversity Order
Complex Gaussian	$T = L$	$\eta_D\eta - 1$
Complex Gaussian	$T \neq L$	$\eta_D\eta$
Real Gaussian	$T = L$	$\eta_D\eta - 2$
Real Gaussian	$T = L + 1$ or $T = L - 1$	$\eta_D\eta - 1$
Real Gaussian	$T = L + 2$ or $T = L - 2$	$\eta_D\eta - 0.5$
Real Gaussian	$\lvert T - L\rvert > 2$	$\eta_D\eta$
Uniform Phase	$T = L = 2$	2.5
Real Spherical Distribution	$T = L = 2$	3
Complex Spherical Distribution	$T = L = 2$	4

- *Uniform phase distribution*: The t-th column of the $L \times T$ randomization matrix is $\mathbf{r}_t = a_t[e^{j\theta_t[1]}, \ldots, e^{j\theta_t[L]}]^T$ where each $\theta_t[l] \sim U(0, 2\pi)$ and $a_t \sim U(1-\epsilon, 1+\epsilon)$ for some small $\epsilon > 0$, where $U(a, b)$ denotes the uniform distribution in the interval (a, b) and all $\theta_t[l], a_t$ are independent of each other.

- *Uniform distribution on a complex/real hypersphere*: The t-th column of the $L \times T$ randomization matrix, $\mathbf{r}_t$, is uniformly selected on the surface of a complex/real hypersphere of radius ρ, i.e. $||\mathbf{r}_t|| = \rho$.

4.5 Average Diversity for Single Randomization Matrices

In calculating the average diversity in the previous sections, we assumed that the group of cooperating nodes changes the randomization matrix several times during the transmission of the packet, at least as frequently as the channel changes. Due to the ergodicity of the random process, the receiver experiences the diversity predicted by the analysis. The question still exists as to what diversity is obtainable if the randomization matrix were kept constant during the entire packet

transmission. The diversity would then be a function of the matrix $\mathbf{R}$

$$d^{(deep-fade)}(\mathbf{R}) = \lim_{SNR\to\infty} \frac{-\ln \Pr(||\mathbf{Rh}||^2 < SNR^{-1}|\mathbf{R})}{\ln SNR}.$$

To calculate the ensemble performance the receiver would expect over many packets, we take the expectation over $\mathbf{R}$ as

$$\delta^{(deep-fade)} \triangleq E_{\mathbf{R}}\{d^{(deep-fade)}(\mathbf{R})\}.$$

Comparing the above expression for $\delta^{(deep-fade)}$ to that of $d^{(deep-fade)}$ in Lemma 6, we see that the expectation is taken in different locations. Noting that $f(x) = -\ln(x)$ is a convex function, we apply Jensen's Inequality, which says $E\{f(X)\} \geq f\left(E\{X\}\right)$. Since f(X) is convex,

$$E_{\mathbf{R}}\{\ln(((\eta-\beta)!)^{-1}SNR^{\beta}\prod_{k=1}^{\eta-\beta}\lambda_k)\} \geq \ln(E_{\mathbf{R}}\{((\eta-\beta)!)^{-1}SNR^{\beta}\prod_{k=1}^{\eta-\beta}\lambda_k\}). \quad (4.34)$$

Clearly, if $E_{\mathbf{R}}\{\ln(|\mathbf{\Phi}_h^{H/2}\mathbf{R}^H\mathbf{R}\mathbf{\Phi}_h^{1/2}|^{-1})\} < \infty$ then from *Corollary* 6 and 8:

$$\delta^{(deep-fade)} = d^{(deep-fade)} = \begin{cases} \eta & \text{flat-fading case} \\ \eta\ \eta_D & \text{frequency-selective case} \end{cases} \quad (4.35)$$

4.6 Specific Space-Time Codes

In [49] several transmission schemes were examined under the framework of distributed randomized cooperation. Specifically, space-time block coding (STBC) and Time-Reversal space-time block coding (TR-STBC) were examined. Here we show the structure of the columns $\mathbf{x}_l$ in (4.20) for these transmission schemes.

4.6.1 Space-Time Block Coding

We consider a message $\mathbf{s}$ of length M which can be evenly parsed into Q substreams $\mathbf{s} = [\mathbf{s}_0^T, ..., \mathbf{s}_{Q-1}^T]$. In space-time block coding, the lth column of the code matrix $\mathbf{G}(\mathbf{s}_q)$ can be expressed as

$$\tilde{\mathbf{x}}_l = \mathbf{A}_l \mathbf{s}_q + \mathbf{B}_l \mathbf{s}_q^*, \tag{4.36}$$

and the matrices $\mathbf{A}_l$ and $\mathbf{B}_l$ uniquely specify the particular space time block code. The columns of the code matrix $\mathbf{G}(\mathbf{s})$ can then be expressed as the concatenation of the code matrices $\mathbf{G}(\mathbf{s}_q)$ for $q = 0, ..., Q-1$ as

$$\mathbf{x}_l = (\mathbf{I} \otimes \mathbf{A}_l)\mathbf{s} + (\mathbf{I} \otimes \mathbf{B}_l)\mathbf{s}^*. \tag{4.37}$$

Let us denote a *vec* operator as $vec[\cdot, \cdot]$, which accumulates all entries of the product on a single column vector. At a single receiver, in order to use linear equalization, we can introduce the vector $\tilde{\mathbf{y}}$ via *vec* operator.

$$\begin{aligned}
\tilde{\mathbf{y}} &\triangleq vec[\mathbf{y}, \mathbf{y}^*] = \mathbf{M}\tilde{\mathbf{s}} + \tilde{\mathbf{w}} \\
\mathbf{M} &\triangleq \begin{pmatrix} \sum_{l=1}^{L} \mathbf{H}_l(\mathbf{I} \otimes \mathbf{A}_l) & \sum_{l=1}^{L} \mathbf{H}_l(\mathbf{I} \otimes \mathbf{B}_l) \\ \sum_{l=1}^{L} \mathbf{H}_l^*(\mathbf{I} \otimes \mathbf{B}_l^*) & \sum_{l=1}^{L} \mathbf{H}_l^*(\mathbf{I} \otimes \mathbf{A}_l^*) \end{pmatrix} \\
\tilde{\mathbf{s}} &\triangleq vec[\mathbf{s}, \mathbf{s}^*] \\
\tilde{\mathbf{w}} &\triangleq vec[\hat{\mathbf{w}}, \hat{\mathbf{w}}^*]
\end{aligned} \tag{4.38}$$

Alternatively, we can use the following mapping:

$$\begin{aligned}
\tilde{\mathbf{y}} &\triangleq vec[\mathfrak{Re}[\mathbf{y}], \mathfrak{Im}[\mathbf{y}]] = \mathbf{M}\tilde{\mathbf{s}} + \tilde{\mathbf{w}} \\
\tilde{\mathbf{s}} &\triangleq vec[\mathfrak{Re}[\mathbf{s}], \mathfrak{Im}[\mathbf{s}]] \\
\tilde{\mathbf{w}} &\triangleq vec[\mathfrak{Re}[\hat{\mathbf{w}}], \mathfrak{Im}[\hat{\mathbf{w}}]]
\end{aligned} \tag{4.39}$$

4.6.2 Time-Reversal Space-Time Block Coding

In the Time-Reversal STBC scheme proposed in [50], the message $\mathbf{s}$ is parsed into two equal length substreams $\mathbf{s} = [\mathbf{s}_1^T, \mathbf{s}_2^T]^T$. The two columns of the code matrix $\mathbf{G}(\mathbf{s})$ can then be expressed as:

$$\mathbf{x}_1 = \begin{bmatrix} \mathbf{s}_1 \\ \mathbf{p} \\ -\acute{\mathbf{s}}_2^* \end{bmatrix}, \quad \mathbf{x}_2 = \begin{bmatrix} \mathbf{s}_2 \\ \mathbf{p} \\ \acute{\mathbf{s}}_1^* \end{bmatrix} \tag{4.40}$$

where $(\acute{\cdot})$ denotes the time-reversal operation, and the vector $\mathbf{p}$ consists of zero guard symbols or a training sequence, in order to avoid inter-block interference. In the Time-Reversal STBC scheme at the single receiver, the second received block $\acute{\mathbf{y}}_2^*$ is time-reversed and conjugated, then combined with the first received block, leading to:

$$\underbrace{\begin{bmatrix} \mathbf{y}_1 \\ \mathbf{y}_2 \end{bmatrix}}_{\mathbf{y}} = \underbrace{\begin{bmatrix} \mathbf{H}_1 & \mathbf{H}_2 \\ \acute{\mathbf{H}}_2^* & -\acute{\mathbf{H}}_1^* \end{bmatrix}}_{\mathbf{H}} \underbrace{\begin{bmatrix} \mathbf{s}_1 \\ \mathbf{s}_2 \end{bmatrix}}_{\mathbf{s}} + \underbrace{\begin{bmatrix} \mathbf{w}_1 \\ \mathbf{w}_2 \end{bmatrix}}_{\mathbf{w}} \tag{4.41}$$

The receiver processes the signal vector $\mathbf{y}$ with the spatio-temporal matched filter $\mathbf{H}^H$ leading to

$$\tilde{\mathbf{y}} = \mathbf{H}^H\mathbf{y} = \mathbf{H}^H\mathbf{H}\mathbf{s} + \mathbf{H}^H\mathbf{w}. \tag{4.42}$$

With frequency-selective channels constant over the two blocks, the spatio-temporal matched filter perfectly decouples the decoding of the data blocks $\mathbf{s}_1$ and $\mathbf{s}_2$. However, in the case of doubly-selective channels, the structure of the channel matrices is no longer Toeplitz but banded.

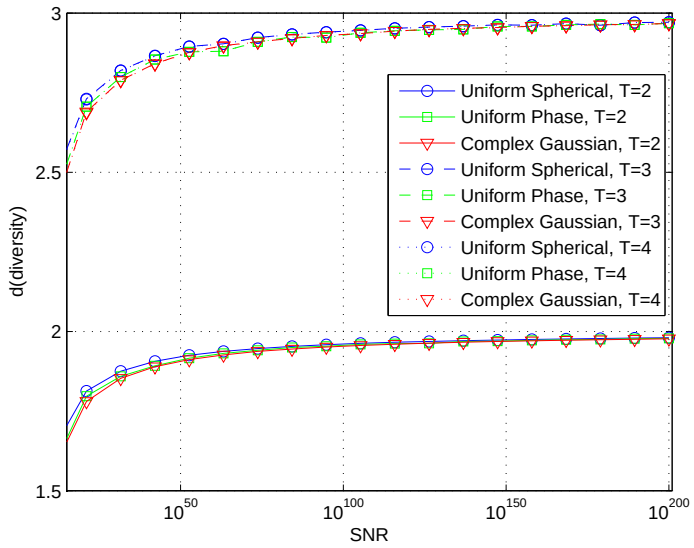

Figure 4.1: Average diversity in terms of deep fade probability over flat fading using (4.16) where $L = 3$ and various T

4.7 Numerical Results

In this section, we present simulations illustrating the performance of the proposed randomized distributed space-time codes in frequency selective channels. In the first set of simulations we will examine the obtainable diversity, using the expression for the diversity in terms of the deep fade event. In the second set of simulations, we examine the time-reversal space-time block code (TR-STBC) scheme for various number of nodes and randomization schemes over frequency selective channels.

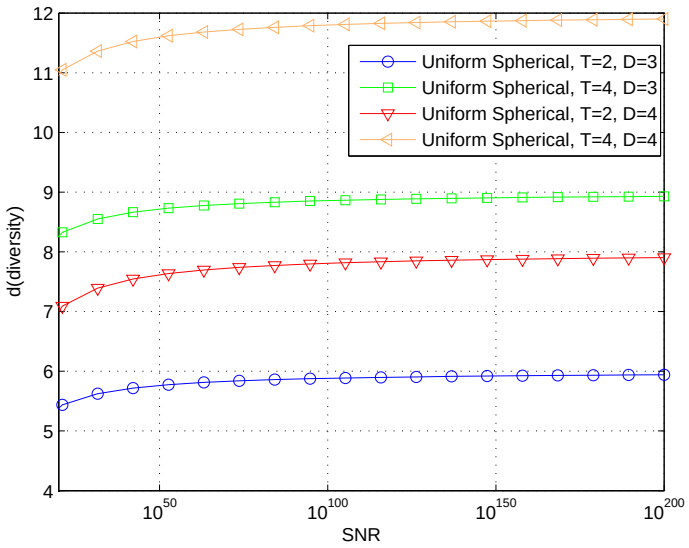

Figure 4.2: Average diversity in terms of deep fade probability over frequency selective fading using (4.30) where $L = 3$, various (T, D), and uniform spherical randomization

4.7.1 Randomized Space-Time Block Coding over Fading Channels

We verify through Monte Carlo simulations that the average diversity of randomized cooperative coding scheme over flat fading and frequency selective fading channel is the same as (4.16) and (4.30), respectively. We assume $L = 3$ and each complex Gaussian channel is independent and identically distributed with zero mean and covariance matrix $\mathbf{\Phi}_h$. As in [42], we perform the randomization over three specific schemes: (i) Uniform spherical randomization, (ii) Uniform phase randomization, and (iii) Complex Gaussian randomization. In this subsection, we use the log-scale with SNR (in linear, not dB) for much clarified visualization.

In Fig. 4.1 we obtain the average diversity at low SNR in the flat-fading case for $L = 3$ and various T. Over any choice of T, we see that the uniform spherical

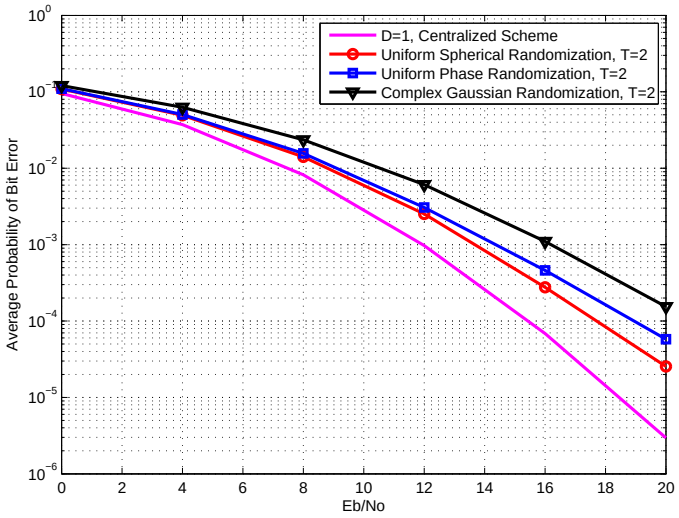

Figure 4.3: Average probability of bit error versus SNR (dB) using TR-STBC scheme where $L = 2$, $T = 2$, $D = 1$

randomization performs best. Our main interest is in what occurs to the average diversity when SNR approaches infinity. For $L > T$ we observe that the average diversity becomes $\eta = \min(L, T)$ in terms of nodes T. For $L \leq T$, we get the full diversity in the level of L for all three randomization schemes.

In Fig. 4.2 we utilize the uniform spherical randomization in the frequency selective case with multi-path channel order D and the results show that (4.30) still holds true. First, we see that with $D = 3$ the average diversity $d^{(deep-fade)}$ goes to 6 ($= \eta \cdot \eta_D$) for $L < T$ and 9 for $L > T$. Second, increasing D by 1 we observe that the average diversity $d^{(deep-fade)}$ goes to 8 for $L < T$ and 12 for $L > T$. In the end we see that increasing channel order enhances the average diversity of randomized cooperative coding scheme in terms of deep-fade probability, provided that the sufficient and necessary condition to achieve full average diversity is satisfied in *Corollary* 8.

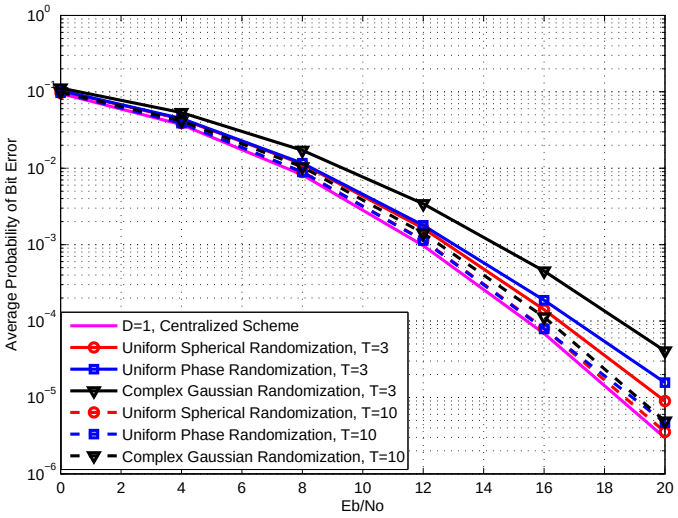

Figure 4.4: Average probability of bit error versus SNR (dB) using TR-STBC scheme where $L = 2$, $D = 1$, and for various T

4.7.2 Randomized Time-Reversal STBC

In these Monte Carlo simulations, we exploit the average probability of error using the TR-STBC scheme. We compare different randomization schemes with the centralized scheme for different values of T. We assume $L = 2$ and the channels between the nodes and a single destination are independent and identically distributed. Further we assume that the taps of the discrete time channel impulse response $\mathbf{h}_{i,t} \sim \mathcal{CN}(0, \frac{1}{D}\mathbf{I})$. Therefore we have $\eta_D = D$. As in Section 4.7.1, we repeat the simulations for three randomization schemes.

In all figures we plot the average probability of bit error with respect to $SNR = E_b/No$ for uncoded 8PSK. In Fig. 4.3 we examine the case of $T = 2$ nodes and a channel with memory $D = 2$, corresponding to two taps in each discrete time channel impulse response. We show the centralized scheme compared to the different randomization schemes. We see that Uniform spherical randomization performs the best. In Fig. 4.4 we examine the case of $D = 2$ for $T = 3$ and $T = 10$

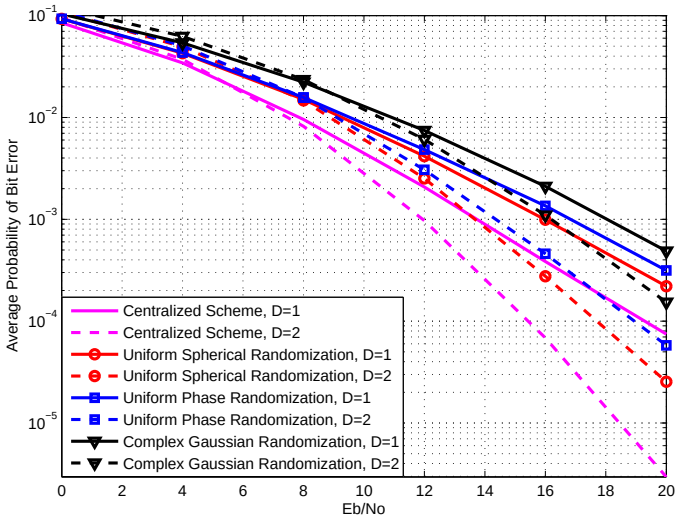

Figure 4.5: Average probability of bit error versus SNR (dB) using TR-STBC scheme where $L = 2$, $T = 2$, for various D

nodes. We see that as the number of nodes is increased, the performance of the distributed schemes approaches the centralized scheme in both diversity and in coding gain. In Fig. 4.5 we let $T = 2$ nodes and vary the channel memory from $D = 1$ to $D = 2$. We see that as we increase the channel memory, the diversity is increased for all randomization schemes, as shown in our previous analysis.

4.8 Summary

In this chapter, we first investigated the asymptotic diversity for the randomized cooperative coding for both flat fading and frequency selective channels. Then the exact average diversity over randomization in multi-path fading environments was derived and the obtained diversity for specific random matrices was characterized. In addition, we numerically verified that as the number of nodes is increased even moderately, the performance of the distributed scheme approaches that of the

centralized scheme both in diversity and coding gain.

APPENDIX 4.A

PROOF OF LEMMA 5

The Laplace-Stieltjes transform of the random variable $SNR||\mathbf{Rh}||^2$ is

$$\Phi_{SNR||\mathbf{Rh}||^2}(s) = E\{e^{-sSNR\sum_{k=1}^{\eta}\lambda_k|\chi_k|^2}\} = \frac{1}{\prod_{k=1}^{\eta}(1+sSNR\lambda_k)}. \tag{4.43}$$

If we denote $\beta = \sum_{k=1}^{\eta}\delta(\lambda_k)$, and make the assumption that $SNR >> 1$ we have the following approximation:

$$\Phi_{SNR||\mathbf{Rh}||^2}(s) \approx \frac{1}{\prod_{k=1}^{\eta-\beta}(\lambda_k SNRs)}. \tag{4.44}$$

By taking the inverse laplace transform we have the following approximation of the density function

$$f_{SNR||\mathbf{Rh}||^2}(y) \approx \frac{1}{(\eta-\beta-1)!}\frac{SNR^{-(\eta-\beta)}}{\prod_{k=1}^{\eta-\beta}\lambda_k}y^{\eta-\beta-1}. \tag{4.45}$$

Using the above approximation for the probability density function, we approximate probability of the deep-fade event conditioned on $\mathbf{R}$ and under the assumption of high SNR as

$$Pr(||\mathbf{Rh}||^2 \leq SNR^{-1}|\mathbf{R}) \approx \frac{1}{(\eta-\beta)!\prod_{k=1}^{\eta-\beta}SNR\lambda_k}. \tag{4.46}$$

This provides me with another means of observing the obtainable diversity with respect to the deep-fade event conditioned on $\mathbf{R}$

$$d^{(deep-fade)}(\mathbf{R}) \approx \lim_{SNR\to\infty}\frac{\ln\left(SNR^{\eta-\beta}(\eta-\beta)!\prod_{k=1}^{\eta-\beta}\lambda_k\right)}{\ln(SNR)} \tag{4.47}$$

$$= \eta-\beta. \tag{4.48}$$

We note that the factor β is also affected by the rank of $\mathbf{\Phi}_h$. If we assume $\mathbf{\Phi}_h$ is full rank, then the sufficient and necessary condition to achieve full rank is $|\mathbf{R}^H\mathbf{R}| \neq 0$.

(Q.E.D.)

APPENDIX 4.B

PROOF OF COROLLARY 7

The empirical eigenvalue distribution of the η largest eigenvalues of $\mathcal{R} = \mathbf{R}^H\mathbf{R}$ is given by

$$\mu_{\mathcal{R}}^{\eta}(x) = \frac{1}{\eta}\sum_{k=1}^{\eta}\delta(x-\lambda_k), \tag{4.49}$$

where δ represents the Dirac delta and λ_k is the k-th largest eigenvalue of $\mathcal{R}$. For the case $T \leq L$ the η largest eigenvalues correspond to the eigenvalues of $\mathbf{R}^H\mathbf{R}$. Central results in random matrix theory state that when the entries of $\mathbf{R}$ are i.i.d. zero mean with variance $1/L$, as $T, L \to \infty$ with $T/L \to c$ the empirical distribution of the eigenvalues almost surely converges to the following Marcenko-Pastur distribution [47]:

$$\mu_c(x) = \max(1-\frac{1}{c},0)\delta(x) + \frac{\sqrt{(x-a)(b-x)}}{2\pi cx}\mathbf{1}_{[a,b]}, \tag{4.50}$$

where $a = (1-\sqrt{c})^2$, $b = (1+\sqrt{c})^2$, and $\mathbf{1}_{[a,b]}$ is the indicator function. When $T/L < 1$, we see the distribution has no mass points at zero. Now for the case that $T > L$, the η largest eigenvalues correspond to the eigenvalues of $\mathbf{R}\mathbf{R}^H$. The empirical distribution converges to the following distribution [47]:

$$\tilde{\mu}_c(x) = \max(1-c,0)\delta(x) + \frac{\sqrt{(x-a)(b-x)}}{2\pi x}\mathbf{1}_{[a,b]} \tag{4.51}$$

Again, we see that since $T/L > 1$, the distribution has no mass points at zero. We now use these results to examine the average obtainable diversity in Lemma 5 assuming the asymptotic case of $\mathbf{R}$. We reach the following expression

$$\ln\left(|\mathbf{R}^H\mathbf{R}|^{-1}\right) = \sum_{k=1}^{\eta}\ln(\frac{1}{\lambda_k}). \tag{4.52}$$

For the asymptotic case where $T, L \to \infty, T/L \to c$

$$\ln\left(|\mathbf{R}^H\mathbf{R}|^{-1}\right) = \begin{cases} \int_a^b \ln(\frac{1}{x})\mu_c(x)dx & \text{if } T < L \\ \int_a^b \ln(\frac{1}{x})\tilde{\mu}_c(x)dx & \text{if } T > L. \end{cases} \tag{4.53}$$

These integrals evaluate to some finite value, and the limit in the corollary is zero. We note that for the case $T = L$

$$\lim_{x \to 0^+} \mu_c(x) = \infty \tag{4.54}$$

and hence we cannot evaluate the limit in *Corollary 7*. (Q.E.D.)

APPENDIX 4.C

PROOF OF LEMMA 8

The probability of deep fade event given $\mathbf{R}$ for the ISI case can be expressed as

$$\begin{aligned}
&\Pr(\|(\mathbf{R}\otimes\mathbf{I})\mathbf{h}\|^2 \leq SNR^{-1}|\mathbf{R}) \\
&= \Pr(\|(\mathbf{R}\boldsymbol{\Phi}_h^{1/2}\otimes\boldsymbol{\Delta}_h^{1/2})(\boldsymbol{\Phi}_h^{-1/2}\otimes\boldsymbol{\Delta}_h^{-1/2})\mathbf{h}\|^2 \leq SNR^{-1}|\mathbf{R}) \qquad (4.55)\\
&= \Pr\left\{\sum_{k=1}^{\eta}\lambda_k\sum_{p=1}^{\eta_D}\gamma_p|\chi_{(k-1)\eta_D+p}|^2 \leq SNR^{-1}|\mathbf{R}\right\} \qquad (4.56)\\
&= Pr\left\{\sum_{k=1}^{\eta\eta_D}\zeta_k|\chi_k|^2 \leq SNR^{-1}|\mathbf{R}\right\}, \qquad (4.57)
\end{aligned}$$

where $\eta = \min(L,T)$, $\eta_D = \text{rank}(\boldsymbol{\Delta}_h)$, and χ_k, $k = 1,\ldots,\eta\eta_D$, are the i.i.d. zero mean, unit variance, complex Gaussian entries of the vector $\boldsymbol{\chi} = (\mathbf{U}^H\otimes\mathbf{V}^H)(\boldsymbol{\Phi}^{-1/2}\otimes\boldsymbol{\Delta}_h^{-1/2})\mathbf{h}$ corresponding to the values ζ_k. Further, the vector $\boldsymbol{\chi}\sim\mathcal{CN}(\mathbf{0},\mathbf{I})$. As in the flat fading case, let $\beta = \sum_{k=1}^{\eta}\mathbf{1}\{\lambda_k\}$, using the same analysis as that in the proof of Lemma 5, we have

$$\Pr(\|(\mathbf{R}\otimes\mathbf{I})\mathbf{h}\|^2 \leq SNR^{-1}|\mathbf{R}) \approx \frac{SNR^{-(\eta-\beta)\eta_D}}{((\eta-\beta)\eta_D)!\prod_{k=1}^{(\eta-\beta)\eta_D}\zeta_k}. \qquad (4.58)$$

Therefore if $\boldsymbol{\Phi}_h$ is full rank, the obtainable diversity given $\mathbf{R}$ is

$$d^{(deep-fade)}(\mathbf{R}) = (\eta-\beta)\eta_D \qquad (4.59)$$

and hence is the lemma proved. (Q.E.D.)

APPENDIX 4.D

PROOF OF COROLLARY 8

We note that $|\mathbf{\Phi}_h^{H/2}\mathbf{R}^H\mathbf{R}\mathbf{\Phi}_h^{1/2} \otimes \mathbf{\Delta}_h|$ is the Kronecker product of the η largest eigenvalues in $\mathbf{\Lambda}$ and the η_D non-zero eigenvalues of $\mathbf{\Delta}_h$. Further, since the η_D eigenvalues γ_ps are necessarily non-zero, a necessary and sufficient condition to obtain the full diversity $d^{(deep-fade)}(\mathbf{R}) = \eta\eta_D$ is

$$|\mathbf{\Phi}_h^{H/2}\mathbf{R}^H\mathbf{R}\mathbf{\Phi}_h^{1/2}|^{-\eta_D} < \infty. \tag{4.60}$$

The value β is affected by both the rank of $\mathbf{\Phi}_h$ and $\mathbf{R}$. If we assume that $\mathbf{\Phi}_h$ is full rank, the necessary and sufficient condition is

$$|\mathbf{R}^H\mathbf{R}|^{-\eta_D} < \infty. \tag{4.61}$$

(Q.E.D.)

APPENDIX 4.E

PROOF OF THEOREM 5

Let us assume that $L \leq T$. Then the probability density function (pdf) of $\mathbf{R}\mathbf{R}^H$ is given as [46]

$$f_{\mathbf{R}\mathbf{R}^H}(\mathbf{Z}) = \frac{1}{c_{L,T}} \int_{\Gamma} p(\sqrt{\mathbf{Z}}\tilde{\mathbf{U}}) \det(\mathbf{Z})^{T-L} \mu(d\mathbf{U}), \tag{4.62}$$

where $L \times L$ matrix $\mathbf{Z} \in \Lambda$, $\mathbf{U} = (u_{ik}) \in \Gamma$, $\tilde{\mathbf{U}} = (u_{ik})_{i=1\ldots L,\ k=1\ldots T}$, $c_{L,T} = \pi^{L(L-1)/2-LT} \prod_{k=1}^{L}(T-k)!$. Also, Γ denotes the set of unitary $T \times T$ matrices and μ is the normalized Haar measure on it, and Λ denotes the set of Hermitian positive definite matrices. By using the formula for the pdf of $\mathbf{R}\mathbf{R}^H$, we conclude that $E\{\det(\mathbf{R}\mathbf{R}^H)^{-1}\} < \infty$ if and only if the integral

$$I \triangleq \int_{\Lambda} \int_{\Gamma} p(\sqrt{\mathbf{Z}}\tilde{\mathbf{U}}) \det(\mathbf{Z})^{T-L-1} \mu(d\mathbf{U}) d\mathbf{Z} \tag{4.63}$$

is finite. The notation $d\mathbf{Z}$ refers to the Lebesgue measure on the set of $L \times L$ dimensional matrices. The proof follows by bounding the integral (4.63) under the given conditions of the Theorem. See [42, Theorem 3] for a similar proof for the flat fading case, i.e., $\eta_D = 1$. For $L \geq T$, the proof can be easily extended by replacing $\mathbf{R}\mathbf{R}^H$ by $\mathbf{R}^H\mathbf{R}$. (Q.E.D.)

CHAPTER 5

DELAY-CONSTRAINED CROSS-LAYER DESIGN OVER MULTIUSER CHANNELS

5.1 Wireless Multiple Access Channels

Wireless multiple access channel has been studied extensively from two perspectives. The first one assumes the simplified random access for wireless packet switched networks, [73]. There under the simplified collision model, the nodes implement decentralized strategies that solve the resource allocation problem of giving channel access to users when buffers are full of data to transmit. The second perspective is the physical layer perspective which studies the optimum resource allocation problem, trying to determine how to multiplex signals from independent sources to approach the limiting efficiency mandated by the multiuser capacity region boundary, [71].

Considering the second perspective, the results in [63] and [66] have shown that, under a sum power constraint, the throughput of a wireless multiple access channel with nodes having equal fading statistics is maximized using a time-sharing policy that assigns the channel to the user that is currently experiencing the maximum channel gain. The policy has been named *opportunistic multiple-access* and it has the interesting property of leading to a logarithmically increasing throughput with the number of users. Remarkably, this outcome is better than the one obtained from multiple access channels without independently faded links. This fact has lead to the concept of *multi-user diversity*. The key assumption behind [63] and [66], and much of the work focused on the physical layer perspective claims that the network objective is to achieve the maximum aggregate throughput. In-

teresting variations of classical packet switched network protocols were introduced in [69] and [70], where the channel state information is used to modify either the retransmission probability (Opportunistic ALOHA) or the priority transmission delay (Opportunistic CSMA) of the nodes contending for the medium. At the cost of having to feedback channel state information to the transmitters, these methods bring multi-user diversity gains in the class of random access methods.

It has been first noted in [68] that both perspectives are somewhat too skewed. The network perspective is that the channel is allocated in response to the state of the users' queues, assuming that the conditions of the channel are equivalent at all times, while the physical layer perspective is that the channel state should drive the resource allocation as if the users are constantly backlogged, the users can wait nearly indefinitely, and the transmission resources are the scarce commodity. Both perspectives do not reflect well the nature of the actual resource allocation problem that network, multiple-access and physical layers have to solve, particularly when dealing with sources that have a limited degree of flexibility, such as for example multi-media sources. Therefore the question posed in [68] was what the allocation policy should be that takes into consideration both the users' backlog as well as the relative condition of their channels.

In fact, the purely PHY layer perspective was formulated in information-theoretic way by Tse's work in [66], where the scheduling of packets transmitted over wireless channels is based on the channel condition without considering the application layer delay constraints. In the meantime, the cross-layer (PHY-MAC) perspective was investigated by Negi et al. in [64], Rajan et al. in [62], and others. Negi et al. in [64] attempted to obtain a Quality of Service (QoS) exponent in time-varying channel, by considering information-theoretically optimal channel

codes with a joint queueing-coding approach. Their joint approach combined large deviation effective capacity with random coding bounds, where it aims to find the ultimate asymptotic limit of delay-bounded communications. Assuming a memoryless independent and identically distributed (i.i.d.) block fading channel, their calculation of the error exponent in decoding error probability was better than that in a pure coding system, implying that the joint approach can provide significantly better QoS, as compared to the pure coding approach.

Rajan et al. in [62] have shown that packet scheduling based on queue state can trade off targeted mean queueing delay with transmitted power. Their goal was to find the efficient transmit-power minimizing schedulers under the queueing delay constraints. Also thanks to subsequent developments by Yeh et al. in [67] it was shown that the strategy called *Longest-Queue-Highest-Possible-Rate* (LQHPR) was the allocation strategy that lead to the maximum stable throughput of the network which interestingly coincides with the capacity region.

The policy works as follows: each corner of the capacity region corresponds to a certain permutation of the users. The rate vector assigned to each user in a greedy manner is determined by the permutation of the queue length vector such that longer queues receive higher rates. Thereafter, Yeh et al. in [67] argued that LQHPR provides the shortest average queue length per user and hence, by means of Little's law, minimizes the average delay of packets with an appropriate rate allocation policy bounded by multi-access capacity region. Finally, the work in [67] imposes a sum power constraint and minimizes the average queue length under such constraint.

5.1.1 Motivation

More often the quality of service constraints for wireless multiple access channels are expressed in terms of delay constraints. The issue then becomes that of finding the minimum average power that can be spent to meet the delay constraint.

Rajan et al. in [62] conjectured that small increases in average delay would allow substantial savings in transmission power, and implemented the optimal scheduler and a sub-optimal scheduler, called as *log-linear* scheduler. Their optimal scheduler was numerically obtained by dynamic programming technique, called as Value Iteration Algorithm (VIA) [74], which had the computational complexity of order of L^3 where L is the buffer length. They also introduced a simple log-linear scheduler. The log-linear scheduler removes a subset of the entries in the buffer. The number of entries removed is a logarithm function proportional to the current queue length at a given time slot. This scheduler had a similar level of delay/power performance as the optimal scheme. However, their work assumed the finite buffer size for a single-user case. Thus their work does not carry over to the case of infinite queues.

In this chapter, we present a powerful suboptimal power/rate control strategy with *modified-linear-rule* (MLR) scheduler, which applies to the multiuser case with unlimited buffer size. Our work extends the results obtained in [62] and numerically verifies the analysis therein.

5.2 System Model

In this section we introduce the basic models and notation used throughout the Chapter to describe both the physical layer and the users' queues dynamics.

5.2.1 Block Flat Fading Model and Capacity Region

We consider a wireless multiple access system with I users over a block flat fading channel model, and we assume Additive White Gaussian Noise (AWGN).

In the lth time slot, N Nyquist samples of the received signal are collected. Then the discrete-time model for the recived samples $R_l[n]$ becomes

$$R_l[n] = \sum_{i=1}^{I} H_{l,i}[n] S_{l,i}[n] + Z_l[n]\,,\ n = 1, ..., N, \tag{5.1}$$

where I is the number of users, $S_{l,i}[n]$ and $H_{l,i}[n]$ denote the transmitted signals and the fading coefficient of the ith user in the lth slot, while $Z_l[n]$ is the complex circularly symmetric white Gaussian noise with variance $\sigma^2 = N_0 W$, where W is the available bandwidth.

For the simple situation where the channel is static over the transmission of the packet, the signal of user i is attenuated by a factor of $h_{l,i}$, i.e. $H_{l,i}[n] = h_{l,i}$ constant for all times n.

Let $\mathbf{H}_l$=$(h_{l,1}, \cdots, h_{l,I})^T$ and $\mathbf{P}_l$=$(P_{l,1}, \cdots ., P_{l,I})^T$ be the channel state vector composed of flat fading channel coefficients and allocated power vector for each user, respectively. Let also, $\mathbf{r}_l$=$(r_{l,1}, \cdots, r_{l,I})^T$ be the vector of user rates and $\mathbf{r}_l(S)$ be the subvector having the entries of $\mathbf{r}_l$ that correspond to the indexes of a specific subset S of users in $\{1, 2, \cdots, I\}$. Assuming that the flat fading parameters are

all known at the transmitters and the receivers, the capacity region $C_G(\mathbf{H}_l, \mathbf{P}_l)$ for the Gaussian multi-access channel becomes [66]

$$C_G(\mathbf{H}_l, \mathbf{P}_l) = \{\mathbf{r}_l : \mathbf{r}_l(S) \leq \frac{1}{2}\log(1 + \frac{\sum_{i\in S}|h_{l,i}|^2 P_{l,i}}{\sigma^2})$$

$$\text{for every } S \subset \{1, 2, ..., I\}\}, \text{ (bits/transmission)} \tag{5.2}$$

The factor of $\frac{1}{2}$ comes from the entropy calculation in Gaussian distribution.

Note that $\mathbf{r}_l(S)$ in (5.2) is characterized by $2^{|S|} - 1$ constraints, where $|S|$ is the cardinality of S. In total we have $I!$ vertices in the positive quadrant, which can be found from one of $I!$ possible orderings by a successive decoding [66].

5.2.2 Queue Model

We mean *packet* by a set of data bits in variable length.

For l-th time slot, let $x_{l,i}$ and $a_{l,i}$ be the number of data bits taken on $[0, L]$ and the number of arriving bits taken on $[0, M]$, respectively. Then, queue state vector and arrival vector can be defined as $\mathbf{x}_l = (x_{l,1}, ..., x_{l,I})^T$ and $\mathbf{a}_l = (a_{l,1}, ..., a_{l,I})^T$. In the case of finite buffer length L for all users, we have the queue state equations for the i-th user as follows:

$$x_{l+1,i} = \min(x_{l,i} + a_{l,i} - r_{l,i}, L), \tag{5.3}$$

which can be written in the following vector form

$$\mathbf{x}_{l+1} = \min(\mathbf{x}_l + \mathbf{a}_l - \mathbf{r}_l, \mathbf{L}) \tag{5.4}$$

where $\mathbf{L} = (L, \cdots, L)^T$. If we denote time average arrival bits per unity of the i-th user as λ_i, i.e. $\lambda_i = E\{a_{l,i}\}$, the average packet delay $\{D_{avg}\}_i$ for the i-th user is

found from the Little's theorem [62]:

$$\{D_{avg}\}_i = \frac{E\{x_{l,i}\}}{\lambda_i}. \tag{5.5}$$

Since we cannot transmit more packets than available in the queue, then we have a constraint $0 \leq r_{l,i} \leq x_{l,i}$. Our intuition is such that the smallest delay would be achieved when all buffered packets are transmitted in each time slot.

A *scheduler*, denoted as α, is a mapping from the current buffer state vector $\mathbf{x}_l$ and the channel state vector $\mathbf{H}_l$ to the vector of rates $\mathbf{r}_l$ and the corresponding power $\mathbf{P}_l$ such that $\alpha : (\mathbf{x_l}, \mathbf{H_l}) \mapsto (\mathbf{r_l}, \mathbf{P_l})$ and it is characterized by the conditional probabilities Prob $((\mathbf{r}_l, \mathbf{P}_l)|(\mathbf{x}_l, \mathbf{H}_l))$. We restrict our scheduler to *zero-outage* scheduler [62], where packets are not dropped at the transmitter and there occur no overflows. Let us denote scalar and vector format of the scheduler, respectively, as $\alpha^{(\mathbf{i})}_{\mathbf{j},\mathbf{k}} = \Pr(r_{l,i} = j | x_{l,i} = k)$ and $\alpha_{\mathbf{j},\mathbf{k}} = \Pr(\mathbf{r}_l = \mathbf{j} | \mathbf{x}_l = \mathbf{k})$, where $\mathbf{j}=(j_1, \cdots, j_I)^T$ and $\mathbf{k}=(k_1, \cdots, k_I)^T$. When the noise is assumed to be additive white Gaussian and $\{\mathbf{H}_l \equiv \mathbf{1}\}$, then we can represent each scheduler by a $(L+1) \times (L+1)$ matrix [62], because buffer size L for each user is identical.

5.3 Multiuser Access Link

In this section we propose low complexity rate allocation strategies that meet the user power constraints. We assume that the fading processes for all users are jointly stationary and ergodic.

5.3.1 Optimal Scheduler

We consider the multi-user rate vector $\mathbf{r}_l$ as the extension of the single-user rate $r_{l,i}$. From results in [75], the capacity function $C_{l,i}$ for the i-th user normalized by the bandwidth W is expressed as:

$$C_{l,i}(P_{l,i}, h_{l,i}) = \log(1 + \frac{|h_{l,i}|^2 P_{l,i}}{\sigma^2}) \text{ , (bits/Hz).} \tag{5.6}$$

The corresponding power control is determined by the maximum reliable rate associated with (5.6) and can be expressed as follows,

$$P_{l,i}(r_{l,i}, h_{l,i}) = \frac{\sigma^2}{|h_{l,i}|^2}(e^{r_{l,i}} - 1). \tag{5.7}$$

Note that $\mathbf{P}_l$ is a strictly convex function of $\mathbf{r}_l$. Thus we can obtain a good estimate of $\mathbf{r}_l$ in the form of $\log(\kappa \mathbf{x}_l)$ (κ: design parameter) since a linear increase in the packets taken from the current queues corresponds to an exponential increase in the required transmit power.

Following Theorem 8 and Lemma 9 in [62], we can generalize characterization of the delay-power region to the multi-user scheduling case. This region is characterized by the minimal average transmit power required for any packet delay over all zero-outage schedulers Θ=$\{\alpha : \alpha \in S, \alpha \text{ is zero outage}\}$. The minimum average power $\{P^\star(D_0)\}_i$ for the i-th user required to achieve average delays no greater than D_0 is (cf. see [62], [77])

$$\{P^\star(D_0)\}_i = \min_{\Theta \cap D} \lim_{l \to \infty} E\{P_{l,i}\} \tag{5.8}$$
$$E[x_{l,i}] \leq \lambda_i D_0$$

where D_0 is the average delay bound.

Provided that packet arrivals are independent and identically distributed (i.i.d.), memoryless property of scheduler guarantees the stationarity of $\mathbf{x}_l$. Then, $\mathbf{x}_l$ be-

comes a Markov chain with the transition probability matrix $\mathbf{T}^{(i)} = [T_{j,k}^{(i)}]$ of the i-th user, where $T_{j,k}^{(i)} = P(x_{l+1,i} = j | x_{l,i} = k)$ is independent of the index of the time-slot l. If we denote buffer state vector $\mathbf{k}$ with each entry k_i of stationary probability as $s_{\mathbf{k}}$, i.e. $P(x_{l,i} = k_i) = s_{k,i}$ where $s_{\mathbf{k}} = (s_{k,1}, \cdots, s_{k,I})^T$, then we have

$$\mathbf{T}^{(i)} s_{k,i} = s_{j,i} \tag{5.9}$$

where $\mathbf{T}^{(i)}$ depends on the choice of scheduler α and $s_{\mathbf{j}}$, $s_{\mathbf{k}}$ are functions of α. The average packet delay $\{D_{avg}(\alpha)\}_i$ and the average transmission power $\{P_{avg}(\alpha)\}_i$ of any scheduler for the user i are obtained by (cf. see [62], [77])

$$\{D_{avg}(\alpha)\}_i = \frac{E\{x_{l,i}\}}{\lambda_i} = \frac{1}{\lambda_i} \sum_{k=0}^{L} k s_{k,i} \tag{5.10}$$

$$\{P_{avg}(\alpha)\}_i = E\{P_{l,i}\} = \sum_{k=0}^{L} s_{k,i} \sum_{j=0}^{k} \alpha_{j,k} P_{l,i}(j, h_{l,i}). \tag{5.11}$$

Let us now consider the two-user uplink case with $\mathbf{j} = (j_1, j_2)$ and $\mathbf{k} = (k_1, k_2)$. In this case the transmission power for each user is $P_{l,i}(j_1, j_2, h_{l,1}, h_{l,2}) = \sigma^2(e^{j_i} - 1)$ for $i = 1, 2$. Then the optimal packet scheduling can be found by solving the following constraint minimization problem [74]:

$$\min_{\alpha_{j,k}} \sum_{k_1=0}^{L} \sum_{k_2=0}^{L} s_{k_1,1} s_{k_2,2} \sum_{j_1=0}^{k_1} \sum_{j_2=0}^{k_2} \alpha_{j,k} P_{l,i}(j_1, j_2, h_{l,1}, h_{l,2})$$

$$\text{s.t.} \quad \sum_{k_i=0}^{L} k_i s_{k_i,i} \leq \lambda_i D_0 \quad \text{for } i = 1, 2. \tag{5.12}$$

In general, in I-user scenario, the transition probability matrix is defined by the relations

$$\begin{aligned} T_{j,k}^{(i)} &= Pr(x_{l+1,i} = j_i | x_{l,i} = k_i) \\ &= Pr(\min(k_i - r_{l,i} + a_{l,i}, L) = j_i | x_{l,i} = k_i) \end{aligned}$$

where for $i = 1, \cdots, I$, k_i, j_i takes an integer value from 0 to L. As mentioned in the Section 5.1.1, we utilize the dynamic programming technique (VIA) to find

the multi-access delay-power region. Let $\mathbf{r}_l^*(\mathbf{x}_l)$ and $\mathbf{P}_l(\mathbf{r}_l, \mathbf{H}_l)$ be the optimal rate vector composed of multi-user rates, i.e. $(r_{l,1}^*, \cdots, r_{l,I}^*)^T$ and the power vector composed of multi-user powers, i.e. $(P_{l,1}, \cdots, P_{l,I})^T$, respectively. Then, from (5.8) our goal is to minimize the cost function $\mathbf{J}_l$ in vector form

$$\mathbf{J}_l \triangleq \mathbf{P}_l(\mathbf{r}_l, \mathbf{H}_l) + \varepsilon(\mathbf{x}_l - \mathbf{L}) \tag{5.13}$$

where ε is the Lagrangian vector used in solving (5.8).

Let m be the number of VIA iterations and $\mathbf{v}_m(\mathbf{j})$ be the difference vector between the m-th and $(m-1)$-st state. Also, $\mathbf{v}_m(\mathbf{j})$ is used to minimize norm of the difference vector between $\mathbf{J}_{l-1}$ and $\mathbf{J}_l$ in (5.13). Then we can generalize (5.12) into an I-user case as follows:

$$\mathbf{r}_l^*(\mathbf{x}_l) = \text{argmin} \left\{ \mathbf{J}_l + \sum_{\mathbf{j}} \mathbf{T}_{\mathbf{j},\mathbf{x}_l}(\mathbf{r}_l)\mathbf{v}_m(\mathbf{j}) \right\} \tag{5.14}$$

where $\mathbf{T}_{\mathbf{j},\mathbf{x}_l}(\mathbf{r}_l)$ is defined as the vector composed of transition probability entries for all I users, that is, $\mathbf{T}_{\mathbf{j},\mathbf{x}_l}(\mathbf{r}_l) = (T_{j,k}^{(1)}, \cdots, T_{j,k}^{(I)})^T$.

The number of states in the VIA increases exponentially and thus the cost of computing the optimal scheduler becomes prohibitively high. Hence in the next section we present a suboptimal log-linear scheduler due to [62] and generalize to a multi-user case which we call a *modified-linear-rule* scheduler.

5.3.2 Suboptimal Schedulers

The single-user *log-linear* scheduler [62] can be easily extended to the multi-user case where it is defined by the following relation (to simplify notations we drop the user index i),

$$\mathbf{r}_l = \min(\mathbf{x}_l, \lfloor \log(\kappa \mathbf{x}_l) \rfloor) \tag{5.15}$$

where κ is chosen to meet the desired delay bound D_0. The parameter κ is found iteratively. In iteration l the approximation κ_l of κ is derived from the previous approximation κ_{l-1} based on the mean arrival rate and has the following form

$$\kappa_l = \kappa_{l-1} + \delta_\kappa(\hat{D}_l - D_0) \tag{5.16}$$

where $\hat{D}_l$ is the sample average delay and δ_κ is the user defined sensitivity factor. The logic behind the policy of the log-linear scheduler is that it tends to choose a rate $\mathbf{r}_l(\mathbf{x}_l)$ so that the power in each time slot is linearly proportional to $\mathbf{x}_l$.

Based on the ideas of the log-linear scheduler we propose a simple *modified-linear-rule* scheduler which can be applied to the case of unlimited buffer size. This scheduler is a generalization of (5.4) without buffer constraint $\mathbf{L}$, and it is modeled by the following relationship

$$\mathbf{r}_l = \min\left(\mathbf{x}_l, \sum_{k=1}^{K} \alpha_k \mathbf{x}_{l-k} + \beta \mathbf{e}_l\right) \tag{5.17}$$

where we define $\mathbf{e}_l$ by an elementary vector with all entries equal to unity, K is the length of recursive filter, and α_ks, β are design parameters found from the typical linear estimation problem. The logic behind the linear rule is to let the queue equations behave similarly to that of a stable feedback filter, which is smoothing the traffic that arrives at the queue. In fact, if the positivity constraint L in (5.7) is removed, for a sufficiently large buffer size ($L \to \infty$), the buffer state equation becomes

$$\mathbf{x}_l = \mathbf{a}_l - \sum_{k=2}^{K} \alpha_k \mathbf{x}_{l-k} + (1-\alpha_1)\mathbf{x}_{l-1} - \beta \mathbf{e}_l \tag{5.18}$$

This policy provides the ability to control mean and variance of $\mathbf{x}_l$ by choosing different smoothing parameters α_k. Since the choice of the parameters affects the power consumption directly, they should be chosen to provide the best compromise between delay and power.

To determine the best choice of α_k's and β analytically, let us introduce the classical linear estimation problem as follows [76]

$$Y \approx g(X) = \sum_{k=1}^{K} a_k X_{l-k} + b \tag{5.19}$$

where by associating (5.18) with (5.19) scalar values Y, X_{l-k} and b correspond to $\mathbf{x}_l$, $\mathbf{x}_{l-k}$'s ($k = 1, \cdots, K$) and $\mathbf{a}_l - \beta \mathbf{e}_l$ in (5.18), and a_k's correspond to the coefficients of $(1 - \alpha_1)$ for $k = 1$ and $-\alpha_k$ for $k = 2, \cdots, K$, which we denote as $\overline{\alpha_k}$. The optimal design parameter β^* is found by taking the expectations on both sides in (5.18):

$$\beta^* = E[\mathbf{x}_l] - \sum_{k=1}^{K} \overline{\alpha}_k E[\mathbf{x}_{l-k}] + E[\mathbf{a}_l] \tag{5.20}$$

where $E[\mathbf{a}_l] \triangleq (\lambda_{l,1}, \cdots, \lambda_{l,I})^T$.

Since all entries of $E[\mathbf{a}_l]$ are deterministic constants, the Minimum Mean Square Error (MMSE) problem is formulated from the difference between the l-th queue state and its best estimate in (5.17) as follows:

$$\min_{\overline{\alpha_k}} E[(\mathbf{x}_l - \sum_{k=1}^{K} \overline{\alpha_k} \mathbf{x}_{l-k} - \beta^*)^2]. \tag{5.21}$$

Let us denote inner product of two vectors as operator $'\odot'$. Then we apply the orthogonal condition [76], which states that the estimate error is orthogonal to the observations, and we have for $k = 1, \cdots, K$

$$E[(\mathbf{x}_l - \beta^* - \sum_{k=1}^{K} \overline{\alpha_k} \mathbf{x}_{l-k}) \odot \mathbf{x}_{l-k}] = 0 \tag{5.22}$$

From a set of K linear equations in (5.22), we construct the following relationship,

$$\begin{bmatrix} E[\mathbf{x}_{l-1} \odot \mathbf{x}_l] \\ E[\mathbf{x}_{l-2} \odot \mathbf{x}_l] \\ \vdots \\ E[\mathbf{x}_{l-K} \odot \mathbf{x}_l] \end{bmatrix} = \mathbf{C} \begin{bmatrix} \overline{\alpha_1} \\ \overline{\alpha_2} \\ \vdots \\ \overline{\alpha_K} \end{bmatrix} + \beta^* \begin{bmatrix} E[\mathbf{x}_{l-1}] \\ E[\mathbf{x}_{l-2}] \\ \vdots \\ E[\mathbf{x}_{l-K}] \end{bmatrix} \tag{5.23}$$

where

$$\mathbf{C} \triangleq \begin{bmatrix} E[\mathbf{x}_{l-1} \odot \mathbf{x}_{l-1}] & E[\mathbf{x}_{l-1} \odot \mathbf{x}_{l-2}] & \cdots & E[\mathbf{x}_{l-1} \odot \mathbf{x}_{l-K}] \\ E[\mathbf{x}_{l-2} \odot \mathbf{x}_{l-1}] & E[\mathbf{x}_{l-2} \odot \mathbf{x}_{l-2}] & \ddots & \vdots \\ E[\mathbf{x}_{l-3} \odot \mathbf{x}_{l-1}] & \ddots & \ddots & \vdots \\ \vdots & \dots & \cdots & E[\mathbf{x}_{l-K} \odot \mathbf{x}_{l-K}] \end{bmatrix}$$

and further we can find the optimal estimates $\overline{\alpha_k^*}$s. Depending on the autocorrelation of the queue state we can obtain a set of sub-optimal coefficients for our *modified-linear-rule* scheduler.

5.4 Numerical Results

5.4.1 Single-user Scheduling

In Fig. 5.1 (L=50, M=6, σ^2=0.5), we plot the average delay-power curve for the optimal scheduler (obtained through VIA) and the log-linear scheduler for AWGN channels ($\mathbf{H}_l \equiv \mathbf{1}$). The log-linear scheduler is clearly sensitive to noise variance, and we realize that the smaller noise leads to the additional power savings, as expected. Instead of updating κ as in the adaptive log-linear scheduler over each iteration, we obtain an typical log-linear scheduler curve by fixing the value of κ=$\frac{10}{D_0}$.

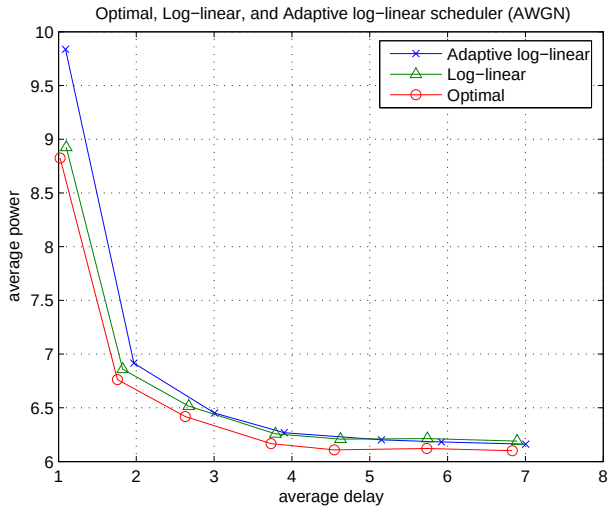

Figure 5.1: Delay-Power curves over AWGN channels (σ^2=0.5)

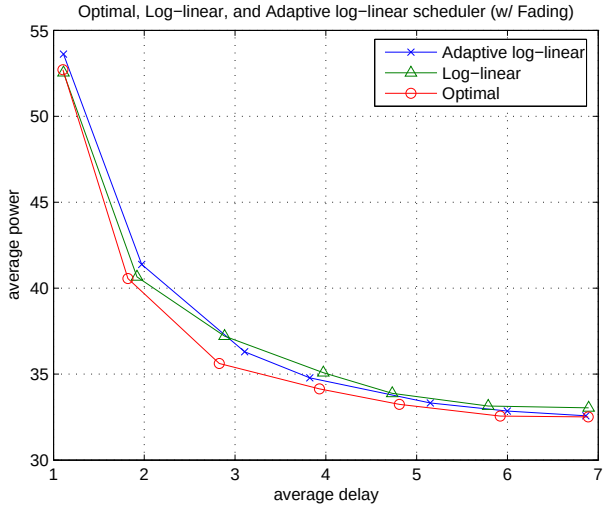

Figure 5.2: Delay-Power curves over Rayleigh fading channels

In Fig. 5.2, the parameters are the same as in Fig. 5.1 except that the channel is modeled as *Rayleigh* fading (σ_H^2=0.15: squared mean value of the channel fading coefficients). We see that in both cases that the optimum and log-linear schedulers perform similarly and that there are significant power savings in relaxing the delay constraints. Also, it is evident that in the delay constrained case, the channel fading causes a considerable additional cost (approximately over 5 times of the AWGN case) in terms of the average power required for the same average delay

constraint compared with Fig. 5.1.

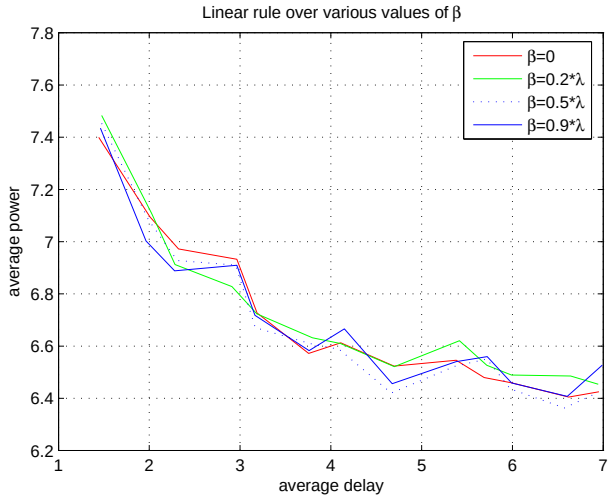

Figure 5.3: Delay-Power curves of the MLR scheduler (proposed)

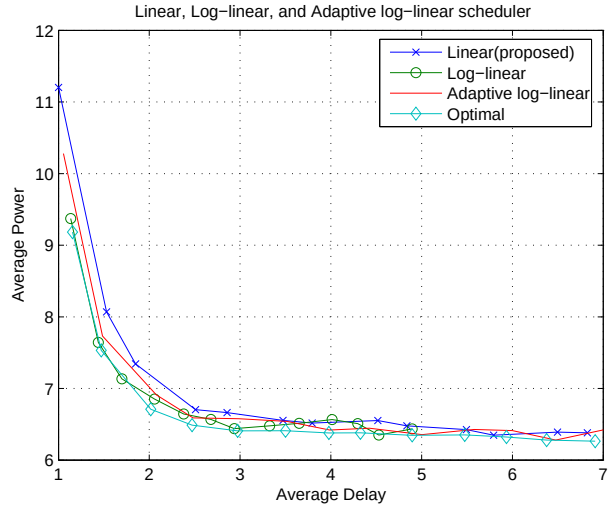

Figure 5.4: Optimal scheduler and various suboptimal schedulers

Fig. 5.3 obtained from 10,000 Monte Carlo simulations provides the performance of the MLR scheduler associated with the various values of β. Changing β in a non-fading case (AWGN, σ^2=0.5), we obtain the best choice of β, which gives the minimum variance of average power for $\beta = 0.5\lambda$: i.e. $var(D_{avg})$=0.0793. As shown in the plots, choosing any β's between 0 and λ does not change performance by much.

In Fig. 5.4 we see the average delay-power curves of both the MLR scheduler (proposed) and the optimal scheduler for a single-user case in *Rayleigh* fading environments (σ_H^2=0.75). Though the MLR scheduler requires on the average a little more transmit power relatively to the optimal scheduler, taking the value of β nearly proportional to the average arrival rate λ offers much simpler scheduler at a low computational cost. Hence, we can determine the best choice of coefficients pair (α,β) for the MLR scheduler for a single-tap case ($K = 1$) from the relation (5.17). Also, by examining performance curves for $\beta = 0 : 0.05\lambda : \lambda$, we see that there exists a local minimizer ($\approx 0.495\lambda$) around the half of the average arrival rate, leading to the minimum variance of average transmit power.

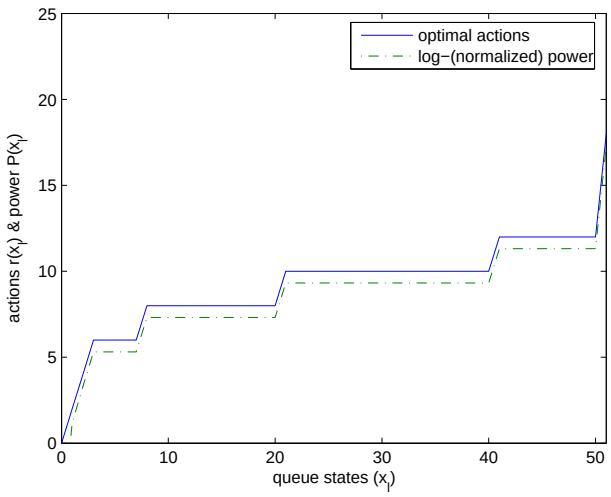

Figure 5.5: Optimal actions (rescaled) and logarithmic power versus queue states in a two-user case

5.4.2 Two-user Scheduling

Fig. 5.5 illustrates the optimal actions for each queue in a two-user case. The performance curves are derived under assumption of the same average arrival rates (λ_1=λ_2=3). Then, we observe that the logarithmic average power curve follows

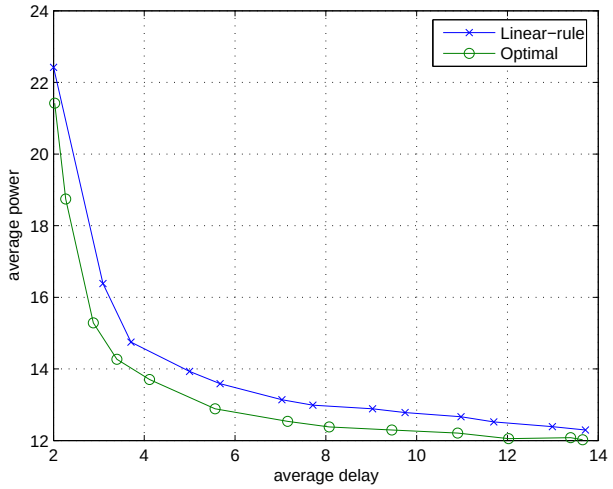

Figure 5.6: Delay-Power curves of the MLR scheduler in a two-user case

the optimal actions taken for two-user queues. In a similar way, we extend and generalize the single-user case in [62] to the multiuser case, finding the optimal number of packets which leave the buffer. Thanks to the exponential relationship of convexity in (5.7) between the queue state and the transmit power, from the comparison of '$r_{l,i}$ - $x_{l,i}$' curve with the 'log $\frac{|h_{l,i}|^2}{\sigma^2}P_{l,i}$ - $x_{l,i}$' curve (normalized), we show that the MLR scheduler with '$r_{l,i} = \alpha x_{l,i} + \beta$' is a simple rate allocation strategy, which leads to '$r_{l,i} - \log \frac{|h_{l,i}|^2}{\sigma^2}P_{l,i} \approx 1.05$' in each flat interval. For this case, we find the suboptimal pair of coefficients equal to $\alpha = 1$ and $\beta = 0.05$.

In Fig. 5.6 (L_1=L_2=50, M_1=M_2=6, σ^2=0.5), assuming that both users have two independent arrivals with the same average arrival rates, the two-user delay-power curve in Rayleigh fading (σ_H^2=0.75) was obtained by applying VIA and using the MLR scheduler where the previous parameters remains the same. As shown in Fig. 5.5 and Fig. 5.6, it turns out that the MLR scheduler requires low complexity but results in delay-power curve close to the optimal scheduler even in the multi-user case.

5.5 Summary

In this chapter we have studied several schedulers over AWGN and fading channels that incorporate buffer and power constraints, in particular which minimize the transmit power under the average delay constraints. We have also provided the characteristics of the optimal delay-power curve for the two-user case. For limited buffer size, we propose a simple *modified-linear-rule* (MLR) scheduler with low cost complexity for large buffer delay. Our MLR scheduler can be substituted for the optimal scheduler at a slightly higher power consumption, but still with a good convergence rate, which could extend to the multiuser access flat-fading channels.

CHAPTER 6

OPTIMAL POWER CONTROL FOR PLC-EMBEDDED COOPERATIVE SYSTEMS

6.1 Hybrid PLC/Wireless Link

In radio propagation environments, there may be blind zones caused by surrounding buildings in the area covered by the transmitter. In such situations several terminals can serve as intermediate nodes which relay the transmitted signal to the receiver. Cooperative relaying is an effective communication technique that offers better quality of communication link and increased channel capacity, [1]-[2]. Information-theoretically, channel capacity depends on the signal-to-noise ratio (SNR) of received signals. In practical systems, there exist resource constraints among those terminals involved in relaying; such as transmit power, encoding/decoding schemes, etc. Therefore, finding the best transmit power allocation strategy between transmitter and relay which achieves maximum SNR at receiver and maximizes channel capacity is an important consideration.

Here we consider cooperative communication with single relay selection, [3]. In that scheme a relay selection mechanism is considered jointly with transmission power control. A set of potential relays determine their transmission power needed to participate in the cooperative communication. The relay which minimizes the overall power consumption is chosen. The relay selection is done in a distributed manner with minimum communication overhead.

6.1.1 Motivation

Due to spatial diversity MIMO techniques based on antenna arrays can dramatically reduce the required transmission power for certain throughput requirements. In cases when each node is limited to a single antenna, multiple nodes could collaborate to form a virtual antenna array to achieve spatial diversity [4]. Compared with multinode cooperative communication schemes, single relay cooperation schemes need neither cooperative beamforming nor distributed space-time coding.

Thus they incur less cooperation overhead and are much easier to implement. Besides, they can potentially achieve the same diversity multiplexing tradeoff as that of multinode cooperative schemes. Hence, single relay selection cooperative strategies are practically appealing, [4]. Most of the work on selective cooperation schemes focuses on the multiplexing diversity tradeoff property, where a fixed power level is usually assumed at the source and relays. Power control issues are investigated in [5]- [8] from an information theoretic point of view based on the outage probability analysis.

It is well known that PLC offers a fully developed infrastructure of electrical power distribution grid for reliable data transmission. Thus we propose to replace a weak wireless link by a stable PLC link. We show that such hybrid scheme can improve overall communication quality. Based on single or two-hop relaying links experiencing Rayleigh fading, we propose an adaptive power allocation scheme under transmit power constraints which guarantees optimal system efficiency. Our proposed scheme involves the decode-and-forward (DF) relaying and orthogonal frequency division multiplexing (OFDM). For a realistic relaying scenario numerical tests indicate that PLC/wireless link performs better then a typical wireless link.

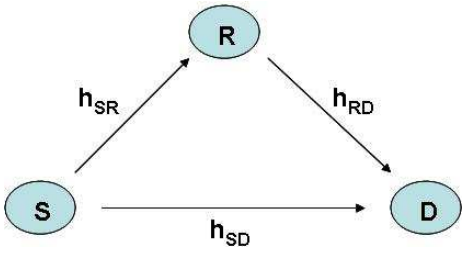

Figure 6.1: Pictorial schematic for a 3-node cooperative network Model

6.2 System Model

We first consider a simple 3-node relay network with source (S), relay (R) and destination (D) nodes as shown in Fig. 6.1. For simplicity we start with analyzing a single-input single-output (SISO) point-to-point communications for each node. We next apply the analysis to a in-home test model shown in Fig. 6.2 which illustrates a hybrid communication scheme involving PLC and WiFi.

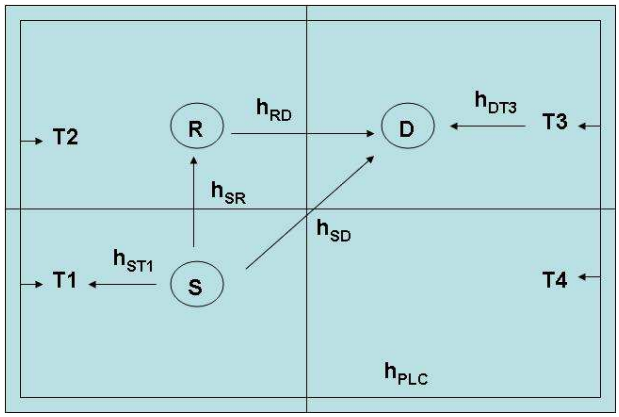

Figure 6.2: A practical model for PLC-embedded cooperative relay Networks

6.2.1 Relay Channel Capacity and Optimal Power Allocation

Denoting transmit and received signals as s and x_i (i=SD, SR, RD), respectively, we can express the received signals as follows:

$$x_{SD} = h_{SD}s + w_{SD} \tag{6.1}$$

$$x_{SR} = h_{SR}s + w_{SR} \tag{6.2}$$

$$x_{RD} = h_{RD}x_{SR} + w_{RD}, \tag{6.3}$$

where h_{SD}, h_{SR} and h_{RD} are mutually independent channel coefficients for the S-D, S-R and R-D links, and w_{SD}, w_{SR} and w_{RD} are assumed to be independently, identically distributed (i.i.d.) and circularly symmetric additive white Gaussian noise with the normalized noise spectral density $N_o = 1$.

Let P_S and P_R denote powers corresponding to each node such that the total power $P^{(tot)}$ is constrained (i.e. $P_S + P_R \leq P^{(tot)}$). We now consider optimal power allocation strategies under the decode-and-forward (DF) scheme that maximizes the channel capacity.

First, if there is no direct link between S and D, the capacity of the relay path will be the smaller of the S-R and R-D link capacities. Then, for non-cooperative relay link we formulate a *max-min* problem as follows:

$$C_{non-coop} = \max_{P_S,P_R} \min \left\{ \frac{1}{2}\log(1 + |h_{SR}|^2 P_S), \frac{1}{2}\log(1 + |h_{RD}|^2 P_R) \right\}, \tag{6.4}$$

where the factor $\frac{1}{2}$ accounts for the fact that a transmission occupies two channel uses, i.e. we have equal time sharing. After some algebraic manipulation, we obtain that optimal power allocation occurs if both link capacities are equal. The

optimal powers are

$$P_S^* = \frac{P_0}{1+\frac{|h_{SR}|^2}{|h_{RD}|^2}}, \tag{6.5}$$

$$P_R^* = \frac{P_0}{1+\frac{|h_{RD}|^2}{|h_{SR}|^2}}. \tag{6.6}$$

On the other hand, if there is a direct link between S and D, we expect that more power will be allocated to S since the transmission involves both paths. For the relay path, we should guarantee that the relay R decodes the message correctly and retransmits it successfully over S-R link, and also guarantee that the destination D receives the message successfully. Thus, the optimal power allocation problem becomes

$$C_{coop} = \max_{P_S,P_R} \min \left\{ \frac{1}{2}\log(1+|h_{SR}|^2 P_S), \frac{1}{2}\log(1+|h_{SD}|^2 P_S + |h_{RD}|^2 P_R) \right\}. \tag{6.7}$$

The cooperative capacity is maximized when P_S^* and P_R^* are as follows:

$$P_S^* = \frac{P_0}{1+\frac{|h_{SR}|^2-|h_{SD}|^2}{|h_{RD}|^2}}, \tag{6.8}$$

$$P_R^* = \frac{P_0}{1+\frac{|h_{RD}|^2}{|h_{SR}|^2-|h_{SD}|^2}}. \tag{6.9}$$

By comparing (6.8) and (6.9) with (6.5) and (6.6) we see that when both direct and relay links cooperate, more power is assigned to the source S than in the case of a single hop relay link.

We now apply the optimal power allocation and wireless relay capacities derived so far to a hybrid indoor situation in which both PLC and wireless links are present. Such situation is illustrated in Fig. 1.1, where T1 through T4 are in-building power outlets for PLC-connected relay links.

We consider the situation when there is no direct wireless link between node S and node D. Thus the communication between node S and D can be realized either by relaying through node R, or by using the PLC link. We want to determine which one of the two connections is preferred over the other. We will refer to this type of communication as PLC-embedded. In our analysis we will assume the following.

(a) Noise components for all links are additive white Gaussian and mutually independent.

(b) Forward and reverse channels of all links are the same, i.e. h_{SR}=h_{RS}.

(c) Once an optimal single hop wireless link is determined, the decision to select wireless transmission or PLC-embedded transmission depends purely on their overall channel characteristics.

Our strategy for adaptive switching between wireless route and PLC-embedded one is developed in several steps below.

(1) We first find an optimal single hop relay network which corporates with a direct link between transmitter and receiver. To find this single hop relay network Lagrange multipliers method is used for minimizing the total power under the total power and data rate constraints. (Or equivalently, the dual problem of the maximum aggregate rate under individual power constraints may be considered.) Hence, only the best relay will participate in the final signal transmitting procedure.

(2) Assume that a relay network with h_{SR} and h_{RD} is found to be optimal. Then, we can concatenate these two discrete time impulse responses and find an overall impulse response $\tilde{h}_1$, where $\tilde{h}_1 \triangleq h_{RD} * h_{SR}$ means discrete time convolution.

(3) By measuring the channel transfer functions $H(f)$, see [9] and [10], we evaluate power line channel capacity for two extreme cases of a channel with high capacity and a channel with low capacity. We label the former as GOOD and the latter as POOR. These channels are segmented into N flat subchannels for OFDM implementation.

(4) By combining h_{PLC} with h_{ST1} and h_{DT3}, we find the overall channel coefficients by discrete time convolution, $\tilde{h}_2 \triangleq h_{DT3} * h_{PLC} * h_{ST1}$.

(5) Since the channel responses over power lines are functions of propagation constants and characteristic impedances, which themselves are functions of cable distance, we do not need to consider the distance of power line segments. Hence, we see that the comparison between $\tilde{h}_1$ and $\tilde{h}_2$ will determine an alternative way for reliable transmission in case when the communication through a direct link is not successful.

6.3 Outage and Ergodic Capacity for Slow and Fast Fading Channels

6.3.1 Single-user MIMO Channel Capacity

In this section we analyze a MIMO channel capacity for several channel conditions and apply it to a multiuser environment. We consider a MIMO system with n_T transmit antennas and n_R receive antennas, which has the following matrix-vector model:

$$\mathbf{x} = \mathbf{H} \cdot \mathbf{s} + \mathbf{w}, \tag{6.10}$$

where received vector $\mathbf{x}$, data vector $\mathbf{s}$, MIMO channel matrix $\mathbf{H}$ and noise vector $\mathbf{w}$ are $n_R \times 1$, $n_T \times 1$, $n_R \times n_T$ and $n_R \times 1$, respectively. We also assume that the noise process is additive white Gaussian.

In general, the MIMO channel capacity C_{MIMO} is represented by

$$C_{MIMO} = \max \log_2 \frac{\det(R_{\mathbf{xx}})}{\det(R_{\mathbf{ww}})}, \tag{6.11}$$

where $R_{\mathbf{xx}} = E\{\mathbf{x}\mathbf{x}^H\}$ and $R_{\mathbf{ww}} = E\{\mathbf{w}\mathbf{w}^H\}$ are received signal and noise covariance matrices, respectively, see [79].

When channel is regarded as slowly fading and we assume the perfect knowledge of the channel state information (CSI), we can approximate single-user (SU) MIMO channel capacity $C_{SU,out}$ in terms of *outage capacity* [78]- [79],

$$C_{SU,out} = \max_{\substack{R_{\mathbf{ss}} \geq \mathbf{0} \\ Tr\{\mathbf{R_{ss}}\} = n_T}} \log_2 \frac{\det(\mathbf{R_{ww}} + \mathbf{H}\mathbf{R_{ss}}\mathbf{H}^H)}{\det(\mathbf{R_{ww}})}, \tag{6.12}$$

where $\mathbf{R_{ss}} = E\{\mathbf{s}\mathbf{s}^H\}$, E_s is the transmit symbol energy and $Tr\{\cdot\}$ denotes the trace operator (the sum of all diagonal entries). With no knowledge of the channel at the transmitter, i.e. when $\tilde{\mathbf{R}}_{\mathbf{ss}} \triangleq \frac{\mathbf{R_{ss}}}{n_T}$ is identical to $\mathbf{I}_{n_T}$, (6.12) reduces to

$$C_{SU,out} \approx \log_2[\det(\mathbf{I}_{n_R} + \frac{E_s}{N_0}\mathbf{\Lambda})], \tag{6.13}$$

where Λ is a matrix of eigenvalues of $\mathbf{H}\mathbf{H}^H$, ($\mathbf{H}\mathbf{H}^H$=$\mathbf{Q}\Lambda\mathbf{Q}^H$ with $\mathbf{Q}$ unitary), and $\rho \triangleq \frac{E_s}{N_0}$ (N_0: noise variance) is the average received signal to noise (SNR) ratio. Equivalently, we can interpret (6.13) as r SISO channels, each having power gain λ_i (i=1, $\cdots$, r), and (6.13) simplifies to

$$C_{SU,out} \approx \sum_{i=1}^{r} \log_2 (1 + \rho\lambda_i)), \tag{6.14}$$

where r is the rank of $\mathbf{\Lambda}$ and λ_i are positive eigenvalues of $\mathbf{H}\mathbf{H}^H$.

When channel is fast fading, we utilize an ensemble average over instant capacities for a specific realization. Then, we have the single user MIMO capacity $C_{SU,erg}$ for fast-fading channels as follow:

$$\begin{aligned} C_{SU,erg} &= E_{\mathbf{H}}\{C_{SU,out}(\mathbf{H})\} \\ &= E_{\mathbf{H}}\{\log_2[\det(\mathbf{I}_{n_R} + \rho\mathbf{H}\tilde{\mathbf{R}}_{\mathbf{ss}}\mathbf{H}^{H})]\}. \end{aligned} \tag{6.15}$$

6.3.2 Multiuser MIMO Channel Capacity

When there are $K > 1$ users, interferences from other users can be treated as noise terms, and the i-th user's MIMO capacity $C^{(i)}_{MU,out}$ in the multiple user (MU) environment can be represented as follows: [12], [79],

$$C^{(i)}_{MU,out} = \max_{\mathbf{R_{ss}}\geq\mathbf{0}, Tr\{\mathbf{R_{ss}}\}=E_s} \log_2[\det(\mathbf{I}_{n_R,i} + (\mathbf{R_{ww}} + \mathbf{H}_i\hat{\mathbf{R}}_{\mathbf{ss},i}\mathbf{H}_i^H)^{-1}\mathbf{H}_i\mathbf{R}_{\mathbf{ss},i}\mathbf{H}_i^H)], \tag{6.16}$$

where $\hat{\mathbf{R}}_{\mathbf{ss},i} = \sum_{j\neq i}^{K}\mathbf{R}_{\mathbf{ss},j}$ for $i = 1, ..., K$.

In a similar way, we expand single user ergodic capacity (6.15) to multiuser ergodic capacity as follows:

$$\begin{aligned} C^{(i)}_{MU,erg} &= E_{\mathbf{H}}\{C^{(i)}_{MU,out}(\mathbf{H})\} \\ &= E_{\mathbf{H}}\{\log_2[\det(\mathbf{I}_{n_R,i} + (\mathbf{R_{ww}} + \mathbf{H}_i\hat{\mathbf{R}}_{\mathbf{ss},i}\mathbf{H}_i^H)^{-1}\mathbf{H}_i\mathbf{R}_{\mathbf{ss},i}\mathbf{H}_i^H)]\}, \end{aligned} \tag{6.17}$$

where the ergodic MU/MIMO capacity is obtained by averaging over a specific realization of $\mathbf{H}$.

Utilizing (6.16) and (6.17), we find a min-max formulation to obtain the overall channel capacity $C^{(tot)}_{MU-MIMO}$ in multi-hop relay networks, depending on whether

the channel is slow fading or fast fading

$$C_{MU-MIMO}^{(tot)} = \begin{cases} \min_i \quad C_{MU,out}^{(i)} & \text{if } \ T_c \gg \tau_d \\ \min_i \quad C_{MU,erg}^{(i)} & \text{if } \ T_c \ll \tau_d, \end{cases} \tag{6.18}$$

where T_c and τ_d are coherence time of the channel and delay requirement, respectively.

6.4 PLC Link Capacity and Adaptive Power Allocation

Now, we consider the power line channel that utilizes orthogonal frequency division multiplexing (OFDM) modulation. The channel is divided into N narrowband flat fading subchannels of bandwidth $\Delta f{=}\frac{B}{N}$, where B is the overall bandwidth, (usually 30 MHz) and we denote symbol period as T_s. The measured transfer function of the k-th frequency samples of the i-th user is $H^{(i)}(k\Delta f)$ ($k{=}1,\cdots,N$). Then, the power line channel capacity $C_{OFDM,i}$ for the i-th user becomes [58]

$$C_{OFDM,i} \approx \frac{\Delta f}{T_s} \sum_{k=1}^{N} \log(1 + \frac{T_s P^{(i)}(k)|H^{(i)}(k\Delta f)|^2}{\Delta f N_o}), \tag{6.19}$$

where each user has the individual and total power constraints that are $\sum_{k=1}^{N} P^{(i)}(k)$ $=P^{(i)}$ $(i = 1, \cdots, K)$ and $\sum_{j=1}^{K} P^{(j)}{=}P^{(tot)}$, respectively.

In order to evaluate h_{PLC} for the scenario illustrated in Fig. 6.2, we consider a single user scenario ($i = 1$) in (6.19) and find N discrete time channel responses $h_{PLC}(n)$ $(n = 1, \cdots, N)$ corresponding to N subcarriers as follows:

$$h_{PLC}(n) = \frac{1}{N} \sum_{k=1}^{N} e^{j2\pi \frac{k \triangle f}{N} n} H(k \triangle f). \tag{6.20}$$

With respect to the k-th subchannel power for the i-th user, we categorize two possible CSI cases and consider uniform and adaptive power loading schemes.

i) No CSI at the transmitter:

We normally resort to equal power loading strategy,

$$P^{(i)}(k) = \frac{1}{NK} P^{(tot)} \,. \tag{6.21}$$

ii) Full CSI at the transmitter:

Using the waterfilling strategy [11], we find optimal power allocation strategy at each subchannel. Combining (6.19) with both individual and total power constraints, we construct a multi-user convex optimization problem, where the single user optimization problem is the following:

$$\begin{aligned} &J(\lambda, \beta, P^{(j)}(k), P^{(j)}) \\ &\triangleq \max \sum_{j=1}^{K} \sum_{k=1}^{N} \log(1+\frac{P^{(j)}(k)}{M^{(j)}(k)}) - \lambda \left\{ \sum_{k=1}^{N} P^{(j)}(k) - P^{(j)} \right\} + \beta \left\{ \sum_{j=1}^{K} P^{(j)} - P^{(tot)} \right\}, \end{aligned} \tag{6.22}$$

where we define $M^{(j)}(k) \triangleq \frac{\triangle f N_o}{T_s |H^{(j)}(k \triangle f)|^2}$. First, if we take the derivative with respect to $P^{(j)}$ in (6.22), we obtain $\lambda = \beta$. Once individual constraints $P^{(j)}$ are given, the objective function $J(\lambda, \beta, P^{(j)}(k), P^{(j)})$ does not depend on β nor $P^{(j)}$ and thus is denoted as $J(\lambda, P^{(j)}(k))$. We can arrange $P^{(j)}$ in nonincreasing order so we have $\overline{P}^{(1)} \geq \overline{P}^{(j)} \geq \cdots \geq \overline{P}^{(K)}$ where the set of $\overline{P}^{(j)}$ is equal to the set $P^{(j)}$.

If we apply to a single user the waterfilling algorithm with parallel subchannels we obtain the following optimal policy

$$[P^{(j)}(k)]^* = (\frac{1}{\lambda} - M^{(j)}(k))^+, \tag{6.23}$$

where $(\cdot)^+ := \max(\cdot, 0)$ and $[P^{(j)}(k)]^*$ in (6.23) satisfies

$$\sum_{k=1}^{N} (\frac{1}{\lambda} - M^{(j)}(k))^+ = P^{(j)}, \tag{6.24}$$

$$\sum_{j=1}^{K} P^{(i)} = P^{(tot)}. \tag{6.25}$$

For the largest power $\overline{P}^{(1)}$, we solve (6.23) under the power constraints (6.24) via waterfilling. Then, we repeat it for the second largest power $\overline{P}^{(2)}$ and so on.

This strategy provides a closed form analysis of the multiuser adaptive power loading problem under both individual and total power constraints and leads to the optimal power loading assignment.

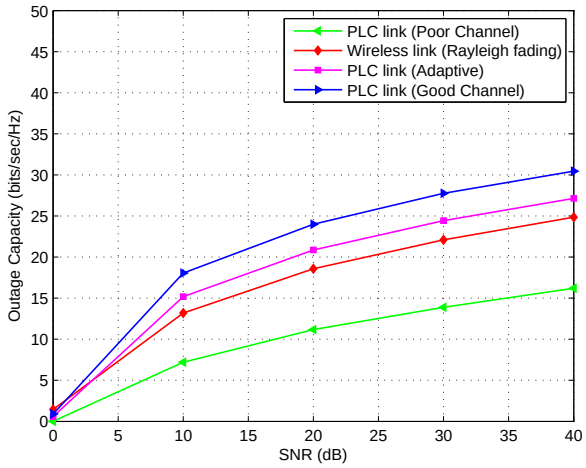

Figure 6.3: Comparison of outage capacities over PLC and wireless link

6.5 Numerical Results

As an illustration of our new analysis we consider the model problem shown in Fig. 1.1. In the model we assume that $\tilde{h}_2 \gg \tilde{h}_1$ where $\tilde{h}_i$, $i = 1, 2$ are defined in steps 2 and 4 of our strategy described in the latter part of Section 6.2.2. In that scenario we transmit 1000 OFDM symbols through both wireless and PLC-embedded wireline relay links and evaluate symbol error rates (SERs) at the receiver. Quadrature phase shift keying (QPSK) modulation is employed per subcarrier and determined

on the basis of the estimated subcarrier SNR. We assume that all other wireless links except for the PLC channel follow Rayleigh fading, and that the additive Gaussian noise at each link is statistically independent. We consider a bandwidth of $B = 32$ MHz, and the total of 128 orthogonal subchannels, which implies $N = 128$ and $\triangle\ f = 250\ kHz$. The measured transfer functions for GOOD and POOR powerline channels and the overall discrete time block channel matrices were taken from [9] and [10].

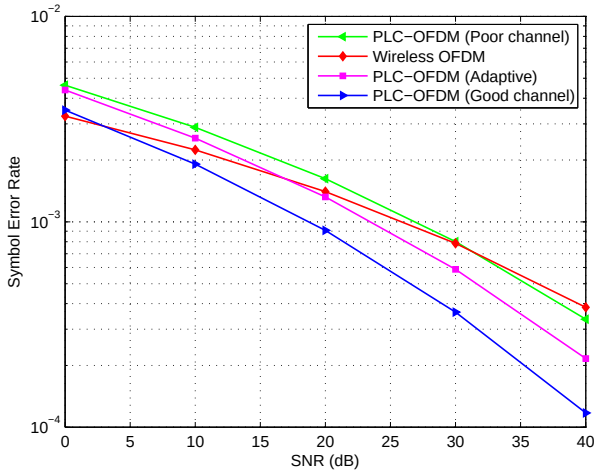

Figure 6.4: Comparison of symbol error rate (SER) over PLC and wireless link

Fig. 6.3 compares three outage capacities over PLC relay links and an outage capacity over typical wireless link (before OFDM modulation). The PLC and wireless outage capacity are calculated according to (6.19) and (6.13), respectively. Instead of (6.14), we made use of (6.13) because only the statistics of Rayleigh-faded wireless channels is known. As seen in Fig. 6.3, the PLC-embedded and wireless links perform comparably at low SNR levels (about up to 10 dB). For higher SNR level the adaptive PLC link outperforms the wireless link.

Fig. 6.4 shows that the wireless OFDM single hop link achieves lower symbol error rate (SER) compared to PLC-embedded OFDM relay link at SNR lev-

els up to around 17dB. Adaptive power loading scheme with bistatic channels (GOOD/POOR) shows that its SER performance lies between those of the POOR and GOOD channels. The gap between POOR and GOOD channels increases when the SNR levels increase. Also when the SNR increases the SER for the wireless channel becomes progressively worse than that of the adaptive PLC channel.

6.6 Summary

In this chapter, we investigated a hybrid PLC-wireless relaying network where power line communication link is introduced in blind zones. We studied relay channel capacities in both full CSI and no CSI environments. Based on the calculated outage and ergodic capacities, we generalized both the single user and multiuser MIMO channel capacities. In particular, for the decode-and-forward (DF) relaying and orthogonal frequency division multiplexing (OFDM) modulation we demonstrated benefits of hybrid wireless/PLC links when transmit powers were allocated optimally at both source and relay nodes under total power constraints. We next applied this strategy to a multiuser power loading scheme over orthogonal subchannels. Numerical simulations showed that the adaptive approach of the PLC/embedded link outperformed the wireless link in both outage capacity and symbol error rate.

CHAPTER 7

CONCLUSIONS

All achievements towards doctoral work are pictorially illustrated in Fig. 7.1, and each chapter is summarized below in details.

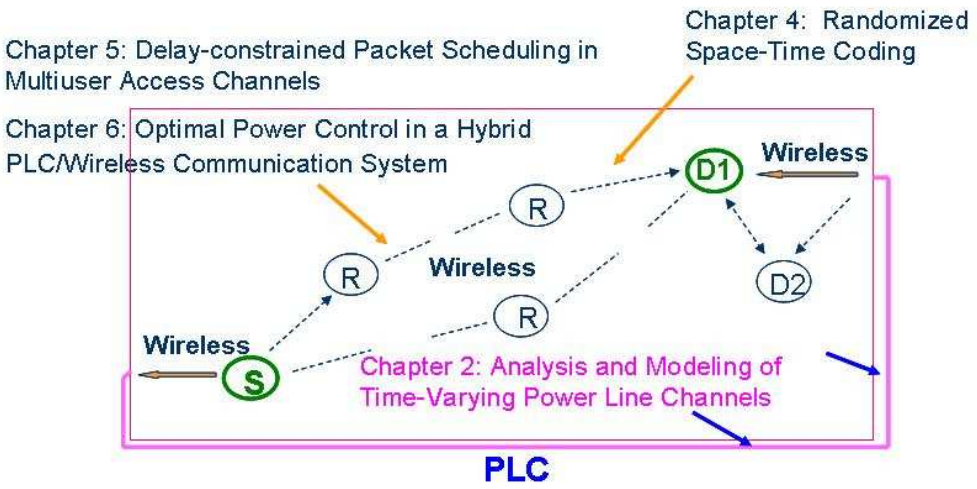

Figure 7.1: Summary of dissertation achievements over PLC and wireless link

Following the Introduction, in Chapter 2 we presented a general approach to characterizing the time-varying nature of power line channel response, and to finding the input output relationship for cascaded discrete time block models. In the considered test channel, we have obtained a close form of bistatic channel capacity for transmission lines and impedances with periodicity of half or a quarter of AC cycles, and compared the symbol error performance with that of classical waterfilling policy.

In Chapter 3, we have addressed a problem of designing a simple, efficient power line network simulator which is embedded with multirate filter bank precoders, i.e. *Wavelet-based MDFB* and *Weighted OFDM*. We also verified that two precoder schemes have trade-offs between error probability and complexity.

In Chapter 4, we studied distributed cooperative communications with randomized space-time coding and theory of the attainable diversity in both flat-fading and frequency-selective channels. Starting with several decentralized randomization schemes, we have shown these schemes are still desirable even in the presence of time dispersion due to asynchronism among nodes and frequency selectivity and also easily adapted to block space-time precoding techniques.

In Chapter 5, we explored packet transmission policies in the cross-layer perspective that minimize the average power consumed by transmitter under the average delay constraints. We have presented a simple packet scheduling policy, called *modified-linear-rule* (MLR) scheduler, which is influenced by both queue and channel states and that can be utilized to trade-off characteristic between queueing delay and transmission power policy. This near-optimal scheme achieves a low-complexity which tends to make the queue evolve as a stable feed-back linear system. In addition, we have generalized the efficiency of simple MLR scheduler even in the multiuser wireless fading, when compared with the performance of the optimal scheduler and the log-linear scheduler.

In Chapter 6, we proposed a hybrid PLC/wireless communication scheme which is realizable in typical indoor communication networks. Towards that goal, we derived analytic forms of single-user and multiuser MIMO channel capacities, and then evaluated relay channel capacities for slow and fast fading channel scenarios. We also investigated optimal allocation of transmit powers for the scheme at both source and relay nodes under total power constraints, and we showed numerical results to justify validity of my analysis.

7.1 Publications

The following is a list of publications/submissions that contain parts of this thesis.

- Tae-Eung Sung, Matthew Sharp, A. Scaglione and B. Sirkeci Mergen, "Randomized distributed multi-antenna systems in multi-path channels, " submitted to *IEEE Transaction on Communications*, (minor revision), 2009.
- Tae-Eung Sung, Anna Scaglione and Stefano Galli, "Novel PLC Embedded Network Topology in Time-Varying Block Transmission Models," submitted to *IEEE Transaction on Signal Processing*, (minor revision), 2009.
- Tae-Eung Sung, Anna Scaglione, and Stefano Galli, "Time-Varying Power Line Block Transmission Models over Doubly Selective Channels," *IEEE International Symposium on Power Line Communications and Its Applications* (ISPLC'08), jeju island, Korea, April 2008.
- Tae-Eung Sung and Adam Bojanczyk, "Cross-layer Delay-constrained Packet Scheduling over Multiuser Wireless Channels," *IEEE Wireless Telecommunications Symposium* (WTS'09), Prague, Czech Republic, April 2009.
- Tae-Eung Sung, "Innovative PLC Network Design for Bit Loading Algorithm and Bistatic Channel Capacity," *IEEE International Symposium on Consumer Electronics* (ISCE'09), Kyoto, Japan, May 2009.
- Tae-Eung Sung and Adam Bojanczyk, "Randomized Cooperative Precoding and Diversity Analysis over Doubly Selective Channels," *IEEE International Conference on Ubiquitous and Future Networks* (ICUFN'09), Hong Kong, June 2009.
- Tae-Eung Sung, "Time-Varying PLC Network Modeling with Wavelet MDFB and Weighted OFDM Precoders," *IEEE International Conference on Com-*

munication Theory, Reliability and Quality of Service (CTRQ'09), Colmar, France, July 2009.

- Tae-Eung Sung, "Cooperative Diversity in Wireless Networks: Randomization over Dispersive Channels," *IEEE Vehicular Technology Conference* (VTC'09 Fall), Anchorage, Alaska, September 2009.

- Tae-Eung Sung, "Cooperation in Decentralized Cognitive Networks: Relaying, Spectrum Sensing and Randomization," *IEEE International Symposium on Personal, Indoor and Mobil Radio Communications* (PIMRC'09), Tokyo, Japan, September 2009.

- Tae-Eung Sung and Adam Bojanczyk, "Optimal Power Control and Relay Capacity for PLC-embedded Cooperative Systems", *IEEE Consumer Communications and Networking Conference* (CCNC2010), Las Vegas, NV, January 2010.

- Tae-Eung Sung, "Multiuser Resource Allocation and Pilot-assisted Channel Estimation in Indoor PLC Cooperative Systems", *IEEE Radio and Wireless Symposium* (RWS2010), New Orleans, LA, January 2010.

- Y. Sung, T. Sung, B.M. Sadler, and L. Tong, "Training/optimal signal design for MIMO," in Space-Time Wireless Systems: From Array Processing to MIMO Communications, edited by H. Bolcskei, D. Gesbert, C. Papadias, and A. J. van der Veen, Cambridge University Press, August, 2006.

- Tae-Eung Sung and Adam Bojanczyk, "Power Line Communications and Smart Grid", in Wireless and Optical Communication Networks, edited by Kris Iniewski , Wiley, Spring, 2010.

BIBLIOGRAPHY

[1] R. Madan, N. B. Mehta, A. F. Molisch and J. Zhang, "Energyefficient cooperative relaying over fading channels with simple relay selection," Mitsubishi Electric Reserach laboratories Technique Report: TR2006-075, Nov 2006.

[2] G. Kramer, M. Gastpar and P. Gupta, "Cooperative strategies and capacity theorems for relay networks," IEEE Trans. Inform. Theory, vol. 51, no. 9, pp. 3037-3063, Sep. 2005.

[3] Z. Zhou, S.Zhou, Z. Cui and S. Cui, "Energy-Efficient Cooperative Communication Based on Power Control and Selective Relay inWireless Sensor Network," IEEE Military Communication Conference, Boston, MA, Oct. 2007.

[4] A. Bletsas, A. Khitsi, D. P. Reed, and A. Lippman, "A simple cooperative diversity method based on network path selection," IEEE Journ. on Select. Areas in Commun., vol. 24, no. 3, pp. 659-672, Mar. 2006.

[5] M. Hasna and M. Alouini, "Optimal power allocation for relayed transmissions over Rayleigh-fading channels," IEEE Trans. Wireless Commun., vol. 3, no. 6, pp. 1999-2004, Nov. 2004.

[6] N. Ahmed, M. Khojastepour, and B. Aazhang, "Outage Minimization and Optimal Power Control for the Fading Relay Channel," IEEE Information Theory Workshop, Houston, pp. 458-462, May 2004.

[7] X. Deng and A. Haimovich, "Powre allocation for cooperative relaying in wireless networks," IEEE Communication Letters, vol. 9, no. 11, pp. 994-996, Nov. 2005.

[8] N. Papandreou and T. Antonakopoulos, "Fair Resource Allocation with Improved Diversity Performance in Indoor Power-Line Networks," IEEE Trans. on Power Delivery, vol. 22, no. 4, pp. 2575-2576, Oct. 2007.

[9] T. Sung, "Innovative PLC Network Design for Bit Loading Algorithm and Bistatic Channel Capacity," *IEEE International Symposium on Consumer Electronics*, Kyoto, Japan, May 2009.

[10] T. Sung, "Time-Varying PLC Network Modeling with Wavelet MDFB and Weighted OFDM Precoders," *IEEE International Conference on Communication Theory, Reliability and Quality of Service*, Colmar, France, July 2009.

[11] T. Cover and J. Thomas, *Elements of Information Theory.* New York: Wiley, 1991.

[12] T. Sung and A. Bojanczyk, "Optimal Power Control and Relay Capacity for PLC-embedded Cooperative Systems", *IEEE Consumer Communications and Networking Conference* (CCNC2010), Las Vegas, NV, January 2010.

[13] S. Galli and T. Banwell, "A Deterministic Frequency-domain Model for the Indoor Power Line Transfer Function," *IEEE Journal on Selected Areas on Comm.*, July 2006.

[14] S. Galli and T. Banwell, "Novel Approach to the Modeling of the Indoor Power Line Channel - Part II: Transfer Function and Its Properties," *IEEE Trans. on Power Delivery*, July 2005.

[15] S. Galli, A. Scaglione, and K. Dostert, "Broadband is Power: Internet Access through the power line network," *IEEE Communication Magazine*, May 2003.

[16] E. Biglieri, S. Galli, Y.-W. Lee, H.V. Poor, H. Vinck, "Power Line Comunications," Guest Editorial for the Special Issue on Power Line Communications, *IEEE J. Select. Areas Commun.*, July 2006.

[17] T. Esmailian, Frank Kschischang and P. Gulak, "In-building power lines as high-speed communication channels: channel characterization and a test channel ensemble," *International Journal of Communication Systems*, May 2003.

[18] A. Scaglione, G. Giannakis, and S. Barbarossa, "Redundant Filterbank Precoders and Equalizers, Part I: Unification and Optimal Designs," *IEEE Trans. on Signal Proc.*, July 1999.

[19] H. Latchman and L. Yonge, "Power line local area networking," Guest Editorial, *IEEE Communication Magazine*, April 2003.

[20] N. Pavlidou, A. J. Han Vinck, J. Yazdani and B. Honary, "Power Line Communications: State of the Art and Future Trends," *IEEE Communications Magazine*, vol. 41, no. 4, pp. 34-39, April 2003.

[21] I. Hakki Cavdar, "Performance Analysis of FSK Power Line Communications Systems Over the Time-Varying Channels: Measurements and Modeling," *IEEE Trans. on Power Delivery*, Jan. 2004.

[22] S. Barmada and A. Musolino, "Innovative Model for Time-Varying Power

Line Communication Channel Response Evaluation," *IEEE Journal on Selected Areas on Comm.*, July 2006.

[23] F. Canete, J. Cortes, L. Diez, and J. Entrambasaguas, "Analysis of the cyclic short-term variation of indoor power line channels," *IEEE J. Select. Areas Commun.*, July 2006.

[24] G. Giannakis and C. Tepedelenlioglu, "Basis Expansion Models and Diversity Techniques for Blind Identification and Equalization of Time-Varying Channels," *Proc. of IEEE*, vol. 86, no 10, October, 1998.

[25] E. Biglieri, "Coding and Modulation for a Horrible Channel," *IEEE Communications Magazine*, vol. 31, no. 5, May 2003.

[26] K. Dostert, *Powerline Communications.* Prentice Hall PTR, 2001.

[27] F. Avram and L. Brown, "A Generalized Holder Inequality and a Generalized Szego Theorem," *Proceedings of the American Mathematical Society*, vol. 107, no. 3, pp. 687-695, Nov. 1989.

[28] L. Moura and I. Darwazeh, *Introduction to linear circuit analysis and modelling : From DC to RF.* published by Newnes, 2005.

[29] P. A. Bello, "Characterization of randomly time-variant linear channels," *IEEE Trans. Commun. Systems*, pp. 360-393, Dec. 1964.

[30] T. Starr, J.M. Cioffi, P.J. Silverman, *Understanding Digital Subscriber Line Technology*, Prentice Hall, 1999.

[31] P. A. Anghel, G. Leus, and M. Kaveh, "Distributed space-time coding in cooperative networks," in *Proc. of 5th NORDIC signal processing symposium*, 2002.

[32] S. Barbarossa and G. Scutari, "Distributed Space-Time Coding for Multihop Networks," in *Proc. of ICC*, vol. 2, pp. 916-920, June 2004.

[33] H. E. Gamal and D. Aktas, "Distributed Space-Time Filtering for Cooperative Wireless Networks," *IEEE Globecom*, vol. 4, pp.1826-1830, Dec. 2003.

[34] J. N. Laneman and D. N. C. Tse and G. W. Wornell, "An Efficient Protocol for Realizing Cooperative Diversity in Wireless Networks," in *Proc. of ISIT*, Washington, DC, June 2001.

[35] E. Moulines, P. Duhamel, J. F. Cardoso, and S. Mayargue, "Subspace Methods for the Blind Edentification of Multichannel FIR Filters," in *IEEE Trans. on Sig. Proc.*, vol. 43, pp. 516 - 525, Feb. 1995.

[36] R. U. Nabar and H. Boelcskei, "Capacity scaling laws in asynchronous relay networks," in *Proc. of Allerton Conference*, Monticello, IL, Oct. 2004.

[37] G. G. Raleigh and J. M. Cioffi, "Spatio-Temporal Coding for Wireless Communication," *IEEE Trans. Commun.*, vol. 46, pp. 357-366, Mar. 1998.

[38] A. Scaglione; Y.W. Hong; "Opportunistic Large Arrays," in *Proc. of, ISWC02*, Victoria, BC, Canada, 2002.

[39] A. Scaglione and Y.-W. Hong, "Opportunistic Large Arrays: Cooperative Transmission in Wireless Multihop Ad-hoc Networks to Reach Far Distances," *IEEE Trans. Signal Proc.*, no. 8, Aug. 2003.

[40] A. Sendonaris, E. Erkip, and B. Aazhang, "Increasing Uplink Capacity via User Cooperation Diversity," in *Proc. of ISIT*, Cambridge, MA, Aug. 1998.

[41] B. Sirkeci-Mergen and A. Scaglione, "Randomized Space-Time Coding for Distributed Cooperative Communication," in *Proc. of ICC*, 2006.

[42] B. Sirkeci-Mergen and A. Scaglione, "Randomized Space-Time Coding for Distributed Cooperative Communication," *IEEE Transactions on Signal Processing*, 2007.

[43] S. Yiu, R. Schober, and L. Lampe, "Distributed space-time block coding," submitted *IEEE Tran. on Comm.*, 2005.

[44] V. Tarokh, H. Jafarkhani, and A. Calderbank, "Space-time block codes from orthogonal designs," *IEEE Trans. Inform. Theory*, vol. 45, no. 5, pp. 1456-1467, July 1999.

[45] S. Wei, D. Goeckel, and M. Valenti, "Asynchronous cooperative diversity," in *Proc. of CISS*, 2004.

[46] V. Girko, *Theory of Random Determinants.* Kluwer Academic Publishers, 1990.

[47] A. M. Tulino and S. Verdú, *Random Matrix Theory and Wireless Communications.* now Publishers Inc., 2004.

[48] D. Tse and P. Viswanath, *Fundamentals of Wireless Communication.* Cambridge University Press, May 2005.

[49] M. Sharp and A. Scaglione and S. Galli, "Distributed Randomized Space-Time Coding for HF Transmission," *MILCOM'06*, Washington, DC, Oct. 2006.

[50] E. Lindskog and A. Paulraj, "A Transmit Diversity Scheme for Channels with Intersymbol Interference," in *IEEE ICC*, vol 1., pp. 307-311, June 2000.

[51] J. N. Lanemen and G. W. Wornell, "Distributed Space-Time Coded Protocols for Exploiting Cooperative Diversity In Wireless Networks," *IEEE Trans. Inform. Theory*, vol. 59, no. 10, Oct. 2003.

[52] J. Mietzner and R. Thobaben and P. A. Hoeher, "Analysis of the Expected Error Performance of Cooperative Wireless Networks Emploting Distributed Space-Time Codes," *Proc. IEEE GLOBECOM'04*, Nov. 2004.

[53] T. Sung and A. Bojanczyk, "Power Line Communications and Smart Grid", in Wireless and Optical Communication Networks, edited by Kris Iniewski , Wiley, Spring, 2010

[54] I. Tasadduq and R. Rao, " Weighted OFDM with Block Codes for Wireless Communication," I*EEE Pacific Rim Conference on Communiction, Computer and Signal Processing*, Aug. 2001.

[55] R. Heath Jr. and G. Giannakis, "Blind channel identification for multirate precoding and OFDM systems," *IEEE Conference on DSP'97*, vol. 1, no. 10, July, 1997.

[56] T. Sung, "Weighted OFDM and MDFB over Time-Varying Power Line Block Transmission Models," *IEEE International Conference on Signal Processing System* (ICSPS'09), Singapore, May 2009.

[57] S. Barmada and A. Musolino, "Innovative Model for Time-Varying Power Line Communication Channel Response Evaluation," *IEEE J. on Select. Areas on Comm.*, July 2006.

[58] T. Sung, A. Scaglione and S. Galli,"Time-Varying Power Line Block Transmission Models over Doubly Selective Channels," *IEEE Int'l Symposium on Power Line Communications and Its Applications* (ISPLC), April 2008.

[59] M. Tzannes, et al., "DMT Systems, DWMT Systems and Digital Filter Banks," in *Proceedings of ICC'94*, 1994, pp 311-315.

[60] S. Galli, H. Koga and N. Kodama, "Advanced Signal Processing for PLCs: Wavelet-OFDM," *IEEE Int'l Symposium on Power Line Communications and Its Applications* (ISPLC), April 2008.

[61] T. Sung and A. Bojanczyk, "Randomized Cooperative Precoding and Diversity Analysis over Doubly Selective Channels," *IEEE International Conference on Ubiquitous and Future Networks* (ICUFN'09), Hong Kong, June 2009.

[62] D. Rajan, A. Sbharwal and B. Aazhang, "Delay-Bounded Packet Scheduling of Bursty Traffic Over Wireless Channels," in *IEEE Trans. Inform. Theory*, vol. 50, pp. 125-144, Jan. 2004.

[63] R. Knopp and P. A. Humblet, "Information Capacity and Power Control in Single-cell Multiuser Communications," in *IEEE Trans. Inform. Theory*, vol. 1, pp. 331-335, Jun. 1995.

[64] R. Negi and S. Goel, "An Information-Theoretic Approach to Queueing in Wireless Channels with Large Delay Bounds," in *Proceedings of IEEE GLOBECOM '04*, vol. 1, pp. 116-122, Nov. 2004.

[65] R. Berry and R. Gallager, "Communication Over Fading Channels with Delay Constraints," *IEEE Trans. Inform. Theory*, 2002.

[66] D. Tse and S. Hanly, "Multi-Access Fading Channels: Part I: Polymatroid Structure, Optimal Resource Allocation and Throughput Capacities," in *IEEE Trans. Inform. Theory*, vol. 44, pp. 2796-2815, Nov. 1998.

[67] E. M. Yeh and A. S. Cohen, "Delay Optimal Rate Allocation in Multiaccess Fading Communications," in *Proc. Allerton Int. Conf. Communication, Control, and Computing*, pp. 140-149, Sep. 2004.

[68] I. E. Teletar and R. G. Gallager, "Combining queueing theory with information theory for multiaccess," in *IEEE J. Select. Areas Commun.*, vol. 13, pp.963-969, Aug. 1995.

[69] P. Venkitasubramaniam, S. Adireddy and L. Tong, "Opportunistic ALOHA and cross layer design for sensor networks," in *MILCOM 2003.* IEEE, vol. 1, pp.705-710, Oct. 2003.

[70] L. Tong, Q. Zhao, and S.Adireddy, "Sensor Networks with Mobile Agilents," in *MILCOM 2003.* IEEE, vol. 1, pp.688-693, Oct. 2003.

[71] T. M. Cover and J. A. Thomas, *Elements of Information Theory.* New York: Wiley, 1991.

[72] R. G. Gallager, *Information Theory and Reliable Communication.* New York: Wiley, 1968.

[73] D. P. Bertsekas and R. G. Gallager, *Data Networks.* Englewood Cliffs, NJ: Prentice-Hall, 1992.

[74] L. I. Sennott, *Stochastic Dynamic Programming and the Control of Queueing Systems.* New York: Wiley, 1999.

[75] C. E. Shannon, "A mathematical theory of communication," *Bell Syst. Tech. J.*, pp. 379-423, Jul. 1948.

[76] A. Leon-Garcia, *Probability and Random Processes for Electrical Engineering.*" Addison-Wesley, 1994.

[77] T. Sung and A. Bojanczyk, "Cross-layer Delay-constrained Packet Scheduling over Multiuser Wireless Channels," *IEEE Wireless Telecommunications Symposium* (WTS'09), Prague, Czech Republic, April 2009.

[78] B. Vucetic and J. Yuan, *Space-Time Coding.* Wiley, 2003.

[79] A. Paulraj, N. Nabar and D. Gore, *Introduction to Space-Time Wireless Communications.* Cambridge University Press, 2003.